THE SPIRALLING BINARY SYSTEM OF BLACK HOLES

By

JAMES KENT BLACKBURN

A DISSERTATION PRESENTED
TO THE GRADUATE SCHOOL
OF THE UNIVERSITY OF FLORIDA IN
PARTIAL FULFILLMENT OF THE REQUIREMENTS
FOR THE DEGREE OF DOCTOR OF PHILOSOPHY

UNIVERSITY OF FLORIDA

1990

To Space Ship Earth

ACKNOWLEDGEMENTS

Many people have contributed to my education and made this dissertation a reality. The individual making the most significant contribution towards this end has been my research advisor, Professor Steven Detweiler. Throughout our collaboration he has bestowed much encouragement and confidence. He possesses a rare talent for communicating the complex in terms of the well understood. He has been more than a mentor guiding his pupil on to greater challenges; he has also been a good friend and I thank him for these qualities.

I am very grateful to Professors Jim Ipser, Jim Fry, Rick Field, and Steve Gottesman for their participation as members of my supervisory committee. I wish to express special thanks to the faculty, postdocs, and graduate students of the astrophysics group in the physics department. Though small in number, they have provided a wealth of dialog and comprehension. I would also like to thank everyone else that has contributed to my understanding in physics, especially my fellow graduate students.

I am endlessly grateful to my parents, my four sisters, and the rest of my relatives for their encouragement, love, and care, especially my two grandmothers who passed away before the completion of my stay in Gainesville.

Finally, I give special thanks to my wife Laddawan Ruamsuwan for her never-ending cheerful disposition while struggling herself with the questions of physics, nature, and the cosmos.

TABLE OF CONTENTS

page

ACKNOWLEDGEMENTS iii

LIST OF TABLES vi

LIST OF FIGURES viii

NOTATION ix

ABSTRACT xii

CHAPTERS

1 INTRODUCTION 1

2 INITIAL VALUE FORMULATION 7

2.1 Foliation of Space-Time 7

2.2 Steady State Equations 19

2.3 Boundary Conditions 23

3 VARIATIONAL PRINCIPLE FOR TOTAL MASS 28

4 TRIAL GEOMETRIES 32

5 NUMERICAL RESULTS 49

5.1 Test Particle Geometry 49

5.2 Equal Mass Geometry 56

5.3 Arbitrary Mass Ratios 70

5.4 Gravitational Radiation 79

5.5 Apparent Horizons 89

6 SUMMARY AND CONCLUSIONS 96

APPENDIX COMPUTER PROGRAM 101
REFERENCES 154
BIOGRAPHICAL SKETCH 157

LIST OF TABLES

TABLE		page
1	Stable Circular Analytical Test Particle Orbits	52
2	Unstable Circular Analytical Test Particle Orbits	52
3	Numerical Test Particle Masses	55
4	Numerical Stable Circular Test Particle Orbits	55
5	Numerical Stable Circular Orbits for Equal Masses	65
6	Comparison of Stable Circular Orbits for Equal Masses	69
7	Numerical Masses for Mass Ratio 0.005	71
8	Numerical Orbits for Mass Ratio 0.005	71
9	Numerical Masses for Mass Ratio 0.02	72
10	Numerical Orbits for Mass Ratio 0.02	72
11	Numerical Masses for Mass Ratio 0.03	73
12	Numerical Orbits for Mass Ratio 0.03	73
13	Numerical Masses for Mass Ratio 0.05	74
14	Numerical Orbits for Mass Ratio 0.05	74
15	Numerical Masses for Mass Ratio 0.10	75
16	Numerical Orbits for Mass Ratio 0.10	75
17	Numerical Masses for Mass Ratio 0.25	76
18	Numerical Orbits for Mass Ratio 0.25	76
19	Numerical Masses for Mass Ratio 0.50	77
20	Numerical Orbits for Mass Ratio 0.50	77

21 Numerical Masses for Mass Ratio 0.75 78
22 Numerical Orbits for Mass Ratio 0.75 78
23 Gravitational Quadrupole Radiation for Equal Masses 84

LIST OF FIGURES

FIGURE		*page*
1	Two Neighboring Spatial Slices of a Foliation	12
2	Hypersurface Topology for Binary System of Black Holes	25
3	Analytical Effective Potential for Test Particle	53
4	Numerical Effective Potential for Test Particle	57
5	Binding Energy of Numerical Test Particle	58
6	Single Parameter Newtonian Circular Orbits	60
7	Post-Newtonian Effective Potential for Equal Masses	63
8	Numerical Effective Potential for Equal Mass Black Holes	66
9	Numerical Binding Energy of Equal Mass Black Holes	67
10	Quadrupole Radiation from Equal Mass Black Holes	85
11	Numerical Binding Energy versus Separation	87
12	Numerical Components of Velocity	88

NOTATION

The conventions used in this dissertation are intended to be consistent with most of the modern references to classical general relativity. In almost all cases, the meaning will be clear from the context. When the possibility for confusion exits, the actual meaning is presented. Geometrized units are employed throughout the text, that is, units having the gravitational constant and the speed of light both set equal to one. The choice of the metric signature is $(- + + +)$. The following is a descriptive list of symbols and their meanings appearing within this dissertation:

$g_{\mu\nu}$	Metric of four dimensional space-time geometry
∇_ν	Covariant derivative associated with space-time metric
$\mathcal{L}_t$	Lie derivative in the direction of the four-vector t
$(\mathrm{M}, \mathrm{g}_{\mu\nu})$	Space-time manifold with metric $g_{\mu\nu}$
Σ_τ	Space-like hypersurface embedded in space-time manifold
τ	Time parameter labeling each hypersurface
$\gamma_{\mu\nu}$	Metric of three dimensional spatial geometry
D_ν	Covariant derivative associated with spatial metric
$K_{\mu\nu}$	Extrinsic curvature tensor
$\pi^{\mu\nu}$	Momentum conjugate to spatial metric
$\Gamma^{\mu}{}_{\nu\delta}$	Christoffel Symbols

$\mathrm{R}_{\alpha\beta\gamma\delta}$	Riemann Tensor of four dimensional spacetime geometry
$R_{\alpha\beta\gamma\delta}$	Riemann Tensor of three dimensional spatial geometry
$\mathrm{R}_{\mu\nu}$	Ricci Tensor of four dimensional spacetime geometry
$R_{\mu\nu}$	Ricci Tensor of three dimensional spatial geometry
R	Ricci Scalar of four dimensional spacetime geometry
R	Ricci Scalar of three dimensional spatial geometry
$\mathrm{G}_{\mu\nu}$	Einstein tensor
$\mathrm{T}_{\mu\nu}$	Stress energy tensor
α	Lapse function
β	Shift vector
Ψ	Reduces to conformal factor in low velocity limit
$\mathcal{L}_G$	Lagrangian density of general relativity
$\mathcal{H}_G$	Hamiltonian density of general relativity
H_G	Hamiltonian of general relativity
s	Separation between the two black holes
m	Schwarzschild test particle mass
E	Energy of Schwarzschild test particle mass
m_1	Mass of first black hole as measured on common sheet of hypersurface
m_2	Mass of second black hole as measured on common sheet of hypersurface
μ	Reduced mass: $m_1 m_2/(m_1 + m_2)$
M_{total}	Mass of both black holes as measured on common sheet
M_1	Irreducible mass of first black hole as measured on first isolated sheet of hypersurface, also called $M_{1_{irreducible}}$
M_2	Irreducible mass of second black hole as measured on second isolated sheet of hypersurface, also called $M_{2_{irreducible}}$
M_o, E_o	Extreme values of the mass determined by Hamiltonian

Ω	Angular frequency of rotation of binary black holes
x_{o_1}	Position of first black hole along x-axis in corotating frame
x_{o_2}	Position of second black hole along x-axis in corotating frame
u	Tangential velocity of first black hole
v	Tangential velocity of second black hole
J_{total}	Total angular momentum
j_{total}	Scaled total angular momentum: $J_{total}/(M_1 M_2)$
$\mathcal{I}_{jl}$	Reduced quadrupole moment tensor
L_{GW}	Dimensionless luminosity of gravitational radiation
$\frac{dJ_{GW}}{dt}$	Rate angular momentum lost to gravitational radiation
$Y_{\ell m}$	Spherical harmonics
$Y^*_{\ell m}$	Complex conjugate to spherical harmonics

Abstract of Dissertation Presented to the Graduate School
of the University of Florida in Partial Fulfillment of the
Requirements for the Degree of Doctor of Philosophy

THE SPIRALLING BINARY SYSTEM OF BLACK HOLES

By

James Kent Blackburn

May 1990

Chairman: Steven Detweiler
Major Department: Physics

A novel approach to the numerical analysis of the dynamic system of two spiralling black holes is developed using the initial value formalism of general relativity. As the two black holes spiral in on each other they will lose energy and angular momentum in the form of gravitational radiation. When the amplitude of this gravitational radiation is small enough, the space-time for the two orbiting black holes can be approximated by a geometry which is unchanging as seen by an observer in a frame of reference corotating with the two black holes. Then a time-like Killing vector field is assumed to exist over a finite region of the space-time geometry. A variational principle is found for the total mass of the binary system based on the Hamiltonian of general relativity and is used to study the dynamics and stability of the close orbits. The emission of gravitational waves within the context of the quadrupole moment approximation is used to determine the secular evolution of the system. For

black holes of equal mass, approximately 3% of the their initial mass, as determined when the two black holes are at rest at large separations, is emitted as gravitational radiation with frequencies less than the quadrupole normal mode frequency of the final coalesced Kerr black hole.

CHAPTER 1
INTRODUCTION

The concept of black holes has been on the minds of men for at least two centuries. In 1783 John Michell, in a letter to Henry Cavendish, discussed the gravitational confinement of light emitted from the surface of a star with the same density as our sun but having a radius 500 times greater.[1] Laplace predicted in 1795 that a spherical object having a large mass of sufficiently small radius would possess a gravitational field so great that even light could not escape from its surface in accord with the Newtonian theory of gravity.[2] Receiving little attention, Laplace removed his early consideration of a black hole from later editions of his work. The consequences of gravitational fields of this strength brought up in these early discussions lie dormant for more than a century, until Einstein's theory of general relativity in 1915.[3]

Schwarzschild was able to formulate an exact solution to the gravitational field surrounding a spherical mass within a month of Einstein's publication of the theory of general relativity.[4] Schwarzschild's solution contains the complete description of the gravitational field associated with a spherically symmetric, nonrotating, electrically neutral black hole. Einstein, not surprisingly, did not expect an exact solution to the field equation of general relativity to exist and commended Schwarzschild on his achievement.

During the next half century black holes would once again be disregarded as an idea with enough physical significance to justify their study. Theoretical

studies of white dwarfs by Chandrasekhar in 1930 lead to the prediction of an upper mass limit for white dwarfs of approximately 1.4 $M_{\odot}$.[5] Above this maximum mass, known as the Chandrasekhar limit, a white dwarf would not be saved from gravitational collapse by the degenerate relativistic electron pressure of Fermi-Dirac statistics. The final state of such a stellar object was now a matter of speculation. Eddington, unhappy with the prospects of black holes, modified the equation of state of a degenerate relativistic gases such that finite equilibrium states existed for stars of any mass.[6] Landau also rejected the idea of black holes as the final resting state of stars with masses greater than the Chandrasekhar Limit. In his elementary explanation of the Chandrasekhar Limit, Landau concludes,"Such masses exist quietly as stars and do not show any such ridiculous tendencies we must conclude that all stars greater than 1.5 $M_{\odot}$ certainly possess regions in which the laws of quantum mechanics are violated."[7]

Chadwick's discovery of the neutron lead to a new class of stellar object, the neutron star.[8] These objects are supported against gravitational collapse by the pressure of degenerate neutrons and the strong interactions between nucleons. The first detailed calculations of neutron star structure were carried out by Oppenheimer and Volkoff in 1939.[9] They also reached the conclusion that a critical mass existed above which neutron stars could not reach a final equilibrium state. Later Oppenheimer and Snyder made a detailed study of the collapse of pressureless neutron stars and concluded that it was unlikely that any law of physics would come to the rescue to prevent the gravitational collapse for some stellar masses.[10]

Lacking observational support, the study of black holes yielded to the opinions of the great astronomers and physicists of this era. In retrospect

Chandrasekhar stated, "Eddington's supreme authority in those years effectively delayed the development of fruitful ideas along these lines for some thirty years."[11] Even with the critical mass limits derived from theory, serious considerations of black holes did not surface again until the later half of this century.

The golden age of black holes began in the 1960s with contributions from many physicists.[12,13,14] Much of the excitement in black holes was sparked by the observations of exotic stellar objects such as pulsars, quasars, and compact X-ray sources.[15] In 1963 Kerr discovered a family of exact solutions to Einstein's vacuum field equations characterizing a chargeless, rotating black hole.[16] Later Newman constructed a charged generalization of this solution for the Einstein-Maxwell field equations.[17] This is the most general exact analytic solution of a black hole known. It is parametrized by just three observable quantities, total mass M, total angular momentum J, and total charge Q. Such a simple parametrization of a black hole led Wheeler to the adage, "A black hole has no hair."[18]

At roughly the same period in time new techniques were being developed to handle the increasing number of global issues surrounding black hole physics. Questions concerned with asymptotic flatness, event horizons, and singularities were resolved using these new global techniques.[19,20,21,22] An extremely useful conformal transformation of space-time developed by Penrose, designed to bring infinity into a finite distance, illustrates the global features of a black hole in what is known as a Penrose diagram.[23] This diagram describes all the causal relationships of past and future singularities, event horizons, space-like, time-like, and null infinities, and the orientation of light cones at all events for a black hole's space-time manifold. It plays a crucial role in formulating the topic of this dissertation.

By the 1970s the studies of a black hole had reached maturity. Yet, the universe as we know it can not be simply modeled by the space-time geometry associated with a single black hole. If Einstein's field equations are to be considered a viable mathematical model of nature, then they must contain the descriptions of any physical system observed. Efforts to find new solutions have been restricted to studies of space-time geometries with so much symmetry that their applications to astrophysics become very limited.[24] Perturbative methods are also applied to problems of significance to astrophysics, but they too are plagued by a limited range of application from perturbation theory's very nature.[25]

Classical theories of physics such as mechanics and electromagnetism have the feature that when initial data is specified in such a way as to satisfy any constraints in the theory, then the initial data can be dynamically evolved in a manner completely and uniquely determined by the specification of initial data. A theory which can be represented by such a description is said to possess an initial value formulation. The general theory of relativity also has an initial value formulation;[26] much of the pioneering development was carried out in the 1960s by Arnowitt, Deser, and Misner.[27]

These efforts laid down the foundation for studying new classes of problems using the initial value formulation of the general theory of relativity. The task of finding solutions is no less involved in this formulation. However, the initial value formulation is well suited for numerical analysis. With the increasing speed and accuracy of the digital computer finding applications in many areas of research, the computer age inevitably was to influence general relativity. Initial data ranging from gravitational radiation to colliding black holes have been studied by these methods.[28,29]

One important unsolved classical problem in general relativity is the binary system of two orbiting black holes. Such a system of black holes will spiral in on each other as a result of the energy and angular momentum losses associated with gravitational radiation emitted by the system. The amplitude of the radiation increases as the system becomes more tightly bound. Eventually, the secular time scale becomes comparable to the orbital period. In the end the black holes coalesce with a highly nonlinear burst of gravitational radiation then settle down into a Kerr black hole. The details of this binary black hole system poses an important challenge to the classical theory of general relativity.[30]

The energy and angular momentum carried off by gravitational radiation will be small throughout most of the evolution of the black holes. While the time scale for secular effects caused by the radiation reaction are large in comparison to the dynamical time scale of the orbit, an observer in a frame of reference rotating with the black holes will see the space-time geometry as approximately time independent. Making the time independence into a global feature of the space-time geometry introduces an important simplification to general relativity. This time independent approximation to the geometry applied to the spiralling binary black hole system is the subject of this dissertation.

The geometry for a finite but sufficiently large region of the space-time manifold is considered. Initial data consistent with the binary system of orbiting black holes and satisfying the necessary constraints is placed on a partial Cauchy surface of the manifold. This initial data evolves inside the future Cauchy development consistently with the time symmetry of the rotating frame of reference. The time translational vector field of this frame will be a Killing

vector field for the geometry. This Killing vector field results in a simplification of the initial value formulation to a set of equations we call the steady state equations. These equations are used in a variational principle for the total mass, which when extremized provides the total mass of circular orbits. The results of this novel technique are compared with calculations from earlier methods when the parametrization of the binary system of black holes overlaps these earlier techniques.

The quadrupole gravitational radiation is used to benchmark the validity of the approximation of a time translational Killing vector for the space-time geometry.[31] As long as the amplitude of the gravitational radiation is small on the boundaries of Cauchy surface approximate asymptotic flatness can be imposed as a boundary condition. Under these circumstances the geometry will be a reasonable approximation to the realistic geometry for this system.

CHAPTER 2
INITIAL VALUE FORMULATION

2.1 Foliation of Space-Time

The search for a mathematical representation of the physical universe in classical general relativity begins with Einstein's field equations

$$G_{\alpha\beta} \equiv R_{\alpha\beta} - \frac{1}{2} g_{\alpha\beta} R = 8\pi T_{\alpha\beta} \tag{2.1}$$

a set of coupled, second order, nonlinear, partial differential equations which relate the inverse of curvature, through second order derivatives of the metric coefficients on the right to sources of curvature, the distribution of mass and energy on the left, for a space-time manifold. The elegant statement of Einstein's equations, that given the mass energy distribution then solve for the geometry of space-time, is misleading. This results from the coupling of the definition of the mass energy distribution to the geometry. Without knowledge of the geometry, the distribution of mass and energy cannot be specified.

In actuality, one can only describe equation (2.1) in terms of sources and expressions for the geometry correctly after separating the initial value data from the future evolution.[32] Of the ten components to Einstein's field equations, four equations relate the distribution of mass energy on a space-like hypersurface to the geometry of the hypersurface, and the remaining six equations determine how the geometry of the hypersurface and the mass energy will evolve. The true statement of Einstein's field equations is that given a

space-like 3-geometry and its time rate of change, and given the fields of mass energy and their time rates of change all at a particular time, solve the space-time 4-geometry at that one time, and then evolve the mass energy fields and 4-geometry to all times. The details of this procedure are at the center of the initial value formulation of general relativity.

In order to apply the initial value formalism to general relativity the space-time manifold $(\mathrm{M}, \mathrm{g}_{\alpha\beta})$, where $g_{\alpha\beta}$ are the metric coefficients, must be well posed. That is, the gravitational field must be the time history of the geometry of a space-like hypersurface viewed as a Cauchy problem.[33] That the space-time manifold $(\mathrm{M}, \mathrm{g}_{\alpha\beta})$ possesses a Cauchy description requires the manifold to be globally hyperbolic with the following features:

- There are no closed causal paths.
- M can be foliated by Cauchy surfaces Σ_τ.
- The Cauchy surface is parametrized by a global time function τ whose gradient is time-like everywhere.
- M has topology $\Sigma \times \Re$ where Σ is the topology of the Cauchy surface.

On such a manifold, $(\mathrm{M}, \mathrm{g}_{\alpha\beta})$, an initial value formulation is well posed.[34] This is shown by using harmonic coordinates x^μ_{HC} which satisfy

$$H^\mu \equiv \nabla_\nu \nabla^\nu x^\mu_{HC} = 0 \; . \tag{2.2}$$

They are used to write Einstein's field equations as a quasilinear, diagonal, second order hyperbolic system

$$-\frac{1}{2} g^{\alpha\beta} \partial_\alpha \partial_\beta g_{\mu\nu} + F_{\mu\nu}(g, \partial g) = 8\pi T_{\mu\nu} \tag{2.3}$$

where the $F_{\mu\nu}(g, \partial g)$ are the nonlinear terms that depend on the metric and its first derivative.[35]

The harmonic coordinates x^{μ}_{HC} of equation (2.2) are not useful in the initial value formalism. However, the coordinates to be used are related by a coordinate transformation to the harmonic coordinates

$$x^{\nu} = x^{\mu}_{HC} \frac{\partial x^{\nu}}{\partial x^{\mu}_{HC}} \ . \tag{2.4}$$

The coordinate transformation does not change the geometry of the space-time, or the physics it contains. It does mean that we are free to work with a set of coordinates which more closely characterize the problem at hand and still be assured that the development of the Cauchy Surface will exist. The initial data on the Cauchy surface has a maximal development; this is the manifold $(\mathrm{M}, \mathrm{g}_{\alpha\beta})$. The extent of the Cauchy development typically is large enough to prove physically interesting.

Having demonstrated that a well posed initial value formalism is consistent with treating the task of finding solutions in general relativity to the Cauchy problem, the initial value formulation can now be described. The space-time manifold $(\mathrm{M}, \mathrm{g}_{\alpha\beta})$ is foliated by Cauchy surfaces, space-like hypersurfaces Σ_{τ}, parametrized by a universal time function τ. Each Cauchy surface will have a time-like normal vector field

$$\mathbf{n} = n^{\alpha} \frac{\partial}{\partial x^{\alpha}} = n^{\beta} \hat{\mathbf{e}}_{\beta} \tag{2.5}$$

satisfying the normalization condition

$$\langle \mathbf{n}, \mathbf{n} \rangle = -1 \tag{2.6}$$

and having components n^{α} in the coordinate basis $\partial/\partial x^{\alpha}$ or components n^{β} in the general basis $\hat{\mathbf{e}}_{\beta}$. The selection of basis is also arbitrary though the choice can lead to a simplification of calculations. As an example, a natural choice for

the initial value formulation, choose $\hat{\mathbf{e}}_0 = \mathbf{n}$, the normal to the hypersurface surface, and $\hat{\mathbf{e}}_i$ where $i = (1,2,3)$, any three tangent vectors spanning this hypersurface Σ_τ. Though not necessary, the three tangent vectors are generally assumed to be the tangents to the coordinates

$$\hat{\mathbf{e}}_i = \frac{\partial}{\partial x^i} \tag{2.7}$$

providing a coordinate basis for the discussion of the three geometry of the hypersurface.

The normal to each hypersurface of the foliation is also described through the dual cotangent basis of vectors $\hat{\mathbf{e}}^\alpha$ by the closed one-form

$$\mathbf{w} = w_\alpha \hat{\mathbf{e}}^\alpha = w_\alpha \mathbf{d}x^\alpha \tag{2.8}$$

where $\hat{\mathbf{e}}^\alpha = \mathbf{d}x^\alpha$ in a coordinate basis, and $\mathbf{w}$ satisfies the relation

$$\langle \mathbf{n}, \mathbf{w} \rangle = 1 \ . \tag{2.9}$$

The one-form $\mathbf{w}$ describes the foliation of space-time and is related to the universal time function τ by the gradient

$$w_\beta = \alpha \nabla_\beta \tau \tag{2.10}$$

where ∇ is the covariant derivative of the space-time manifold and α is the lapse function. The lapse function α is a measure of the local rates of clock on the hypersurface. Imposing these choices insures that $\mathbf{n}$ points in the direction of increasing τ, and gives the four-velocity vector field of observers instantaneously at rest in the slice Σ_τ.

An important point to make about $\mathbf{n}$ is that, for a particular foliation of the space-time manifold, it is not the most natural choice of orthogonal vector fields for connecting each slice. Reconsidering equation (2.9)

$$\langle \mathbf{n}, \mathbf{w} \rangle = \langle \mathbf{n}, \alpha \nabla \tau \rangle = \langle \alpha \mathbf{n}, \nabla \tau \rangle \tag{2.11}$$

reveals that the orthogonal vector field with components $N^\beta = \alpha n^\beta$ is the natural choose since the proper time interval between two nearby hypersurfaces parametrized by τ is $\alpha\delta\tau$. However, $\mathbf{N}$ is not the most general vector to measure this proper time interval, see Figure 1. Removing the restriction of orthogonality, a general vector field $\mathbf{t}$ of the form

$$\mathbf{t} = t^\sigma \hat{\mathbf{e}}_\sigma = (\alpha n^\sigma + \beta^\sigma)\hat{\mathbf{e}}_\sigma \tag{2.12}$$

with $\beta^\sigma w_\sigma = \beta_\sigma n^\sigma = 0$, will also satisfy the normalization condition

$$\langle \mathbf{t}, \nabla\tau \rangle = 1 \ . \tag{2.13}$$

The arbitrary spatial vector $\beta^\sigma \hat{\mathbf{e}}_\sigma$ is the shift vector and represents the remaining kinematic freedom associated with describing a particular space-time foliation. The vector field $\mathbf{t}$ is the tangent to a congruence of curves parametrized by τ connecting the hypersurfaces Σ_τ of the foliation on $(M, g_{\alpha\beta})$.

The space-time metric $g_{\alpha\beta}$ of M induces the space-like metric $\gamma_{\alpha\beta}$ on the hypersurface Σ_τ given by

$$\gamma_{\alpha\beta} = g_{\alpha\beta} + w_\alpha w_\beta \tag{2.14}$$

with the inverse space-like metric given by

$$\gamma^{\alpha\beta} = g^{\alpha\beta} + n^\alpha n^\beta \ . \tag{2.15}$$

That the metric $\gamma_{\alpha\beta}$ is a spatial tensor results from

$$\gamma_{\alpha\beta} n^\beta = 0 \ . \tag{2.16}$$

The mixed form $\gamma^\alpha{}_\beta$, one covariant index and one contravariant index, is the unit operator of projection onto the hypersurface.

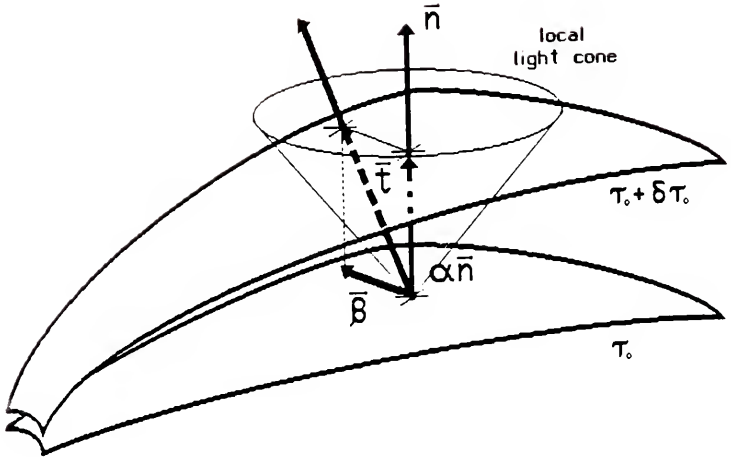

FIGURE 1: Two Neighboring Spatial Slices of a Foliation. Two neighboring hypersurfaces of the space-time foliation illustrating the relationship between the "time" vector $\mathbf{t}$, the lapse function α, the shift vector β, and the normal $\mathbf{n}$ in the expression $\mathbf{t} = (\alpha n^\sigma + \beta^\sigma)\hat{\mathbf{e}}_\sigma$.

The covariant derivative ∇ of the space-time manifold also induces a covariant derivative D on the hypersurface though the action of the projection operation. Consider a scalar function Φ defined on the hypersurface. The covariant derivative on Σ_τ of Φ is given by

$$\mathrm{D}_\beta \Phi \equiv \gamma^\alpha{}_\beta \nabla_\alpha \Phi \ . \tag{2.17}$$

Next consider a spatial vector existing in the hypersurface with contravariant components v^σ where $v^\sigma w_\sigma = 0$. The covariant derivative on Σ_τ of v^σ is given by

$$\mathrm{D}_\beta v^\sigma \equiv \gamma^\alpha{}_\beta \gamma^\sigma{}_\lambda \nabla_\alpha v^\lambda \ . \tag{2.18}$$

As a last example consider the second rank mixed spatial tensor $t^\alpha{}_\beta$ which satisfies $t^\alpha{}_\beta w_\alpha = t^\alpha{}_\beta n^\beta = 0$. The covariant derivative on Σ_τ of $t^\alpha{}_\beta$ is given by

$$\mathrm{D}_\nu t^\alpha{}_\beta \equiv \gamma^\mu{}_\nu \gamma^\alpha{}_\sigma \gamma^\lambda{}_\beta \nabla_\mu t^\sigma{}_\lambda \ . \tag{2.19}$$

When the covariant derivative D on the hypersurface acts on the spatial metric $\gamma_{\alpha\beta}$ the following result

$$\mathrm{D}_\kappa \gamma_{\alpha\beta} = \gamma^\sigma{}_\kappa \gamma^\mu{}_\alpha \gamma^\nu{}_\beta \nabla_\sigma (g_{\mu\nu} + n_\mu n_\nu) = 0 \tag{2.20}$$

using $\nabla_\sigma g_{\mu\nu} = 0$, and $\gamma^\alpha{}_\beta n^\beta = 0$, shows D to be the unique covariant derivative operator on the hypersurface σ_τ associated with the metric $\gamma_{\alpha\beta}$ of the hypersurface.

Having established a metric $\gamma_{\alpha\beta}$ and covariant derivative D on the hypersurface Σ_τ, the usual constructs of differential geometry can be defined on the 3-geometry of the hypersurface. The Riemannian curvature tensor $R(\gamma)$ is given by requiring that all spatial cotangent vectors $\omega_\nu \mathbf{d}x^\nu$ satisfy

$$\mathrm{D}_{[\alpha}\mathrm{D}_{\beta]}\omega_\nu \equiv \frac{1}{2}(\mathrm{D}_\alpha \mathrm{D}_\beta - \mathrm{D}_\beta \mathrm{D}_\alpha)\omega_\nu = \frac{1}{2} R^\mu{}_{\nu\beta\alpha}\omega_\mu \ . \tag{2.21}$$

To complete the initial data for the Cauchy surface also requires the extrinsic curvature tensor $K_{\sigma\rho}$. The following are equivalent expressions for the extrinsic curvature:

$$\begin{aligned} K_{\sigma\rho} &= \gamma^{\mu}{}_{\sigma}\gamma^{\nu}{}_{\rho}\nabla_{(\mu}\alpha\nabla_{\nu)}\tau \\ &= \gamma^{\mu}{}_{\sigma}\gamma^{\nu}{}_{\rho}\nabla_{(\mu}w_{\nu)} \\ &= \frac{1}{2}\gamma^{\mu}{}_{\sigma}\gamma^{\nu}{}_{\rho}(\nabla_{\mu}w_{\nu} + \nabla_{\nu}w_{\mu}) \\ &= -\frac{1}{2}\gamma^{\mu}{}_{\sigma}\gamma^{\nu}{}_{\rho}(\nabla_{\mu}n_{\nu} + \nabla_{\nu}n_{\mu}) \\ &= -\frac{1}{2}\gamma^{\mu}{}_{\sigma}\gamma^{\nu}{}_{\rho}(g_{\xi\nu}\nabla_{\mu}n^{\xi} + g_{\mu\xi}\nabla_{\nu}n^{\xi}) \\ &= -\frac{1}{2}\gamma^{\mu}{}_{\sigma}\gamma^{\nu}{}_{\rho}(n^{\xi}\nabla_{\xi}g_{\mu\nu} + g_{\xi\nu}\nabla_{\mu}n^{\xi} + g_{\mu\xi}\nabla_{\nu}n^{\xi}) \\ &= -\frac{1}{2}\gamma^{\mu}{}_{\sigma}\gamma^{\nu}{}_{\rho}\mathcal{L}_{\mathrm{n}}g_{\mu\nu} \\ &= -\frac{1}{2}\gamma^{\mu}{}_{\sigma}\gamma^{\nu}{}_{\rho}\mathcal{L}_{\mathrm{n}}\gamma_{\mu\nu} \\ &= -\frac{1}{2}\mathcal{L}_{\mathrm{n}}\gamma_{\sigma\rho} \end{aligned} \tag{2.22}$$

where $\mathcal{L}$ is the Lie derivative. The Lie derivative $\mathcal{L}_{\mathrm{n}}$ in the direction of the time-like normal $\mathbf{n}$ to the Cauchy surface acts as a time derivative. The equation $\mathcal{L}_{\mathrm{n}}\gamma^{\mu}{}_{\nu} = 0$ was used in the last two equalities. The final expression provides an interpretation of the extrinsic curvature as the time rate of evolution, or velocity, of the spatial metric. The extrinsic curvature's role in the initial data formulation is to express the bending of the embedded hypersurface Σ_{τ} in the space-time manifold $(\mathrm{M}, g_{\alpha\beta})$. The extrinsic curvature, as a spatial tensor, depends on the vector field $\mathbf{n}$ only on the Cauchy surface. Thus, one slice of the foliation of space-time is characterized by $(\Sigma_{\tau}, \gamma_{\alpha\beta}, K_{\alpha\beta})$, and provides the initial data for the space-time manifold $(\mathrm{M}, g_{\alpha\beta})$.

As previously mentioned, the 3-geometry is found first, followed by the determination of the 4-geometry for that one value of the universal time τ.

The geometry of the hypersurface is related to the space-time geometry by the Gauss-Codazzi equations

$$\gamma^{\rho}{}_{\alpha}\gamma^{\sigma}{}_{\beta}\gamma^{\mu}{}_{\lambda}\gamma^{\nu}{}_{\delta}\mathrm{R}_{\rho\sigma\mu\nu} = R_{\alpha\beta\lambda\delta} + K_{\alpha\lambda}K_{\beta\delta} - K_{\alpha\delta}K_{\beta\lambda} \tag{2.23a}$$

$$\gamma^{\rho}{}_{\alpha}\gamma^{\sigma}{}_{\beta}\gamma^{\mu}{}_{\delta}\mathrm{R}_{\rho\sigma\mu\nu}n^{\nu} = \mathrm{D}_{\alpha}K_{\beta\delta} - \mathrm{D}_{\beta}K_{\alpha\delta} \tag{2.23b}$$

where the roman $\mathrm{R}_{\rho\sigma\mu\nu}$ are the components of the Riemannian tensor of the space-time geometry, and the italic $R_{\alpha\beta\lambda\delta}$ are the components of the Riemannian tensor of the hypersurface, which results from the projection onto the Cauchy surface of the commutator of the space-time covariant derivatives, $\nabla_{[\alpha}\nabla_{\beta]}$, applied to any spatial vector, and applied to the normal vector. Using the symmetries of the Riemannian curvature tensor, and the equivalence of this tensor to the Ricci tensor in three dimensions

$$\begin{aligned} \mathrm{R}_{\sigma\rho\mu\nu} &= \mathrm{R}_{[\mu\nu][\sigma\rho]} \\ \mathrm{R}_{[\sigma\rho\mu]\nu} &= 0 \end{aligned} \tag{2.24}$$

and

$$R_{\sigma\rho\mu\nu} = 2\gamma_{\sigma[\mu}R_{\nu]\rho} + 2\gamma_{\rho[\nu}R_{\mu]\sigma} + \gamma_{\sigma[\nu}\gamma_{\mu]\rho}R \tag{2.25}$$

the Gauss-Codazzi equations relate 14 of the 20 components of the space-time Riemannian curvature tensor to the initial data on each hypersurface Σ_{τ}. These equations are consistent for any three dimensional geometry embedded in a four dimensional geometry.

Requiring that the space-time geometry $(\mathrm{M}, g_{\alpha\beta})$ satisfy Einstein's field equations (2.1) will impose several constraints on the initial data for the Cauchy surface. Einstein's equations involve the Ricci tensor $\mathrm{R}_{\mu\nu}$, and Ricci scalar R of the space-time geometry. The Gauss-Codazzi equations relate the Riemannian tensor of the space-time geometry to the initial data of the hypersurface. In order to impose Einstein's equations, the Gauss-Codazzi equations must be

contracted into a form involving the Ricci tensor and Ricci scalar. Contracting the indices α and λ in equation (2.23a) and using equation (2.14) gives

$$\gamma^{\sigma}{}_{\beta}\gamma^{\nu}{}_{\delta}\mathrm{R}_{\sigma\nu} + n^{\rho}n^{\mu}\mathrm{R}_{\rho\beta\mu\delta} - n^{\rho}n^{\sigma}n^{\mu}w_{\beta}\mathrm{R}_{\rho\sigma\mu\delta} + n^{\rho}n^{\sigma}n^{\mu}n^{\nu}w_{\beta}w_{\delta}\mathrm{R}_{\rho\sigma\mu\nu}$$
$$= R_{\beta\delta} + K^{\lambda}{}_{\lambda}K_{\beta\delta} - K^{\lambda}{}_{\delta}K_{\beta\lambda} \ .$$

Using the symmetries of the Riemannian tensor this reduces to

$$\gamma^{\sigma}{}_{\beta}\gamma^{\nu}{}_{\delta}\mathrm{R}_{\sigma\nu} + n^{\rho}n^{\mu}\mathrm{R}_{\rho\beta\mu\delta} = R_{\beta\delta} + K^{\lambda}{}_{\lambda}K_{\beta\delta} - K^{\lambda}{}_{\delta}K_{\beta\lambda} \ . \tag{2.26}$$

Contracting this equation over the indices β and δ gives

$$\mathrm{R} + 2n^{\rho}n^{\mu}\mathrm{R}_{\rho\mu} = R + K^{\lambda}{}_{\lambda}K^{\delta}{}_{\delta} - K^{\lambda\delta}K_{\lambda\delta} \ . \tag{2.27}$$

This expression relating the Ricci scalar and Ricci tensor of the space-time geometry to the Ricci scalar and extrinsic curvature of the hypersurface. Similarly, by contracting the indices α and δ in equation (2.23b) and using equation (2.14) gives

$$\gamma^{\sigma}{}_{\beta}\mathrm{R}_{\sigma\nu}n^{\nu} + \gamma^{\sigma}{}_{\beta}n^{\rho}n^{\mu}n^{\nu}\mathrm{R}_{\rho\sigma\mu\nu} = \mathrm{D}_{\alpha}K^{\alpha}{}_{\beta} - \mathrm{D}_{\beta}K^{\alpha}{}_{\alpha} \ .$$

Again using the symmetries of the Riemannian tensor this reduces to

$$\gamma^{\sigma}{}_{\beta}\mathrm{R}_{\sigma\nu}n^{\nu} = \mathrm{D}_{\alpha}K^{\alpha}{}_{\beta} - \mathrm{D}_{\beta}K^{\alpha}{}_{\alpha} \tag{2.28}$$

which relates the Ricci tensor of the space-time geometry to the covariant derivative of the extrinsic curvature in the hypersurface.

Before invoking Einstein's field equations on equations (2.27), and (2.28), consider the trace of equation (2.1)

$$\mathrm{G}^{\alpha}{}_{\alpha} \equiv \mathrm{R}^{\alpha}{}_{\alpha} - \frac{1}{2}g^{\alpha}{}_{\alpha}\mathrm{R} = 8\pi\mathrm{T}^{\alpha}{}_{\alpha}$$

which reduces to

$$\mathrm{R} = -8\pi\mathrm{T}^{\alpha}{}_{\alpha} \ . \tag{2.29}$$

This can now be substituted back into equation (2.1) giving

$$R_{\alpha\beta} = 8\pi(T_{\alpha\beta} - \frac{1}{2}g_{\alpha\beta}T^{\alpha}{}_{\alpha}) \tag{2.30}$$

which is an equivalent expression to Einstein's field equations. Substituting equations (2.29), and (2.30) into equation (2.27) gives

$$16\pi\rho = 16\pi n^{\sigma}n^{\mu}T_{\sigma\mu} = R + K^{\lambda}{}_{\lambda}K^{\delta}{}_{\delta} - K^{\lambda\delta}K_{\lambda\delta} \tag{2.31}$$

where $\rho \equiv n^{\sigma}n^{\mu}T_{\sigma\mu}$ is the energy density measured by an observer that is moving with the hypersurface Σ_{τ}. Making these same substitutions in equation (2.28) gives

$$8\pi j_{\beta} = 8\pi\gamma^{\sigma}{}_{\beta}T_{\sigma\nu}n^{\nu} = D_{\alpha}K^{\alpha}{}_{\beta} - D_{\beta}K^{\alpha}{}_{\alpha} \tag{2.32}$$

where $j_{\beta} \equiv \gamma^{\sigma}{}_{\beta}T_{\sigma\nu}n^{\nu}$ is the momentum density vector measured by the same observer moving with the hypersurface Σ_{τ}. Equations (2.31), and (2.32) are constraints on the initial data of the Cauchy surface imposed by Einstein's field equations. Equation (2.31) is known as the Hamiltonian constraint equation, and equation (2.32) is known as the momentum constraint equation.

Having satisfied these equations, the initial data of the hypersurface can be evolved forward in time along the congruence of curves parametrized by τ, having $\mathbf{t} = (\alpha n^{\sigma} + \beta^{\sigma})\hat{\mathbf{e}}_{\sigma}$ as tangents. In order to evolve the initial data, consider the Lie derivative of the extrinsic curvature $\mathcal{L}_{\mathrm{n}}K_{\sigma\rho}$. This will provide the remaining 6 components of the space-time Riemannian curvature tensor. The 6 components of the space-time curvature tensor involving second order derivatives in a time-like direction are given by

$$\begin{aligned}\mathcal{L}_{\mathrm{n}}K_{\sigma\rho} &= \mathcal{L}_{\mathrm{n}}\left(\gamma^{\mu}{}_{\sigma}\gamma^{\nu}{}_{\rho}\nabla_{(\mu}w_{\nu)}\right) = \mathcal{L}_{\mathrm{n}}\left(\gamma^{\mu}{}_{\sigma}\gamma^{\nu}{}_{\rho}\nabla_{\mu}w_{\nu}\right) \\ &= \gamma^{\mu}{}_{\sigma}\gamma^{\nu}{}_{\rho}n^{\delta}n^{\lambda}R_{\delta\mu\lambda\nu} - K_{\sigma\delta}K^{\delta}{}_{\rho} - \frac{1}{\alpha}D_{\sigma}D_{\rho}\alpha\ .\end{aligned} \tag{2.33}$$

In order to impose Einstein's field equations, the space-time Riemannian tensor is replaced by expressions involving the space-time Ricci tensor and the initial data on the hypersurface by substituting equation (2.26) into equation (2.33) giving

$$\mathcal{L}_{\mathrm{n}} K_{\sigma\rho} = -\gamma^{\delta}{}_{\sigma}\gamma^{\lambda}{}_{\rho}\mathrm{R}_{\delta\lambda} + R_{\sigma\rho} + K^{\lambda}{}_{\lambda}K_{\sigma\rho} - 2K_{\sigma\lambda}K^{\lambda}{}_{\rho} - \frac{1}{\alpha}\mathrm{D}_{\sigma}\mathrm{D}_{\rho}\alpha \ . \tag{2.34}$$

Next the Einstein's field equations are imposed through the substitution of equation (2.30) into equation (2.34) giving

$$\begin{aligned}\mathcal{L}_{\mathrm{n}} K_{\sigma\rho} = &-8\pi\gamma^{\delta}{}_{\sigma}\gamma^{\lambda}{}_{\rho}\mathrm{T}_{\delta\lambda} + 4\pi\gamma_{\sigma\rho}\mathrm{T}^{\lambda}{}_{\lambda} \\ &+ R_{\sigma\rho} + K^{\lambda}{}_{\lambda}K_{\sigma\rho} - 2K_{\sigma\lambda}K^{\lambda}{}_{\rho} - \frac{1}{\alpha}\mathrm{D}_{\sigma}\mathrm{D}_{\rho}\alpha \ .\end{aligned} \tag{2.35}$$

This can now be put into a form representing the Lie derivative of the extrinsic curvature in the direction of the tangents to the congruence of curves parametrized by τ using the linearity of the Lie derivative

$$\mathcal{L}_{\mathrm{t}} K_{\sigma\rho} = \alpha\mathcal{L}_{\mathrm{n}} K_{\sigma\rho} + \mathcal{L}_{\beta} K_{\sigma\rho} \ . \tag{2.36}$$

Applying equation (2.36) to equation (2.35) and defining the projection of the spatial stress tensor $S_{\sigma\rho} \equiv \gamma^{\delta}{}_{\sigma}\gamma^{\lambda}{}_{\rho}\mathrm{T}_{\delta\lambda}$ gives

$$\begin{aligned}\mathcal{L}_{\mathrm{t}} K_{\sigma\rho} = &-8\pi\alpha S_{\sigma\rho} + 4\pi\alpha\gamma_{\sigma\rho}\mathrm{T}^{\lambda}{}_{\lambda} \\ &+ \alpha R_{\sigma\rho} + \alpha K^{\lambda}{}_{\lambda}K_{\sigma\rho} - 2\alpha K_{\sigma\lambda}K^{\lambda}{}_{\rho} - \mathrm{D}_{\sigma}\mathrm{D}_{\rho}\alpha + \mathcal{L}_{\beta} K_{\sigma\rho}\end{aligned} \tag{2.37}$$

which is the evolution equation for the initial data of the Cauchy surface Σ_{τ}.

Conservation of energy and momentum, $\nabla_{\alpha}\mathrm{T}^{\alpha\beta} = 0$, for a space-time manifold $(\mathrm{M}, g_{\alpha\beta})$ is a consequence of the contracted Bianchi identity

$$\nabla_{\mu}\mathrm{G}^{\mu\nu} = 0 \ . \tag{2.38}$$

This is shown by taking the divergence of Einstein's field equations

$$\nabla_{\mu}\mathrm{G}^{\mu\nu} \equiv \nabla_{\mu}\mathrm{R}^{\mu\nu} - \frac{1}{2}g^{\mu\nu}\nabla_{\mu}\mathrm{R} = 8\pi\nabla_{\mu}\mathrm{T}^{\mu\nu} \ . \tag{2.39}$$

Observers moving with the hypersurface measure the stress energy tensor using the previously defined quantities ρ, j^μ, and $S^{\mu\nu}$ to be

$$\mathrm{T}^{\mu\nu} = \rho n^\mu n^\nu + 2j^{(\mu} n^{\nu)} + S^{\mu\nu} \ . \tag{2.40}$$

Projecting the contracted Bianchi identities onto the normal $\mathbf{n}$ to the hypersurface and imposing Einstein's equations in terms of equation (2.40) gives the continuity equation

$$\mathcal{L}_\mathrm{t}\rho = \alpha S^{\mu\nu} K_{\mu\nu} + \alpha\rho K^{\mu}{}_{\mu} - \alpha \mathrm{D}_\mu j^\mu - 2j^\mu \mathrm{D}_\mu \alpha + \mathcal{L}_\beta \rho \ . \tag{2.41}$$

Similarly, by projecting the contracted Bianchi identities onto the hypersurface and imposing Einstein's equations in terms of equation (2.40) gives the Euler equation

$$\mathcal{L}_\mathrm{t} j^\mu = 2\alpha K^{\mu\nu} j_\nu + \alpha j^\mu K^{\nu}{}_{\nu} - \alpha \mathrm{D}_\nu S^{\mu\nu} + S^{\mu\nu}\mathrm{D}_\nu \alpha + \rho\gamma^{\mu\nu}\mathrm{D}_\nu\alpha + \mathcal{L}_\beta j^\mu \ . \tag{2.42}$$

An important consequence of the contracted Bianchi identities (2.38) is that initial data which satisfies the constraint equations (2.31), and (2.32), will continue to satisfy these constraint equations as it is evolved along the congruence of curves parametrized by τ from one slice to the next by the evolution equation (2.37).

2.2 Steady State Equations

When specializing classical general relativity to the study of black holes, the stress energy tensor, $\mathrm{T}_{\alpha\beta}$, is set equal to the classical vacuum value of zero. The gravitational field itself becomes the source of curvature through the nonlinearity of Einstein's field equations (2.1). Equation (2.29) for zero

stress energy restricts the Ricci scalar of the space-time geometry to zero. Substituting these vacuum values into Einstein's field equations gives

$$G_{\mu\nu}^{(vacuum)} = R_{\mu\nu} = 0 \ . \tag{2.43}$$

The Ricci tensor for the vacuum space-time geometry must be zero. The initial value formalism applied to vacuum space-times will also have zero stress energy. The related quantities of energy density, momentum density vector, and spatial stress tensor measured by an observer comoving with the hypersurface are also zero

$$\begin{aligned} \rho &= 0 \\ j^{\mu} &= 0 \\ S^{\mu\nu} &= 0 \ . \end{aligned} \tag{2.44}$$

Applying these vacuum restrictions to the constraint equations (2.31), and (2.32) of the initial value formalism gives the Hamiltonian constraint for the vacuum

$$R + K^{\lambda}_{\ \lambda} K^{\delta}_{\ \delta} - K^{\lambda\delta} K_{\lambda\delta} = 0 \ , \tag{2.45}$$

and the momentum constraints for vacuum

$$D_{\alpha} K^{\alpha}_{\ \beta} - D_{\beta} K^{\alpha}_{\ \alpha} = 0 \ . \tag{2.46}$$

Finally, applying the vacuum restrictions to the evolution equation (2.37) gives

$$\mathcal{L}_{t} K_{\sigma\rho} = \alpha R_{\sigma\rho} + \alpha K^{\lambda}_{\ \lambda} K_{\sigma\rho} - 2\alpha K_{\sigma\lambda} K^{\lambda}_{\ \rho} - D_{\sigma} D_{\rho} \alpha + \mathcal{L}_{\beta} K_{\sigma\rho} \ . \tag{2.47}$$

The continuity equation (2.41), and the Euler equation (2.42) are trivially satisfied in a vacuum space-time geometry.

The initial value formalism for vacuum simplifies further when the tangent vector t^{σ} is a Killing vector field. A vector field ξ^{σ} on any space-time manifold $(M, g_{\alpha\beta})$ satisfying

$$\mathcal{L}_{\xi} g_{\mu\nu} = \nabla_{\mu} \xi_{\nu} + \nabla_{\nu} \xi_{\mu} = 0 \tag{2.48}$$

is known as a Killing vector field. Such a vector field results from the presence of a symmetry on the space-time manifold. This symmetry gives rise to the conserved quantity $\xi_\sigma u^\sigma$ along geodesics having u^σ for a tangent, as is shown by evaluation of the expression

$$\begin{aligned} u^\mu \nabla_\mu (\xi_\nu u^\nu) &= u^\mu u^\nu \nabla_\mu \xi_\nu + \xi_\nu u^\mu \nabla_\mu u^\nu \\ &= 0 \end{aligned} \tag{2.49}$$

which is useful for integrating the geodesic equation $u^\mu \nabla_\nu u^\mu = 0$, when symmetries are present.

As discussed in the introduction, the spiralling binary black hole problem possesses no symmetries. This is a consequence of the gravitation radiation the system emits associated with the acceleration each black hole experiences. Energy and angular momentum are carried off to null infinity by the gravitational radiation causing the binary system of black holes to spiral in on itself. However, when the holes are reasonably far apart and orbiting in near circular orbits, the secular time scale for decay of the orbit will be large when compared with the dynamical time scale of the orbital motion. Then as an approximation, the circular orbits will be stable. An observer corotating with the black holes will see a space-time geometry which is constant in time. This approximation will then possess a time symmetry in the corotating observers frame. The corotating observer's Killing vector field is then

$$\mathbf{t}' = \frac{\partial}{\partial t'} \tag{2.50}$$

where the prime denotes a quantity observed in the corotating frame. In the inertial frame of reference, the black holes rotate at the angular frequency Ω as viewed from spatial infinity. The shift vector connecting the coordinates of the

inertial frame to the coordinates of the corotating frame in the asymptotically flat region is given by

$$\beta^\sigma \frac{\partial}{\partial x^\sigma} = \Omega \frac{\partial}{\partial \phi} \ . \tag{2.51}$$

The natural choice of orthogonal vector field connecting the hypersurfaces in the asymptotically flat regions of space-time for the inertial frame is

$$\mathbf{N} = \alpha n^\sigma \hat{\mathbf{e}}_\sigma = \frac{\partial}{\partial t} \ . \tag{2.52}$$

The Killing vector field for the asymptotically flat region of the space-time geometry in the inertial frame of reference is given by equation (2.12). Substituting the asymptotically flat results of equations (2.51), and (2.52) gives

$$\mathbf{t} = t^\sigma \frac{\partial}{\partial x^\sigma} = \frac{\partial}{\partial t} + \Omega \frac{\partial}{\partial \phi} \tag{2.53}$$

as a coordinate transformation of equation (2.50) also reveals. The Killing vector field for all other regions requires that the space-time geometry be known. Equation (2.53) is an asymptotic boundary condition on the Killing vector field in the inertial frame of reference.

Having chosen the appropriate lapse function α, and shift vector β^σ to make the tangent $\mathbf{t} = (\alpha n^\sigma + \beta^\sigma)\hat{\mathbf{e}}_\sigma$ a Killing vector field, then $\mathcal{L}_\mathrm{t}$, the Lie derivatives in the direction of $\mathbf{t}$, of various geometric quantities of the space-time manifold $(\mathrm{M}, \mathrm{g}_{\alpha\beta})$ will be zero. In particular

$$\mathcal{L}_\mathrm{t} \gamma_{\mu\nu} = 0 \tag{2.54}$$

and

$$\mathcal{L}_\mathrm{t} K_{\mu\nu} = 0 \tag{2.55}$$

will be satisfied. In addition equations (2.22) and (2.54) allow the extrinsic curvature to be written as

$$\alpha K_{\sigma\rho} = \mathrm{D}_{(\sigma} \beta_{\rho)} \ . \tag{2.56}$$

The vacuum constraint equations, (2.45) and (2.46) are unchanged by this symmetry. However, the vacuum evolution equation reduces to

$$\alpha R_{\sigma\rho} + \alpha K^{\lambda}{}_{\lambda} K_{\sigma\rho} - 2\alpha K_{\sigma\lambda} K^{\lambda}{}_{\rho} - \mathrm{D}_{\sigma}\mathrm{D}_{\rho}\alpha + \mathcal{L}_{\beta} K_{\sigma\rho} = 0 \ . \tag{2.57}$$

The last term in equation (2.57) is equivalent to

$$\mathcal{L}_{\beta} K_{\sigma\rho} = \beta^{\mu}\mathrm{D}_{\mu} K_{\sigma\rho} + 2K_{\mu(\sigma}\mathrm{D}_{\rho)}\beta^{\mu} \ . \tag{2.58}$$

Substituting into equation (2.57) gives

$$\alpha R_{\sigma\rho} + \alpha K^{\lambda}{}_{\lambda} K_{\sigma\rho} - 2\alpha K_{\sigma\lambda} K^{\lambda}{}_{\rho} - \mathrm{D}_{\sigma}\mathrm{D}_{\rho}\alpha + \beta^{\mu}\mathrm{D}_{\mu} K_{\sigma\rho} + 2K_{\mu(\sigma}\mathrm{D}_{\rho)}\beta^{\mu} = 0 \ . \tag{2.59}$$

Under the symmetry of this Killing vector field, the initial value formalism simplifies to a set of equations referred to as the steady state equations[36]

$$\alpha K_{\sigma\rho} = \mathrm{D}_{(\sigma}\beta_{\rho)} \tag{2.60a}$$

$$R + K^{\lambda}{}_{\lambda} K^{\delta}{}_{\delta} - K^{\lambda\delta} K_{\lambda\delta} = 0 \tag{2.60b}$$

$$\mathrm{D}_{\alpha} K^{\alpha}{}_{\beta} - \mathrm{D}_{\beta} K^{\alpha}{}_{\alpha} = 0 \tag{2.60c}$$

$$\mathrm{D}_{\sigma}\mathrm{D}_{\rho}\alpha - \beta^{\mu}\mathrm{D}_{\mu} K_{\sigma\rho} - 2K_{\mu(\sigma}\mathrm{D}_{\rho)}\beta^{\mu} - \alpha R_{\sigma\rho} - \alpha K^{\lambda}{}_{\lambda} K_{\sigma\rho} + 2\alpha K_{\sigma\lambda} K^{\lambda}{}_{\rho} = 0 \tag{2.60d}$$

which are collected here in summary. Equations (2.60a) through (2.60d) are the fundamental vacuum initial value formulae for the approximate symmetry associated with the Killing vector field $\mathbf{t}$ used in the analysis of spiralling binary black holes discussed in this dissertation.

2.3 Boundary Conditions

The boundary conditions for the space-time geometry select the particular solution to equation (2.43). In the spiralling binary black holes approximation, these boundary conditions are specified on the Cauchy surface. This is

due to the simplification introduced by the steady state symmetry. The spatial geometry of the Cauchy surface chosen for the binary black holes consists of three separate asymptotically flat regions each possessing its own spatial infinity as shown in Figure 2. The top sheet of the Cauchy surface contains two black holes connected to the two lower isolated sheets by bridges similar to the Einstein-Rosen bridge of the Schwarzschild black hole.[37] This differs from the inversion symmetric spatial geometry used in earlier studies which consisted of just two asymptotically flat regions.[38] Unlike the inversion symmetric geometry which requires that boundary conditions be placed at the two throats of the black holes as well as at the two spatial infinities, the Cauchy surface having three asymptotically flat regions has the advantage of requiring boundary conditions only at the three spatial infinities.

The conditions on initial data for the Cauchy surface which guarantee asymptotic flatness were found by Ashtekar and Hansen.[39] In a coordinate component manner when asymptotic Euclidean coordinates are used, these conditions on the initial data require that the spatial metric of the hypersurface approach the flat Euclidean spatial metric in the following limit

$$\lim_{r\to\infty} \gamma_{\mu\nu} = f_{\mu\nu} + O(\frac{1}{r}) \tag{2.61}$$

where $f_{\mu\nu}$ is the flat spatial metric of Euclidean geometry and r is the radial component of flat spherical coordinates. The components of the extrinsic curvature in these coordinates must approach zero at least as fast as

$$\lim_{r\to\infty} K_{\mu\nu} = O(\frac{1}{r^2}) \tag{2.62}$$

and the Ricci curvature tensor of the spatial hypersurface must approach zero

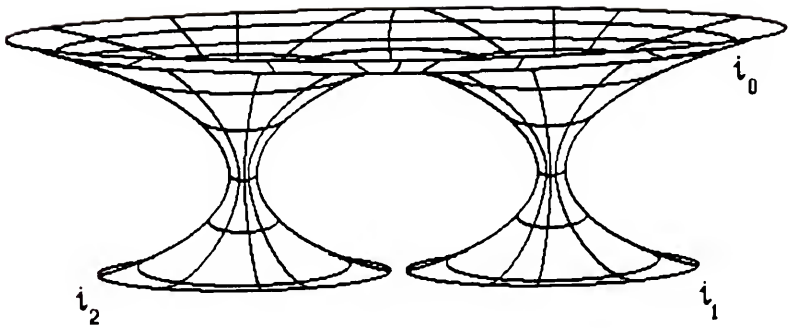

FIGURE 2: Hypersurface Topology for Binary System of Black Holes. A space-like slice with three asymptotically flat regions, one on each sheet, connected by two wormholes.

at the rate

$$\lim_{r\to\infty} R_{\mu\nu} = O(\frac{1}{r^3}) \tag{2.63}$$

or faster in this Euclidean coordinate system.[27]

For a space-time manifold which is asymptotically flat the mass and angular momentum of the geometry is found using two dimensional spherical surface integrals near space-like infinity.[40] The mass is given by the integral

$$16\pi M_i = \lim_{r\to\infty_i} \oint \nabla_\nu (h^{\mu\nu} - f^{\mu\nu} h^\sigma{}_\sigma) \mathrm{d}\Sigma_\mu \tag{2.64}$$

where $h_{\mu\nu} = \gamma_{\mu\nu} - f_{\mu\nu}$, and ∇_ν is the flat derivative operator. The linear momentum is given by the surface integral

$$8\pi P_i^\mu = \lim_{r\to\infty_i} \oint (K^{\mu\nu} - \gamma^{\mu\nu} K^\sigma{}_\sigma) \mathrm{d}\Sigma_\nu \tag{2.65}$$

and the angular momentum is given by the surface integral

$$8\pi J_i^\mu = \lim_{r\to\infty_i} \oint \epsilon^{\mu\nu\delta} \xi_\delta (K^\rho{}_\nu - \gamma^\rho{}_\nu K^\sigma{}_\sigma) \mathrm{d}\Sigma_\rho \tag{2.66}$$

where ξ^ρ is the axial Killing vector field at each spatial infinity and $\epsilon^{\mu\nu\delta}$ is the total anti-symmetric tensor. The subscript i is used to distinguish each of the three asymptotically flat regions which the radial coordinate r is approaching in the above limits.

Finally, the Killing vector field generated by imposing the time symmetry on the space-time geometry is inconsistent with the exact geometry as a result of the gravitational radiation, as already pointed out. In the frame of the corotating observers, the gravitational radiation must have standing waveforms at large radial distances from the binary black holes. In a Euclidean background geometry gravitational radiation falls off as $1/r$ and has an energy density which falls off as $1/r^2$. Thus the contribution to the total energy from

large radial distances is divergent. However, if the amplitude is sufficiently small, then a large radial value r_{max} can be found such that the contribution to the total energy from the gravitational radiation is much less than the mass of the black holes and r_{max} is sufficiently distant to make the assumptions of asymptotic flatness valid in the Euclidean sense. This does mean that the initial data is being satisfied on a partial Cauchy surface which will have a finite future Cauchy development consistent with causality and the Killing vector field. Outside this future Cauchy development the geometry is unspecified and not determined by the initial data. Only under these conditions will the time symmetric approximation to the spiralling binary black holes be sufficiently adequate.

CHAPTER 3
VARIATIONAL PRINCIPLE FOR TOTAL MASS

Determination of the variational principle for the mass begins with the Hamiltonian density of general relativity[27]

$$\mathcal{H}_G = \pi^{\mu\nu}\dot{\gamma}_{\mu\nu} - \mathcal{L}_G \tag{3.1}$$

where the dot over the spatial metric denotes Lie derivative in the time direction

$$\dot{\gamma}_{\mu\nu} \equiv \mathcal{L}_t\gamma_{\mu\nu} = -2\alpha K_{\mu\nu} + \mathrm{D}_\mu\beta_\nu + \mathrm{D}_\nu\beta_\mu \ . \tag{3.2}$$

The conjugate momentum tensor density is related to the extrinsic curvature by

$$\pi^{\mu\nu} = \frac{\partial\mathcal{L}_G}{\partial\dot{\gamma}_{\mu\nu}} = -\sqrt{\gamma}\,(K^{\mu\nu} - \gamma^{\mu\nu}K^{\sigma}{}_{\sigma}) \tag{3.3}$$

and the Lagrangian density $\mathcal{L}_G$ of general relativity is given by

$$\mathcal{L}_G = \sqrt{-g}\,\mathrm{R} \ . \tag{3.4}$$

The Lagrangian density can be rewritten in terms of the initial value formalism and the initial data of the hypersurface by using the following relationships:

$$\sqrt{-g} = \alpha\sqrt{\gamma} \tag{3.5}$$

$$\mathrm{R} = 2(\mathrm{G}_{\mu\nu} - \mathrm{R}_{\mu\nu})n^\mu n^\nu \ . \tag{3.6}$$

Using the vacuum Hamiltonian constraint equation (2.45), the first term in (3.6) becomes

$$2\mathrm{G}_{\mu\nu}n^\mu n^\nu = R - K_{\mu\nu}K^{\mu\nu} + K^{\mu}{}_{\mu}K^{\nu}{}_{\nu} \ . \tag{3.7}$$

From the definition of the Riemann Tensor the second term in equation (3.6) can be evaluated,

$$\begin{aligned} \mathrm{R}_{\mu\nu}n^{\mu}n^{\nu} &= \mathrm{R}_{\mu\sigma\nu}{}^{\sigma}n^{\mu}n^{\nu} \\ &= n^{\mu}(\nabla_{\sigma}\nabla_{\mu} - \nabla_{\mu}\nabla_{\sigma})n^{\sigma} \\ &= K^{\mu}{}_{\mu}K^{\sigma}{}_{\sigma} - K_{\mu\sigma}K^{\mu\sigma} - \nabla_{\mu}(n^{\mu}\nabla_{\sigma}n^{\sigma}) + \nabla_{\sigma}(n^{\mu}\nabla_{\mu}n^{\sigma}) \; . \end{aligned} \tag{3.8}$$

The last two terms in equation (3.8) are total divergences and will be dropped temporarily since they result in surface terms which will be described later. Combining equations (3.5), (3.6), (3.7), and (3.8) in equation (3.4) gives the Lagrangian density in terms of the initial value data

$$\mathcal{L}_G = \alpha\sqrt{\gamma}\,(R + K_{\mu\nu}K^{\mu\nu} - K^{\mu}{}_{\mu}K^{\nu}{}_{\nu}) + \textit{neglected divergences} \; . \tag{3.9}$$

Finally substituting this expression for the Lagrangian density (3.9) into the Hamiltonian density (3.1) along with equations (3.2) and (3.3) gives

$$\begin{aligned} \mathcal{H}_G = -\sqrt{\gamma}\,[\alpha(R - K_{\mu\nu}K^{\mu\nu} + K^{\mu}{}_{\mu}K^{\nu}{}_{\nu}) - 2\beta_{\mu}\mathrm{D}_{\nu}(K^{\mu\nu} - \gamma^{\mu\nu}K^{\sigma}{}_{\sigma})] \\ - \textit{neglected divergences} \end{aligned} \tag{3.10}$$

where all divergent terms have been suppressed until later discussion.

The Hamiltonian is given by the integration of the Hamiltonian density (3.10) over the three dimensional space-like hypersurface Σ_{τ}

$$\mathrm{H}_G = \int_{\Sigma_{\tau}} \mathcal{H}_G \; . \tag{3.11}$$

This Hamiltonian, using the Hamiltonian density of equation (3.10), is known to be correct for a closed universe having the closed hypersurface Σ_{τ}.[26] However, when the space-time geometry is asymptotically flat the variation $\delta\mathrm{H}_E$ of this Hamiltonian does not lead to Einstein's field equations. In order to correct this shortcoming the Hamiltonian in equation (3.10) must be supplemented by the addition of surface integrals which result from the careful treatment of the

previously neglected divergences. In a geometry with asymptotic flatness this leads to [41]

$$\mathrm{H}_E = \mathrm{H}_G + E \tag{3.12}$$

where E is given by

$$E = \lim_{r\to\infty_o} \oint \alpha \nabla_\nu (h^{\mu\nu} - f^{\mu\nu} h^\sigma{}_\sigma) \mathrm{d}\Sigma_\mu \ . \tag{3.13}$$

Variations $\delta \mathrm{H}_E$ which preserve asymptotic flatness do lead to Einstein's field equations, and the value of H_E for solutions to Einstein's field equations is E. From equation (2.64) this value is shown to be

$$\{\mathrm{H}_E\}_{(\delta \mathrm{H}_E = 0)} = \{E\}_{(\delta \mathrm{H}_E = 0)} = 16\pi \mathrm{M}_o \ . \tag{3.14}$$

Solving equation (3.14) for M_o gives the mass of the system

$$\mathrm{M}_o = \frac{1}{16\pi} \{\mathrm{H}_E\}_{(\delta \mathrm{H}_E = 0)} = \frac{1}{16\pi} \{\mathrm{H}_G + E\}_{(\delta \mathrm{H}_E = 0)} \ . \tag{3.15}$$

Substituting the integrals (3.13) and (3.11) into equation (3.15) produces the equation to be evaluated in a variational method for the mass

$$\begin{aligned} \mathrm{M}_o = {} & \frac{1}{16\pi} \lim_{r\to\infty_o} \oint \alpha \nabla_\nu (h^{\mu\nu} - f^{\mu\nu} h^\sigma{}_\sigma) \mathrm{d}\Sigma_\mu \\ & - \frac{1}{16\pi} \int_{\Sigma_\tau} \sqrt{\gamma} \left[\alpha (R - K_{\mu\nu} K^{\mu\nu} + K^\mu{}_\mu K^\nu{}_\nu) - 2\beta_\mu \mathrm{D}_\nu (K^{\mu\nu} - \gamma^{\mu\nu} K^\sigma{}_\sigma) \right] \mathrm{d}V \end{aligned} \tag{3.16}$$

where ∇_ν is again the flat derivative operator and the surface integral is evaluated at the shared infinity of the hypersurface.

As demonstrated by equation (3.15), $\delta \mathrm{H}_E = 0$ must be satisfied in order for M_o to be the mass of the system in equation (3.16). To study the variation of H_E consider a test geometry for the binary black holes system possessing the time symmetry in a corotating frame as described by the steady state approximation and characterized by the initial value data, α, β^μ, $K^{\mu\nu}$, and

$\gamma_{\mu\nu}$ with their respective infinitesimal variations $\delta\alpha$, $\delta\beta^{\mu}$, $\delta K^{\mu\nu}$, and $\delta\gamma_{\mu\nu}$. The quantity $\delta \mathrm{H}_E$ is given by[30]

$$\delta \mathrm{H}_E = 16\pi\delta \mathrm{M}_{\circ}$$

$$= \int \{\delta\alpha[\![b]\!] + \delta\beta^{\mu}[\![c]\!]_{\mu} + \delta K^{\mu\nu}[\![a]\!]_{\mu\nu} + \delta\gamma_{\mu\nu}[\![a,b,c,d]\!]^{\mu\nu}\}\mathrm{dV} \qquad (3.17)$$

$$+ \Omega_{\circ}\delta J_{\circ} - \alpha_1\delta M_1 + \Omega_1\delta J_1 - \alpha_2\delta M_2 + \Omega_2\delta J_2 \ .$$

The $[\![\,]\!]$ denotes linear combinations of the equation numbers (2.60a) through (2.60d) enclosed, which will vanish when the steady state equations are satisfied. The δJ_i's represent variations in the angular momentum at each of the three asymptotically flat regions of the hypersurface Σ_{τ}. Similarly, the Ω_i's are the angular frequencies, and the $\delta \mathrm{M}_i$'s are the variations in masses measured at each of the three asymptotically flat regions.

The variational principle for $\mathrm{M}_{\circ}$ can now be described. Given a trial geometry on the hypersurface Σ_{τ} characterized by α, β^{μ}, $K^{\mu\nu}$, and $\gamma_{\mu\nu}$ then any arbitrary infinitesimal variations, $\delta\alpha$, $\delta\beta^{\mu}$, $\delta K^{\mu\nu}$, and $\delta\gamma_{\mu\nu}$ which do not change the total angular momentum at each of the three asymptotically flat regions of Σ_{τ} and also do not change the mass at the two asymptotically flat regions associated with the interiors of the binary black holes, will satisfy the condition $\delta \mathrm{H}_E = 0$ for trial geometries which also satisfy the steady state equations. The total mass $\mathrm{M}_{\circ}$ is an extremum since it satisfies $\delta \mathrm{M}_{\circ} = 0$. This signifies that an accurate determination of the total mass $\mathrm{M}_{\circ}$ can be obtained when only a rough estimate of the geometry is available.

Application of the variational principle follows as such, given the trial geometry for the hypersurface, evaluate equation (3.16) throughout the parameter space of the classes of variations preserving the restrictions described above for the extremum. The mass of the system is given by this extremum value. An error of order $O(\epsilon)$ in the trial geometry will produce an error of order $O(\epsilon^2)$ in the extremum value of the total mass $\mathrm{M}_{\circ}$ for the geometry.

CHAPTER 4
TRIAL GEOMETRIES

The trial geometry to be used in the variational principle for the mass must be a physically reasonable approximation to the binary black hole system. In addition the meaning of asymptotically flat must be made precise in order that the surface integrations appearing in the variation of the Hamiltonian of equation (3.11) vanish. The detailed variation of $\mathcal{H}_G$ is

$$\begin{aligned}\delta\mathcal{H}_G = &\int \{H\delta\alpha + H_\mu\delta\beta^\mu + A^{\mu\nu}\delta\gamma_{\mu\nu} + B_{\mu\nu}\delta\pi^{\mu\nu}\}\mathrm{dV} \\ &- \sum_i \lim_{r_i\to\infty_i} \oint G^{\mu\nu\sigma\rho}\{\alpha(\mathrm{D}_\sigma\delta\gamma_{\mu\nu}) - (\mathrm{D}_\sigma\alpha)\delta\gamma_{\mu\nu}\}\mathrm{d}\Sigma_\rho \\ &- \sum_i \lim_{r_i\to\infty_i} \oint \{2\beta_\sigma\delta\pi^{\sigma\rho} + (2\beta^\sigma\pi^{\nu\rho} - \beta^\rho\pi^{\nu\sigma})\delta\gamma_{\nu\sigma}\}\mathrm{d}\Sigma_\rho\end{aligned} \tag{4.1}$$

where the two surface integrals are evaluated at each of the three asymptotically flat regions of the hypersurface Σ_τ. The terms appearing in the integrand are

$$H = \sqrt{\gamma}(\pi_{\mu\nu}\pi^{\mu\nu} - \frac{1}{2}(\pi^\nu{}_\nu)^2 - R) \tag{4.2}$$

which is proportional to the Hamiltonian constraint,

$$H_\mu = -2\mathrm{D}_\nu\pi_\mu{}^\nu \tag{4.3}$$

which is proportional to the momentum constraint,

$$A^{\mu\nu} = \alpha\sqrt{\gamma}(2\pi^{\mu\nu} - \gamma^{\mu\nu}\pi^\nu{}_\nu) + \gamma^{\rho\nu}\mathrm{D}_\rho\beta^\mu + \gamma^{\rho\mu}\mathrm{D}_\rho\beta^\nu \tag{4.4}$$

which is the functional derivative of the Hamiltonian with respect to the spatial metric tensor $\gamma_{\mu\nu}$,

$$\begin{aligned} B_{\mu\nu} = & -\alpha\sqrt{\gamma}(R_{\mu\nu} - \frac{1}{2}\gamma_{\mu\nu}R) + \frac{1}{2\sqrt{\gamma}}\alpha\gamma_{\mu\nu}(\pi^{\sigma\rho}\pi_{\sigma\rho} - \frac{1}{2}(\pi^{\sigma}{}_{\sigma})^2) \\ & - \frac{2}{\sqrt{\gamma}}\alpha(\pi_{\mu\sigma}\pi^{\sigma}{}_{\nu} - \frac{1}{2}\pi_{\mu\nu}\pi^{\rho}{}_{\rho}) + \sqrt{\gamma}(\mathrm{D}_{\mu}\mathrm{D}_{\nu}\alpha - \gamma_{\mu\nu}\gamma^{\sigma\rho}\mathrm{D}_{\sigma}\mathrm{D}_{\rho}\alpha) \\ & + \mathrm{D}_{\sigma}(\pi_{\mu\nu}\beta^{\sigma}) - (\mathrm{D}_{\sigma}\beta_{\mu})\pi^{\sigma}{}_{\nu} - (\mathrm{D}_{\sigma}\beta_{\nu})\pi^{\sigma}{}_{\mu} \end{aligned} \tag{4.5}$$

which is the functional derivative of the Hamiltonian with respect to the conjugate momentum tensor density $\pi_{\mu\nu}$, and the super-metric

$$G^{\mu\nu\sigma\rho} = \frac{1}{2}\sqrt{\gamma}(\gamma^{\mu\sigma}\gamma^{\nu\rho} + \gamma^{\mu\rho}\gamma^{\nu\sigma} - 2\gamma^{\mu\nu}\gamma^{\sigma\rho}) \, . \tag{4.6}$$

The particular asymptotic behavior for the initial data necessary to apply the Hamiltonian (3.12) and the variational principle for the mass (3.16) are given for the spatial metric by[41]

$$\gamma_{\mu\nu} - f_{\mu\nu} \propto \frac{1}{r} \, , \tag{4.7}$$

and the gradient of the metric by the behavior

$$\gamma_{\mu\nu,\sigma} \propto \frac{1}{r^2} \, . \tag{4.8}$$

The conjugate momentum tensor density has the asymptotic behavior given by

$$\pi_{\mu\nu} = -\sqrt{\gamma}\,(K_{\mu\nu} - \gamma_{\mu\nu}K^{\sigma}{}_{\sigma}) \propto \frac{1}{r^2} \, . \tag{4.9}$$

The lapse function has the asymptotic behavior given by

$$\alpha - 1 \propto \frac{1}{r} \, , \tag{4.10}$$

and the gradient of the lapse function has the asymptotic behavior

$$\alpha_{,\sigma} \propto \frac{1}{r^2} \, . \tag{4.11}$$

The shift vector has the asymptotic behavior given by

$$\beta^{\nu} \propto \frac{1}{r} , \tag{4.12}$$

and the gradient of the shift vector has the asymptotic behavior

$$\beta^{\nu}{}_{,\sigma} \propto \frac{1}{r^2} . \tag{4.13}$$

Where the r for each behaves as the Schwarzschild radial coordinate in the asymptotic limit

$$r = \sqrt{x^2 + y^2 + z^2} . \tag{4.14}$$

These are sufficient specifications on the asymptotic behavior of the geometry to use equation (3.16) as a variational principle for the mass.

The trial geometry should also approximate several limiting cases where analytical results can be used as a bases for comparison. These limiting cases consist of the following list of properties:

- At each of the three distinct infinities of the Cauchy surface the spatial geometry must be asymptotically flat as outlined above in order to guarantee well defined masses, linear momenta, and angular momenta.
- When the separation between the two black holes is large, the geometry must approach the superposition of two boosted black holes with arbitrary velocities.
- For very small black hole velocities the Hamiltonian constraint (2.60b) and the momentum constraint (2.60c) must be satisfied by the geometry to order $O(v^2)$ in the velocities.
- In the limit that one of the masses is much less than the other, the test particle limit, the analytic results for geodesics of the Schwarzschild black hole are reproduced.

The first requirement is necessary to establish well defined physical quantities. The second and third requirements are consistent with special relativity and Newtonian gravity. The last requirement allows for comparison to analytic results of general relativity. This list of requirements is not necessarily complete, however it does provide a reasonable basis of test for the trial geometry.

The infinitesimal line element for the four dimensional space-time geometry is given by

$$ds^2 = g_{\mu\nu} dx^\mu dx^\nu \ . \tag{4.15}$$

Once the four dimensional space-time has been foliated into constant τ spacelike hypersurfaces Σ_τ as previously outlined the infinitesimal line element in terms of the lapse function α, the shift vector β^μ, and the three dimensional spatial metric $\gamma_{\mu\nu}$, is given by

$$ds^2 = -\alpha^2 dt^2 + \gamma_{\mu\nu}(dx^\mu + \beta^\mu dt)(dx^\nu + \beta^\nu dt) \ . \tag{4.16}$$

The form of the spatial metric for the trial geometry in a coordinate basis which approaches Cartesian coordinates in the asymptotic limit is given by

$$\gamma_{\mu\nu} dx^\mu dx^\nu = \Psi^4 (dx^2 + dy^2 + dz^2) - \left[\frac{u^2({\alpha_1}^2 - {\psi_1}^2)}{(1-u^2)} + \frac{v^2({\alpha_2}^2 - {\psi_2}^2)}{(1-v^2)} \right] dy^2 \ . \tag{4.17}$$

The functions Ψ, ψ_1, ψ_2, α_1, and α_2 are chosen to make the spatial metric on the hypersurface Σ_τ model the geometry of two black holes in circular orbits, with asymptotic boundary conditions, as close as possible. They are defined in the trial geometry by

$$\Psi = 1 + \frac{m_1}{2\rho_1} + \frac{m_2}{2\rho_2} \tag{4.18}$$

where m_1 and m_2 are the masses of the two black holes as measured on the upper (shared) sheet of the hypersurface Σ_τ, also ρ_1 and ρ_2 are radial measures of

distance from each black hole given by the relationships to the quasi-Cartesian coordinates

$$\rho_1{}^2 = (x - x_{o_1})^2 + \frac{y^2}{1-u^2} + z^2 \tag{4.19}$$

and

$$\rho_2{}^2 = (x - x_{o_2})^2 + \frac{y^2}{1-v^2} + z^2 \tag{4.20}$$

where x_{o_1} and u are the position along the x-direction and 3-velocity of the black hole of mass m_1, and the x_{o_2} and v are the position along the x-direction and 3-velocity of the black hole of mass m_2. The functions ψ_1 and ψ_2 are chosen to be

$$\psi_1 = 1 + \frac{m_1}{2\rho_1} + \frac{m_2 m_1^2}{2s(m_1{}^2 + 4\rho_1{}^4)} \tag{4.21}$$

and

$$\psi_2 = 1 + \frac{m_2}{2\rho_2} + \frac{m_1 m_2^2}{2s(m_2{}^2 + 4\rho_2{}^4)} \tag{4.22}$$

where s is the separation between the two black holes and is given by

$$s = x_{o_1} - x_{o_2} \ . \tag{4.23}$$

The functions α_1 and α_2 are chosen to be

$$\alpha_1 = \frac{\left(1 - \frac{m_1}{2\rho_1(1+\frac{m_2}{2\rho_2})}\right)}{\left(1 + \frac{m_1}{2\rho_1(1+\frac{m_2}{2\rho_2})}\right)} \left(1 + \frac{m_2 m_1^2}{2s(m_1{}^2 + 4\rho_1{}^4)}\right)^2 \tag{4.24}$$

and

$$\alpha_2 = \frac{\left(1 - \frac{m_2}{2\rho_2(1+\frac{m_1}{2\rho_1})}\right)}{\left(1 + \frac{m_2}{2\rho_2(1+\frac{m_1}{2\rho_1})}\right)} \left(1 + \frac{m_1 m_2^2}{2s(m_2{}^2 + 4\rho_2{}^4)}\right)^2 . \tag{4.25}$$

In addition the shift vector β and the lapse function α are needed in order to specify the four dimensional space-time metric $g_{\mu\nu}$. The lapse function α

provides a measure for the rate of proper time over the hypersurface Σ_τ and is chosen to be

$$\begin{aligned}\alpha =& \frac{\left(1-\frac{m_1}{2\rho_1(1+\frac{m_2}{2\rho_2})}\right)}{\left(1+\frac{m_1}{2\rho_1(1+\frac{m_2}{2\rho_2})}\right)}\frac{\left(1-\frac{m_2}{2\rho_2(1+\frac{m_1}{2\rho_1})}\right)}{\left(1+\frac{m_2}{2\rho_2(1+\frac{m_1}{2\rho_1})}\right)} \\ &\times\left(\frac{\Psi^2}{\sqrt{\Psi^4-\frac{u^2}{1-u^2}({\alpha_1}^2-{\psi_1}^4)-\frac{v^2}{1-v^2}({\alpha_2}^2-{\psi_2}^4)}}\right) \\ &\times\left\{\left(1+\frac{m_2}{2s}\right)^2\left(1+\frac{m_2}{2s(1+\frac{m_1}{2\rho_1})}\right)^2\left(\frac{{m_1}^2{\rho_2}^2}{{m_1}^2{\rho_2}^2+4{\rho_1}^4}\right)\right. \\ &+\left(1+\frac{m_1}{2s}\right)^2\left(1+\frac{m_1}{2s(1+\frac{m_2}{2\rho_2})}\right)^2\left(\frac{{m_2}^2{\rho_1}^2}{{m_2}^2{\rho_1}^2+4{\rho_2}^4}\right) \\ &\left.+\left(1-\frac{{m_1}^2{\rho_2}^2}{{m_1}^2{\rho_2}^2+4{\rho_1}^4}-\frac{{m_2}^2{\rho_1}^2}{{m_2}^2{\rho_1}^2+4{\rho_2}^4}\right)\right\}.\end{aligned} \tag{4.26}$$

The arbitrary spatial shift vector β is chosen to co-rotate each point on the hypersurface Σ_τ with the orbiting black holes. In this quasi-Cartesian coordinate system the shift vector has components given by

$$\beta^x = -\Big(1+(\frac{u^2}{1-u^2})(\frac{{m_1}^2{\rho_2}^2}{{m_1}^2{\rho_2}^2+4{\rho_1}^4})+(\frac{v^2}{1-v^2})(\frac{{m_2}^2{\rho_1}^2}{{m_2}^2{\rho_1}^2+4{\rho_2}^4})\Big)\Omega y \tag{4.27a}$$

$$\beta^y = \Omega x + \frac{\left((\frac{u^2}{1-u^2})({\alpha_1}^2-{\psi_1}^4)+(\frac{v^2}{1-v^2})({\alpha_2}^2-{\psi_2}^4)\right)}{\left(\Psi^4-\frac{u^2}{1-u^2}({\alpha_1}^2-{\psi_1}^4)-\frac{v^2}{1-v^2}({\alpha_2}^2-{\psi_2}^4)\right)} \tag{4.27b}$$

$$\beta^z = 0\,. \tag{4.27c}$$

The quantity Ω appearing in the components of the shift vector β is the orbital angular frequency of the black holes and is given by

$$\Omega = \frac{u}{x_{o_1}} = \frac{v}{x_{o_2}}\,. \tag{4.28}$$

The Christoffel symbols are needed in order that the covariant derivative and the scalar curvature for the spatial geometry can be calculated. The covariant Christoffel symbols are derived from the spatial metric using

$$\Gamma_{\mu\nu\delta} = \frac{1}{2}\Big(\frac{\partial\gamma_{\mu\nu}}{\partial x^\delta}+\frac{\partial\gamma_{\mu\delta}}{\partial x^\nu}-\frac{\partial\gamma_{\nu\delta}}{\partial x^\mu}\Big)\,. \tag{4.29}$$

By having a diagonal spatial metric, these take on a particularly simple form:

$$\Gamma_{xxx} = \frac{1}{2}\frac{\partial \gamma_{xx}}{\partial x} \tag{4.30}$$

$$\Gamma_{xxy} = \Gamma_{xyx} = \frac{1}{2}\frac{\partial \gamma_{xx}}{\partial y} \tag{4.31}$$

$$\Gamma_{xxz} = \Gamma_{xzx} = \frac{1}{2}\frac{\partial \gamma_{xx}}{\partial z} \tag{4.32}$$

$$\Gamma_{xyy} = -\frac{1}{2}\frac{\partial \gamma_{yy}}{\partial x} \tag{4.33}$$

$$\Gamma_{xyz} = \Gamma_{xzy} = 0 \tag{4.34}$$

$$\Gamma_{xzz} = -\frac{1}{2}\frac{\partial \gamma_{zz}}{\partial x} \tag{4.35}$$

$$\Gamma_{yxx} = -\frac{1}{2}\frac{\partial \gamma_{xx}}{\partial y} \tag{4.36}$$

$$\Gamma_{yxy} = \Gamma_{yyx} = \frac{1}{2}\frac{\partial \gamma_{yy}}{\partial x} \tag{4.37}$$

$$\Gamma_{yxz} = \Gamma_{yzx} = 0 \tag{4.38}$$

$$\Gamma_{yyy} = \frac{1}{2}\frac{\partial \gamma_{yy}}{\partial y} \tag{4.39}$$

$$\Gamma_{yyz} = \Gamma_{yzy} = \frac{1}{2}\frac{\partial \gamma_{yy}}{\partial z} \tag{4.40}$$

$$\Gamma_{yzz} = -\frac{1}{2}\frac{\partial \gamma_{zz}}{\partial y} \tag{4.41}$$

$$\Gamma_{zxx} = -\frac{1}{2}\frac{\partial \gamma_{xx}}{\partial z} \tag{4.42}$$

$$\Gamma_{zxy} = \Gamma_{zyx} = 0 \tag{4.43}$$

$$\Gamma_{zxz} = \Gamma_{zzx} = \frac{1}{2}\frac{\partial \gamma_{zz}}{\partial x} \tag{4.44}$$

$$\Gamma_{zyy} = -\frac{1}{2}\frac{\partial \gamma_{yy}}{\partial z} \tag{4.45}$$

$$\Gamma_{zyz} = \Gamma_{zzy} = \frac{1}{2}\frac{\partial \gamma_{zz}}{\partial y} \tag{4.46}$$

$$\Gamma_{zzz} = \frac{1}{2}\frac{\partial \gamma_{zz}}{\partial z}\,. \tag{4.47}$$

The contravariant Christoffel symbols are given by

$$\Gamma^{\mu}{}_{\nu\delta} = \frac{1}{2}\gamma^{\mu\sigma}\Big(\frac{\partial\gamma_{\sigma\nu}}{\partial x^{\delta}} + \frac{\partial\gamma_{\sigma\delta}}{\partial x^{\nu}} - \frac{\partial\gamma_{\nu\delta}}{\partial x^{\sigma}}\Big) \tag{4.48}$$

which also are rather simple expressions when the spatial metric is diagonal:

$$\Gamma^{x}{}_{xx} = \frac{1}{2\gamma_{xx}}\frac{\partial\gamma_{xx}}{\partial x} \tag{4.49}$$

$$\Gamma^{x}{}_{xy} = \Gamma^{x}{}_{yx} = \frac{1}{2\gamma_{xx}}\frac{\partial\gamma_{xx}}{\partial y} \tag{4.50}$$

$$\Gamma^{x}{}_{xz} = \Gamma^{x}{}_{zx} = \frac{1}{2\gamma_{xx}}\frac{\partial\gamma_{xx}}{\partial z} \tag{4.51}$$

$$\Gamma^{x}{}_{yy} = -\frac{1}{2\gamma_{xx}}\frac{\partial\gamma_{yy}}{\partial x} \tag{4.52}$$

$$\Gamma^{x}{}_{yz} = \Gamma^{x}{}_{zy} = 0 \tag{4.53}$$

$$\Gamma^{x}{}_{zz} = -\frac{1}{2\gamma_{xx}}\frac{\partial\gamma_{zz}}{\partial x} \tag{4.54}$$

$$\Gamma^{y}{}_{xx} = -\frac{1}{2\gamma_{yy}}\frac{\partial\gamma_{xx}}{\partial y} \tag{4.55}$$

$$\Gamma^{y}{}_{xy} = \Gamma^{y}{}_{yx} = \frac{1}{2\gamma_{yy}}\frac{\partial\gamma_{yy}}{\partial x} \tag{4.56}$$

$$\Gamma^{y}{}_{xz} = \Gamma^{y}{}_{zx} = 0 \tag{4.57}$$

$$\Gamma^{y}{}_{yy} = \frac{1}{2\gamma_{yy}}\frac{\partial\gamma_{yy}}{\partial y} \tag{4.58}$$

$$\Gamma^{y}{}_{yz} = \Gamma^{y}{}_{zy} = \frac{1}{2\gamma_{yy}}\frac{\partial\gamma_{yy}}{\partial z} \tag{4.59}$$

$$\Gamma^{y}{}_{zz} = -\frac{1}{2\gamma_{yy}}\frac{\partial\gamma_{zz}}{\partial y} \tag{4.60}$$

$$\Gamma^{z}{}_{xx} = -\frac{1}{2\gamma_{zz}}\frac{\partial\gamma_{xx}}{\partial z} \tag{4.61}$$

$$\Gamma^{z}{}_{xy} = \Gamma^{z}{}_{yx} = 0 \tag{4.62}$$

$$\Gamma^{z}{}_{xz} = \Gamma^{z}{}_{zx} = \frac{1}{2\gamma_{zz}}\frac{\partial\gamma_{zz}}{\partial x} \tag{4.63}$$

$$\Gamma^{z}{}_{yy} = -\frac{1}{2\gamma_{zz}}\frac{\partial\gamma_{yy}}{\partial z} \tag{4.64}$$

$$\Gamma^{z}{}_{yz} = \Gamma^{z}{}_{zy} = \frac{1}{2\gamma_{zz}}\frac{\partial \gamma_{zz}}{\partial y} \tag{4.65}$$

$$\Gamma^{z}{}_{zz} = \frac{1}{2\gamma_{zz}}\frac{\partial \gamma_{zz}}{\partial z} \ . \tag{4.66}$$

The covariant derivative D_μ is defined using these Christoffel symbols. As an example, consider the gradient of a second rank mixed tensor T^{β}_{α}

$$\mathrm{D}_\mu T^{\beta}_{\alpha} = \frac{\partial T^{\beta}_{\alpha}}{\partial x^\mu} + \Gamma^{\beta}{}_{\delta\mu} T^{\delta}{}_{\alpha} + \Gamma^{\delta}{}_{\alpha\mu} T^{\beta}{}_{\delta} \ . \tag{4.67}$$

Other applications of the covariant derivative follow from this example with the exception that the gradient of a scalar function is merely

$$\mathrm{D}_\mu \Phi = \frac{\partial \Phi}{\partial x^\mu} \ . \tag{4.68}$$

All of which is in agreement with the standard definitions of differential geometry.

The scalar curvature R also is derivable from the spatial metric of the hypersurface Σ_τ and will be required for the variational principle. For a diagonal metric of the form

$$\gamma_{\mu\nu} = \begin{pmatrix} \gamma_{xx} & 0 & 0 \\ 0 & \gamma_{yy} & 0 \\ 0 & 0 & \gamma_{zz} \end{pmatrix} \tag{4.69}$$

such as the spatial metric for the hypersurface Σ_τ of equation (4.17), the scalar curvature becomes the relatively modest expression

$$\begin{aligned} R = & -\frac{\frac{\partial^2 \gamma_{xx}}{\partial y \partial y}}{(\gamma_{xx}\gamma_{yy})} - \frac{\frac{\partial^2 \gamma_{xx}}{\partial z \partial z}}{(\gamma_{xx}\gamma_{zz})} - \frac{\frac{\partial^2 \gamma_{yy}}{\partial x \partial x}}{(\gamma_{xx}\gamma_{yy})} - \frac{\frac{\partial^2 \gamma_{yy}}{\partial z \partial z}}{(\gamma_{yy}\gamma_{zz})} - \frac{\frac{\partial^2 \gamma_{zz}}{\partial x \partial x}}{(\gamma_{xx}\gamma_{zz})} - \frac{\frac{\partial^2 \gamma_{zz}}{\partial y \partial y}}{(\gamma_{yy}\gamma_{zz})} \\ & + \frac{\left(\frac{\partial \gamma_{xx}}{\partial y}\frac{\partial \gamma_{xx}}{\partial y}\right)}{(2\gamma_{xx}\gamma_{xx}\gamma_{yy})} + \frac{\left(\frac{\partial \gamma_{xx}}{\partial z}\frac{\partial \gamma_{xx}}{\partial z}\right)}{(2\gamma_{xx}\gamma_{xx}\gamma_{zz})} + \frac{\left(\frac{\partial \gamma_{yy}}{\partial x}\frac{\partial \gamma_{yy}}{\partial x}\right)}{(2\gamma_{xx}\gamma_{yy}\gamma_{yy})} + \frac{\left(\frac{\partial \gamma_{yy}}{\partial z}\frac{\partial \gamma_{yy}}{\partial z}\right)}{(2\gamma_{yy}\gamma_{yy}\gamma_{zz})} \\ & + \frac{\left(\frac{\partial \gamma_{zz}}{\partial x}\frac{\partial \gamma_{zz}}{\partial x}\right)}{(2\gamma_{xx}\gamma_{zz}\gamma_{zz})} + \frac{\left(\frac{\partial \gamma_{zz}}{\partial y}\frac{\partial \gamma_{zz}}{\partial y}\right)}{(2\gamma_{yy}\gamma_{zz}\gamma_{zz})} + \frac{\left(\frac{\partial \gamma_{xx}}{\partial x}\frac{\partial \gamma_{yy}}{\partial x}\right)}{(2\gamma_{xx}\gamma_{xx}\gamma_{yy})} + \frac{\left(\frac{\partial \gamma_{xx}}{\partial x}\frac{\partial \gamma_{zz}}{\partial x}\right)}{(2\gamma_{xx}\gamma_{xx}\gamma_{zz})} \\ & + \frac{\left(\frac{\partial \gamma_{xx}}{\partial y}\frac{\partial \gamma_{yy}}{\partial y}\right)}{(2\gamma_{xx}\gamma_{yy}\gamma_{yy})} - \frac{\left(\frac{\partial \gamma_{xx}}{\partial y}\frac{\partial \gamma_{zz}}{\partial y}\right)}{(2\gamma_{xx}\gamma_{yy}\gamma_{zz})} - \frac{\left(\frac{\partial \gamma_{xx}}{\partial z}\frac{\partial \gamma_{yy}}{\partial z}\right)}{(2\gamma_{xx}\gamma_{yy}\gamma_{zz})} + \frac{\left(\frac{\partial \gamma_{xx}}{\partial z}\frac{\partial \gamma_{zz}}{\partial z}\right)}{(2\gamma_{xx}\gamma_{zz}\gamma_{zz})} \\ & - \frac{\left(\frac{\partial \gamma_{yy}}{\partial x}\frac{\partial \gamma_{zz}}{\partial x}\right)}{(2\gamma_{xx}\gamma_{yy}\gamma_{zz})} + \frac{\left(\frac{\partial \gamma_{yy}}{\partial y}\frac{\partial \gamma_{zz}}{\partial y}\right)}{(2\gamma_{yy}\gamma_{yy}\gamma_{zz})} + \frac{\left(\frac{\partial \gamma_{yy}}{\partial z}\frac{\partial \gamma_{zz}}{\partial z}\right)}{(2\gamma_{yy}\gamma_{zz}\gamma_{zz})} \end{aligned} \tag{4.70}$$

which results from a computation similar to that of the Dingle formula.[42] Actually, a simplification exist for the spatial metric of equation (4.17) since there the γ_{xx} and γ_{zz} components are equal. However, this simplification was not used to its full advantage in the application of the variational principle and will be left out here.

The complete set of initial data for the hypersurface Σ_τ requires in addition to the spatial metric $\gamma_{\mu\nu}$, the lapse function α, and the shift vector β^ν, that the extrinsic curvature $K_{\mu\nu}$ be defined as given by equation (2.22). However, this is a rather complicated expression when applied to the trial geometry above. In the variational method outlined, only a reasonable approximation to the extrinsic curvature is needed. Consider the linear superposition of the extrinsic curvatures associated with two separate boosted black holes.The spacetime geometry for a single black hole in isotropic spherical coordinates is given by the infinitesimal line element[31]

$$ds^2 = -\alpha_{iso}^2 dt^2 + \Psi_{iso}^4 (d\rho_{iso}^2 + \rho_{iso}^2 d\theta^2 + \rho_{iso}^2 d\phi^2) \tag{4.71}$$

where

$$\alpha_{iso} = \frac{(1 - \frac{M}{2\rho_{iso}})}{(1 + \frac{M}{2\rho_{iso}})} \tag{4.72}$$

and

$$\Psi_{iso} = (1 + \frac{M}{2\rho_{iso}}) \, . \tag{4.73}$$

The isotropic radial coordinate ρ_{iso} is related to the Schwarzschild radial coordinate r_{Sch} by

$$r_{Sch} = \left(1 + \frac{M}{2\rho_{iso}}\right)^2 \rho_{iso} \, . \tag{4.74}$$

By making a Lorentz transformation on this metric the infinitesimal line element for a single boosted black hole is obtained. For the quasi-Cartesian coordinates it is found to be

$$\begin{aligned} ds^2 = &-\Big(\frac{\alpha_{iso}^2 - v^2\Psi_{iso}^4}{1-v^2}\Big)dt^2 + \Big(\frac{2v(\alpha_{iso}^2 - \Psi_{iso}^4)}{1-v^2}\Big)dydt \\ &+ \Big(\frac{\Psi_{iso}^4 - v^2\alpha_{iso}^2}{1-v^2}\Big)dy^2 + \Psi_{iso}^4(dx^2 + dz^2) \end{aligned} \tag{4.75}$$

with the position of the boosted black hole given by

$$y_{BBH}(t) = y_{o_1} + vt \tag{4.76}$$

where v is the boost velocity of the black hole and y_{o_1} is the coordinate offset of the black hole from the origin along the y axis. In order to put a spatial slice of this geometry into the moving frame of reference, introduce the new set of coordinates

$$t = t' \tag{4.77a}$$

$$x = x' \tag{4.77c}$$

$$y = y' + vt \tag{4.77b}$$

$$z = z' \,. \tag{4.77d}$$

Then the infinitesimal line element is given by

$$\begin{aligned} ds^2 = &-\Big(\frac{(1-v^2)\alpha_{iso}^2\Psi_{iso}^4}{\Psi_{iso}^4 - v^2\alpha_{iso}^2}\Big)dt'^2 \\ &+ \Big(\frac{\Psi_{iso}^4 - v^2\alpha_{iso}^2}{1-v^2}\Big)\Big[dy' + \Big(\frac{v(1-v^2)\alpha_{iso}^2}{\Psi_{iso}^4 - v^2\alpha_{iso}^2}\Big)dt'\Big]^2 \\ &+ \Psi_{iso}^4(dx'^2 + dz'^2) \,. \end{aligned} \tag{4.78}$$

Comparison of this infinitesimal line element to the general form for infinitesimal line elements given by equation (4.15) leads to the definition of the square of the lapse function A_{BBH}^2 for the single boosted black hole

$$A_{BBH}^2 = \frac{(1-v^2)\alpha_{iso}^2\Psi_{iso}^4}{\Psi_{iso}^4 - v^2\alpha_{iso}^2} \,. \tag{4.79}$$

The definition of the shift vector is found to be

$$\beta^{\mu}_{BBH}\frac{\partial}{\partial x^{\mu}} = \left(\frac{v(1-v^2)\alpha^2_{iso}}{\Psi^4_{iso} - v^2\alpha^2_{iso}}\right)\frac{\partial}{\partial y'} \tag{4.80}$$

And the spatial metric $\gamma^{BBH}_{\mu\nu}$, given by the three dimensional infinitesimal line element becomes

$$\gamma^{BBH}_{\mu\nu}dx^{\mu}dx^{\nu} = \Psi^4_{iso}(dx'^2 + dz'^2) + \left(\frac{\Psi^4_{iso} - v^2\alpha^2_{iso}}{1-v^2}\right)dy'^2 \tag{4.81}$$

which agrees with the spatial slice of the boosted black hole geometry given in equation (4.75). This boosted black hole geometry will be used to construct an adequate extrinsic curvature tensor for the binary black holes' geometry. The extrinsic curvature for this boosted black hole geometry is given by

$$2A_{BBH}K^{BBH}_{\mu\nu} = -\mathcal{L}_{\mathrm{t}}\gamma^{BBH}_{\mu\nu} + \mathcal{L}_{\beta}\gamma^{BBH}_{\mu\nu} \ . \tag{4.82}$$

In the comoving frame the first term vanishes

$$\mathcal{L}_{\mathrm{t}}\gamma^{BBH}_{\mu\nu} = 0 \ . \tag{4.83}$$

Thus the extrinsic curvature for the boosted black hole geometry becomes

$$\begin{aligned} 2A_{BBH}K^{BBH}_{\mu\nu} &= \mathcal{L}_{\beta}\gamma^{BBH}_{\mu\nu} \\ &= \beta^{\sigma}_{BBH}\frac{\partial}{\partial x^{\sigma}}\gamma^{BBH}_{\mu\nu} + \gamma^{BBH}_{\sigma\nu}\frac{\partial}{\partial x^{\mu}}\beta^{\sigma}_{BBH} + \gamma^{BBH}_{\mu\sigma}\frac{\partial}{\partial x^{\nu}}\beta^{\sigma}_{BBH} \ . \end{aligned} \tag{4.84}$$

In order to generate the extrinsic curvature for the binary black holes geometry consider the two separate geometries for two independent boosted black holes, one with boost velocity u offset from the origin by x_{o_1} along the x axis and the second with boost velocity v offset from the origin by x_{o_2} along the x axis. The extrinsic curvature is then approximated by

$$K_{\mu\nu} = K_{1\mu\nu} + K_{2\mu\nu} \ , \tag{4.85}$$

where $K_{1\mu\nu}$ and $K_{2\mu\nu}$ are constructed by comparison with the boosted black hole's extrinsic curvature given in equation (4.84). The difference is that in the place of the isotropic lapse function and conformal factor α_{iso} and Ψ_{iso} appearing in the expression for the boosted black hole's extrinsic curvature are placed the functions α_1, α_2 and ψ_1, ψ_2 of the binary black holes given by equations (4.24), (4.25), (4.21), and (4.22). In addition the shift vector of the boosted black hole β_{BBH} is replaced by the shift vector of the binary black holes with components given by equations (4.27a) through (4.27c). Once this analogy is complete, the extrinsic curvature for the binary black holes geometry has the following components:

$$\begin{aligned} K_{xx} &= K_{1xx} + K_{2xx} \\ &= \frac{u\alpha_1 \frac{\partial \rho_1}{\partial y}\frac{\partial \gamma_{xx}}{\partial \rho_1}}{2\sqrt{\Psi^4 \gamma_{yy}}} + \frac{v\alpha_2 \frac{\partial \rho_2}{\partial y}\frac{\partial \gamma_{xx}}{\partial \rho_2}}{2\sqrt{\Psi^4 \gamma_{yy}}} \end{aligned} \tag{4.86}$$

$$\begin{aligned} K_{yy} &= K_{1yy} + K_{2yy} \\ &= \frac{u(-\alpha_1 \frac{\partial \rho_1}{\partial y}\frac{\partial \gamma_{yy}}{\partial \rho_1} + 4\gamma_{yy}\frac{\partial \rho_1}{\partial y}\frac{\partial \alpha_1}{\partial \rho_1})}{2\sqrt{\Psi^4 \gamma_{yy}}} \\ &+ \frac{v(-\alpha_2 \frac{\partial \rho_2}{\partial y}\frac{\partial \gamma_{yy}}{\partial \rho_2} + 4\gamma_{yy}\frac{\partial \rho_2}{\partial y}\frac{\partial \alpha_2}{\partial \rho_2})}{2\sqrt{\Psi^4 \gamma_{yy}}} \end{aligned} \tag{4.87}$$

$$\begin{aligned} K_{zz} &= K_{1zz} + K_{2zz} \\ &= \frac{u\alpha_1 \frac{\partial \rho_1}{\partial y}\frac{\partial \gamma_{zz}}{\partial \rho_1}}{2\sqrt{\Psi^4 \gamma_{yy}}} + \frac{v\alpha_2 \frac{\partial \rho_2}{\partial y}\frac{\partial \gamma_{zz}}{\partial \rho_2}}{2\sqrt{\Psi^4 \gamma_{yy}}} \end{aligned} \tag{4.88}$$

$$
\begin{aligned}
K_{xy} = K_{yx} &= K_{1xy} + K_{2xy} \\
&= u\sqrt{\frac{\gamma_{yy}}{\Psi^4}}\frac{\partial\rho_1}{\partial x}\left(\frac{\partial\alpha_1}{\partial\rho_1} - \frac{\alpha_1\frac{\partial\gamma_{yy}}{\partial\rho_1}}{2\gamma_{yy}}\right) \\
&+ v\sqrt{\frac{\gamma_{yy}}{\Psi^4}}\frac{\partial\rho_2}{\partial x}\left(\frac{\partial\alpha_2}{\partial\rho_2} - \frac{\alpha_2\frac{\partial\gamma_{yy}}{\partial\rho_2}}{2\gamma_{yy}}\right)
\end{aligned}
\tag{4.89}
$$

$$
\begin{aligned}
K_{yz} = K_{zy} &= K_{1yz} + K_{2yz} \\
&= u\sqrt{\frac{\gamma_{yy}}{\Psi^4}}\frac{\partial\rho_1}{\partial z}\left(\frac{\partial\alpha_1}{\partial\rho_1} - \frac{\alpha_1\frac{\partial\gamma_{yy}}{\partial\rho_1}}{2\gamma_{yy}}\right) \\
&+ v\sqrt{\frac{\gamma_{yy}}{\Psi^4}}\frac{\partial\rho_2}{\partial z}\left(\frac{\partial\alpha_2}{\partial\rho_2} - \frac{\alpha_2\frac{\partial\gamma_{yy}}{\partial\rho_2}}{2\gamma_{yy}}\right)
\end{aligned}
\tag{4.90}
$$

$$
\begin{aligned}
K_{xz} = K_{zx} &= K_{1xz} + K_{2xz} \\
&= 0 \, .
\end{aligned}
\tag{4.91}
$$

The masses associated with this trial geometry for each of the three asymptotically flat regions of the spatial hypersurface Σ_τ are given by evaluating the integral of equation (2.64). On the top sheet which contains both black holes, the value of the total mass is found to be

$$
M_{total} = \frac{m_1}{\sqrt{1-u^2}} + \frac{m_2}{\sqrt{1-v^2}} \, . \tag{4.92}
$$

When solving for the masses at each of the bottom sheets of the hypersurface, the trial geometry must be evaluated in the limit that ρ_1 and ρ_2 approach zero. The value of the masses associated with each of these bottom sheets are referred to as irreducible masses, and are found to be

$$
M_{1_{irreducible}} = m_1\left(1 + \frac{m_2(1-u^2)}{2s}\right) \tag{4.93}
$$

for the asymptotically flat region containing only the one black hole located at x_{o_1}, and

$$M_{2_{irreducible}} = m_2\left(1 + \frac{m_1(1-v^2)}{2s}\right) \tag{4.94}$$

for the asymptotically flat region containing only the one black hole located at x_{o_2}. The variable s is the separation between the two holes. It is the irreducible masses which must be fixed in value for the purpose of comparing neighboring geometries in the variations of the Hamiltonian of equation (3.16).

The linear momentum for each sheet of the hypersurface is defined by equation (2.65). Evaluated on the top sheet, the magnitude of the total linear momentum for this trial geometry is given by

$$P_{total} = \frac{m_1 u}{\sqrt{1-u^2}} + \frac{m_2 v}{\sqrt{1-v^2}} \ . \tag{4.95}$$

The total linear momentum can freely be chosen to have the value

$$P_{total} = 0 \tag{4.96}$$

restricting the frame of reference to the center of mass frame. Then the value of the second velocity v is restricted by the value of the first velocity u though the constraint

$$\frac{m_1 u}{\sqrt{1-u^2}} = -\frac{m_2 v}{\sqrt{1-v^2}} \ . \tag{4.97}$$

The values of the linear momenta as measured on each of the bottom two sheets of the hypersurface are both zero.

The Angular momentum for each sheet of the hypersurface is defined by equation (2.66). Again evaluated on the top sheet, the magnitude of the total angular momentum for this trial geometry is given by

$$J_{total} = \frac{m_1 u x_{o_1}}{\sqrt{1-u^2}} + \frac{m_2 v x_{o_2}}{\sqrt{1-v^2}} \ . \tag{4.98}$$

The values of the angular momenta as measured on each of the bottom two sheets of the hypersurface are both zero.

These equations taken in combination provide a single parameter for the variational principle as follows. Select a choice of irreducible masses for the two black holes $M_{1_{irreducible}}$ and $M_{2_{irreducible}}$ along with a choice of the total angular momentum J_{total} for the geometry, the above equations (4.93), (4.94), (4.95), and (4.98) provide self consistent values for the velocities u and v, the masses of the two black holes on the top sheet of the hypersurface m_1 and m_2, and the positions along the x-axis x_{o_1} and x_{o_2}, given any value for the separation s between the two black holes. The correct value of the separation for these values of irreducible masses and total angular momentum is found by numerical application of the variational method for the Hamiltonian of equation (3.16) on a computer.

A concise algorithmic description of the numerical code applied to a universal Turing machine consists of the following:[43]

- Choose an interesting set of values for the irreducible masses and total angular momentum along with a reasonable estimate for the separation between the two black holes. This estimate may be found through application of Newtonian mechanics, post-Newtonian analysis, or the test particle limit of the Schwarzschild geometry.
- Evaluate equation (3.16) over a sufficiently large region of three dimensional hypersurface Σ_τ to cover all three sheets of the slice out to their respective asymptotically flat regions. Note that the surface integral in equation (3.16) can actually be evaluated analytically for this trial geometry and has the value of $(-\Omega J_{total})$.

- Use the results of the evaluation of equation (3.16) in an extremizing algorithm which efficiently alters the value of the separation between the two black holes to a value corresponding to the minimum or maximum value of the Hamiltonian of equation (3.16). This value of the Hamiltonian is the mass of the binary black hole system and the separation provides the best trial geometry to the system.

In practice the procedure is much more complex as a result of the limitations of modern computer programming languages. The actual numerical procedure is in the form of a C program, a programming language not often used in physics but one of the least limited in terms of flexibility. The C program has been extensively tested where comparisons to analytically known results apply and performs admirably.

CHAPTER 5
NUMERICAL RESULTS

5.1 Test Particle Geometry

In the limit that one of the black hole's mass approaches zero, the trial geometry used in the variational principle should reproduce the results obtainable from the test particle geodesics of the Schwarzschild geometry. In this test particle limit, the trial geometry does not satisfy the steady state equations, (2.60a) through (2.60d), nevertheless the numerical results in this limit are remarkably accurate.

The test particle geodesics are analytically derivable, and can easily be expressed in a concise functional form.[44] Since the constraints on the trial geometry of equation (4.17) restrict the motion of the two black holes to circular orbits of fixed radial separation, only the analytic results for the test particle in circular orbits about a Schwarzschild black hole will be applicable for comparison in this limit. The analytic expressions for orbital equations of motion about a Schwarzschild black hole are found using the following set of coupled differential equations in the usual Schwarzschild coordinates of (r, θ, ϕ):

$$\left(\frac{dr}{d\tau}\right)^2 = \left(\frac{E}{m}\right)^2 - V_{eff}(r) \tag{5.1}$$

where the effective potential $V_{eff}(r)$ is given by

$$V_{eff}(r) = \left(1 - \frac{2M}{r}\right)\left(1 + \frac{\left(\frac{J_{total}}{m}\right)^2}{r^2}\right) \tag{5.2}$$

also

$$\frac{d\phi}{d\tau} = \frac{\left(\frac{J_{total}}{m}\right)^2}{r^2} \tag{5.3}$$

and

$$\frac{dt}{d\tau} = \frac{\left(\frac{E}{m}\right)}{\left(1 - \frac{2M}{r}\right)} \ . \tag{5.4}$$

The equation (5.1) though (5.4) together can be solved for motion, $r(\tau)$, $\phi(\tau)$ and $t(\tau)$ for a test particle of mass m orbiting a Schwarzschild black hole of mass M with particle energy E and total angular momentum J_{total}. In general, the equation for $r(\tau)$ involves an elliptic integral. However, by restricting considerations to the circular orbits which satisfy

$$\left(\frac{dr}{d\tau}\right) = 0 \ , \tag{5.5}$$

the solution for $r(\tau)$ becomes simple. The circular orbits are found by setting

$$\frac{dV_{eff}(r)}{dr} = 0 \ . \tag{5.6}$$

Thus the square of the energy per test particle mass equals the effective potential

$$\left(\frac{E}{m}\right)^2 = V_{eff}(r) \ . \tag{5.7}$$

Figure 3 illustrates $(V_{eff})^{\frac{1}{2}}$ for several values of J_{total}/mM. Differentiating the effective potential with respect to the radius leads to the expression for the radius of the circular orbits

$$Mr^2 - \left(\frac{J_{total}}{m}\right)^2 r + 3M\left(\frac{J_{total}}{m}\right)^2 = 0 \ . \tag{5.8}$$

Equation (5.8) has two solutions for the radii of the circular orbits. The outer radial solutions, shown in Table 1, correspond to stable circular orbits, while

the inner radial solutions, shown in Table 2, correspond to unstable circular orbits. Finally, there are no circular orbits, stable or unstable, for a test particle with $J_{total} < 2\sqrt{3}mM$, a result which does not appear in Newtonian considerations. Combining equations (5.7) and (5.8), the following relationships for the total angular momentum and energy are derived

$$J_{total} = mr\sqrt{\frac{M}{r-3M}} \tag{5.9}$$

$$E = \frac{m(r-2M)}{\sqrt{r(r-3M)}} \, . \tag{5.10}$$

The equations of motion (5.1) through (5.4) also provide the following expressions for the tangential velocity

$$v^{\phi} = \frac{J_{total}}{rE}\sqrt{1-\frac{2M}{r}} \tag{5.11}$$

and the angular frequency

$$\Omega = \sqrt{\frac{M}{r^3}} \tag{5.12}$$

as measured by an observer at infinity. Circular orbits exist down to radii of $3M$. But stable circular orbits exist only for radii greater than $6M$ in these Schwarzschild coordinates.

The binding energy per unit mass of a test particle in the innermost stable orbit at $r = 6M$ is given by

$$\frac{E_{Binding}}{m} = \left(\frac{m-E}{m}\right) = 1 - \left(\frac{8}{9}\right)^2 \approx 5.7191\% \, . \tag{5.13}$$

This percentage of the rest-mass energy of the particle is available for emission in the form of gravitational radiation as the particle slowly spirals in from an initial state of rest at infinity inward to the innermost stable circular orbit at $r = 6M$.

TABLE 1: Stable Circular Analytical Test Particle Orbits

j_{total}	r_{Sch}/M	ρ_{iso}/M	E/m	ΩM_1	v^ϕ
3.46†	6.0000	4.9495	0.94280904	0.0680414	0.5000
3.50	7.0000	5.9580	0.94491118	0.0539949	0.4472
3.85	10.6453	9.6193	0.95830523	0.0287914	0.3401
4.00	12.0000	10.9772	0.96225045	0.0240563	0.3162
4.50	16.5876	15.5716	0.97167430	0.0148210	0.2618
5.00	21.5139	20.5017	0.97776736	0.0100213	0.2264
5.50	26.8730	25.8633	0.98201155	0.0071784	0.2005
6.00	32.6969	31.6891	0.98511216	0.0053486	0.1805
6.50	39.0000	37.9934	0.98745695	0.0041059	0.1644
7.00	45.7897	44.7841	0.98927822	0.0032274	0.1511
7.50	53.0703	52.0655	0.99072367	0.0025866	0.1399
8.00	60.8444	59.8402	0.99189151	0.0021070	0.1304
8.50	69.1138	68.1102	0.99284942	0.0017404	0.1221
9.00	77.8798	76.8766	0.99364540	0.0014550	0.1148
9.50	87.1430	86.1401	0.99431433	0.0012293	0.1084
10.00	96.9042	95.9016	0.99488211	0.0010483	0.1026

Note: Units with $G = c = 1$.
†Actual value of $j_{total} \equiv J_{total}/mM$ is $2\sqrt{3}$.

TABLE 2: Unstable Circular Analytical Test Particle Orbits

j_{total}	r_{Sch}/M	ρ_{iso}/M	E/m	ΩM_1	v^ϕ
3.46†	6.0000	4.9495	0.94280904	0.0680414	0.5000
3.50	5.2500	4.1903	0.94561086	0.0831306	0.5547
3.85	4.1772	3.0965	0.98181765	0.1171314	0.6777
4.00	4.0000	2.9142	1.00000000	0.1250000	0.7071
4.50	3.6624	2.5649	1.06732488	0.1426781	0.7756
5.00	3.4861	2.3811	1.14159110	0.1536336	0.8203
5.50	3.3770	2.2667	1.22039216	0.1611404	0.8522
6.00	3.3036	2.1889	1.30239038	0.1665808	0.8760
6.50	3.2500	2.1328	1.38675049	0.1706770	0.8944
7.00	3.2103	2.0908	1.47291437	0.1738502	0.9090
7.50	3.1798	2.0583	1.56049136	0.1763645	0.9207
8.00	3.1556	2.0326	1.64919827	0.1783936	0.9302
8.50	3.1361	2.0119	1.73882411	0.1800567	0.9381
9.00	3.1202	1.9949	1.82920807	0.1814379	0.9448
9.50	3.1070	1.9808	1.92022523	0.1825981	0.9505
10.00	3.0958	1.9690	2.01177698	0.1835827	0.9553

Note: Units with $G = c = 1$.
†Actual value of $j_{total} \equiv J_{total}/mM$ is $2\sqrt{3}$.

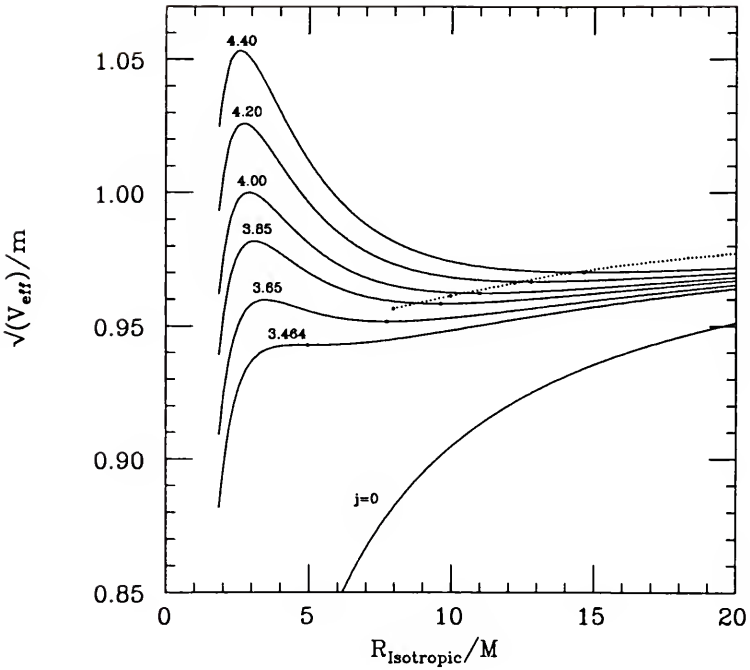

FIGURE 3: Analytical Effective Potential for Test Particle. Stable circular orbits are located at the minima. Unstable circular orbits are located at the maxima. No orbits exist for $J_{total} < 2\sqrt{3}mM$, where J_{total} is the total angular momentum, m is the mass of the test particle and M is the mass of the black hole. The dotted line locates the positions of the numerically derived stable circular orbits.

This is one of the most efficient mechanisms in nature for converting mass into energy. The burning of nuclear fuel in the cores of stars is only 0.9% efficient as hydrogen is combined to form iron.[44] Such efficiency is a major reason for studying black holes as a source of gravitational radiation and as candidates for high energy compact objects.

By taking the black hole of mass m_1 to be the more massive black hole and the black hole of mass m_2 to be the less massive black hole in the trial metric, then a relationship between the analytical results, for a test particle in circular orbit about a Schwarzschild black hole, to the numerical results for the variation method, requires the following identifications:

$$M = M_{1_{irreducible}} \tag{5.14}$$

$$m = M_{2_{irreducible}} \, . \tag{5.15}$$

In addition the coordinates used in the analytical analysis are Schwarzschild coordinates, (r, θ, ϕ). The trial metric is expressed in isotropic coordinates (ρ, θ, ϕ). The two radial coordinates are related through equation (4.74). Taking these factors into account, the numerical results for black hole masses of $M_{1_{irreducible}} = 1.00$, and $M_{2_{irreducible}} = 0.01$, can be used to benchmark the trial geometry with a test particle orbiting a Schwarzschild black hole. The values of m_1 and m_2 appearing in equation (4.92) are summarized in Table 3 for these values of irreducible masses along with the total mass M_{total} defined by equation (4.92) and the extreme value of the mass returned by the variational principle.

Table 4 provides a list of numerical results which can be compared to the analytic results of Table 1. In Table 4 the quantity j_{total} is the total angular momentum divided by the mass of each black hole, s is the separation between

TABLE 3: Numerical Test Particle Masses

j_{total}	m_1	m_2	M_{total}	$E_\circ$
3.85	0.99940862	0.00940862	1.01000214	1.009565079
4.00	0.99952198	0.00952198	1.00986509	1.009612864
4.10	0.99957026	0.00957026	1.00983177	1.009638584
4.20	0.99960644	0.00960644	1.00981706	1.009661131
4.33	0.99963959	0.00963959	1.00981405	1.009686699
4.40	0.99965838	0.00965838	1.00981109	1.009699110
4.50	0.99968070	0.00968070	1.00981099	1.009715259
4.60	0.99969985	0.00969985	1.00981313	1.009729954
4.80	0.99973405	0.00973405	1.00981890	1.009755968
5.00	0.99976203	0.00976203	1.00982694	1.009777992
6.00	0.99984429	0.00984429	1.00987175	1.009852113
7.00	0.99988955	0.00988955	1.00990319	1.009893937
8.00	0.99991788	0.00991788	1.00992474	1.009919656
9.00	0.99993595	0.00993595	1.00994011	1.009937049
10.00	0.99994865	0.00994865	1.00995125	1.009949368

Note: Units with $G = c = 1$, and $M_2 = 0.01M_1$.
All masses in units of the irreducible mass M_1.
$E_\circ$ is the extremized mass.

TABLE 4: Numerical Stable Circular Test Particle Orbits

j_{total}	s/M_1	$(E_\circ - M_1)/M_2$	ΩM_1	u^ϕ	v^ϕ
3.85	7.950	0.9565079	0.0581753	0.00485	0.4576
4.00	9.955	0.9612864	0.0394575	0.00402	0.3888
4.10	11.130	0.9638584	0.0326053	0.00369	0.3592
4.20	12.200	0.9661131	0.0279352	0.00344	0.3374
4.33	13.368	0.9686699	0.0240683	0.00324	0.3185
4.40	14.132	0.9699110	0.0219325	0.00311	0.3068
4.50	15.155	0.9715259	0.0195468	0.00297	0.2933
4.60	16.153	0.9729954	0.0176149	0.00285	0.2817
4.80	18.296	0.9755968	0.0143674	0.00262	0.2602
5.00	20.506	0.9777992	0.0119365	0.00244	0.2423
6.00	31.606	0.9852113	0.0060513	0.00190	0.1894
7.00	44.764	0.9893937	0.0035240	0.00156	0.1562
8.00	60.380	0.9919656	0.0022150	0.00133	0.1324
9.00	77.556	0.9937049	0.0015107	0.00116	0.1160
10.00	96.875	0.9949368	0.0010760	0.00103	0.1032

Note: Units with $G = c = 1$, and $M_2 = 0.01M_1$.
M_1 and M_2 are irreducible masses.
$E_\circ$ is the extremized mass.

the black holes, $\frac{(M_1-E_o)}{M_2}$ is the energy per mass of the less massive black hole, Ω is the angular frequency, u^ϕ is the tangential velocity of the more massive black hole and v^ϕ is the tangential velocity of the less massive black hole. The most obvious difference in the test particle tables is the limiting value of J_{total}/mM. The numerical results have no stable circular orbits for $J_{total} < 3.85mM$ which is roughly 11% larger than the analytic limit. A comparison of the energy per mass of the particle with angular momentum $J_{total} = 3.85mM$ reveals a difference of 0.2% between the analytical and numerical results. However, the binding energy per mass for the numerical result is 4.35%, while the analytic result is 4.17%. This translates into a 4.3% difference in the percentage of rest-mass energy available for the emission of gravitational radiation between the two results.

Using the Hamiltonian of equation (3.16) as the effective potential energy, a series of curves can be generated which locate the stable circular orbits as their minima. The numerically derived effective potentials for several values of J_{total}/mM are illustrated in Figure 4. For a fixed value of angular momentum the variational principle provides the extremum of mass to second order in accuracy, while providing the position of the extremum only to first order. Thus the numerical results for the extremized mass are most accurately presented as functions of the angular momentum as shown in Figure 5.

5.2 Equal Mass Geometry

When the two black holes are of comparable masses, no analytic solutions exist for circular orbits. The form chosen for the trial geometry does reduce

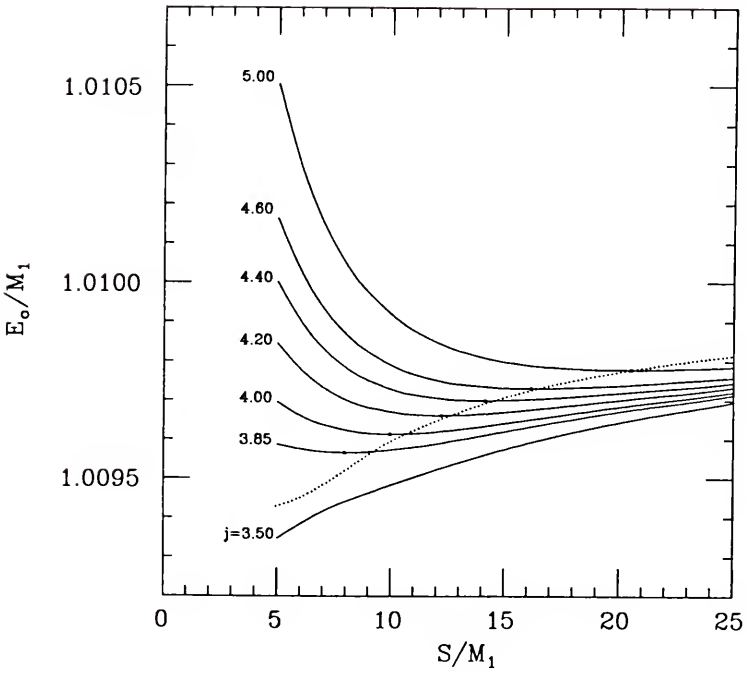

FIGURE 4: Numerical Effective Potential for Test Particle. Stable circular orbits are located at the minima. Maxima were not found with this trial geometry. No orbits exist for $J_{total} < 3.85 M_1 M_2$, where J_{total} is the total angular momentum and M_1 and M_2 are the irreducible masses of the black holes. The position of the analytic stable circular orbits for a test particle orbiting a Schwarzschild black hole are represented by the dotted line.

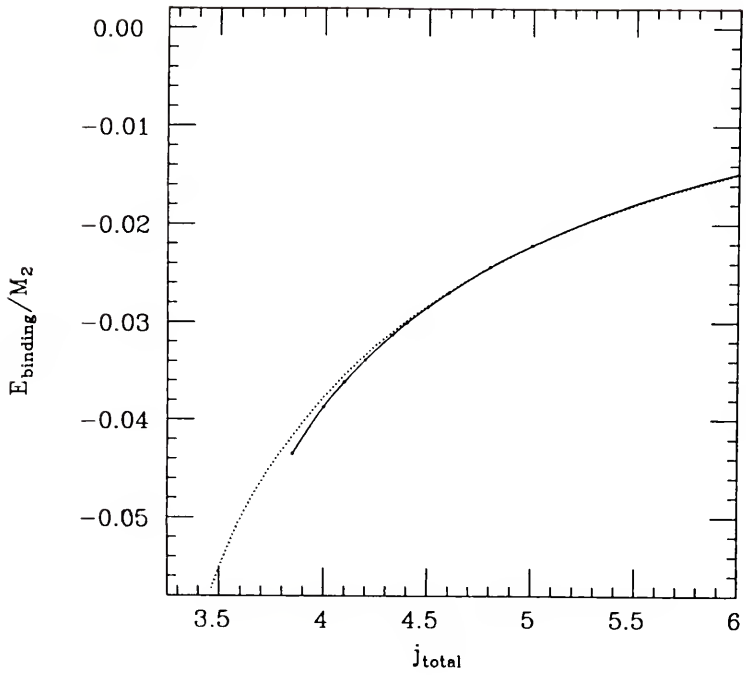

FIGURE 5: Binding Energy of Numerical Test Particle. The binding energy per mass of the smaller black hole $(E_o - M_1 - M_2)/M_2$ for the stable circular orbits is plotted against $j_{total} = J_{total}/(M_1 M_2)$ for the case of $M_2 = 0.01 M_1$ where M_1 and M_2 are the irreducible masses. The dotted line represents the stable circular orbits for the analytic test particle.

to the time symmetric solution for any separation when the speeds of the two black holes approach zero.[45] In addition, when the separation is very large the trial geometry reduce to two boosted black holes having arbitrarily large speeds. The trial geometry will not be exact in any other limits. Still, the numerical solutions can be compared to Newtonian calculations, as well as, post-Newtonian calculations.

A Newtonian binary system of two point masses, m_1, and m_2, in circular orbits, move about their common center of mass under the influence of the Newtonian gravitational force

$$\vec{F} = \frac{m_1 m_2}{r_{12}^2} \hat{r}_{12} \ . \tag{5.16}$$

This is in units with the universal gravitational constant $G = 1$, and the speed of light $c = 1$. Next introduce two new mass variables, the total mass

$$M_{total} = m_1 + m_2 \tag{5.17}$$

and the reduced mass

$$\mu = \frac{m_1 m_2}{(m_1 + m_2)} \ . \tag{5.18}$$

Then the Newtonian expression for the separation between the two point masses in circular orbits is given by

$$s_N = \frac{J_{total}^2}{\mu^2 M_{total}} = j_{total}^2 M_{total} \tag{5.19}$$

where J_{total} is the total angular momentum of the binary system. The scaled angular momentum j_{total} is related to the total angular momentum by

$$J_{total} = j_{total}(\mu M_{total}) = j_{total}(m_1 m_2) \ . \tag{5.20}$$

The total energy of the binary system of point masses, including the rest mass energy of the two masses, is given by

$$E_N = M_{total} - \frac{\mu^3 M_{total}^2}{2 J_{total}^2} = M_{total} - \frac{\mu}{2 j_{total}^2} \ . \tag{5.21}$$

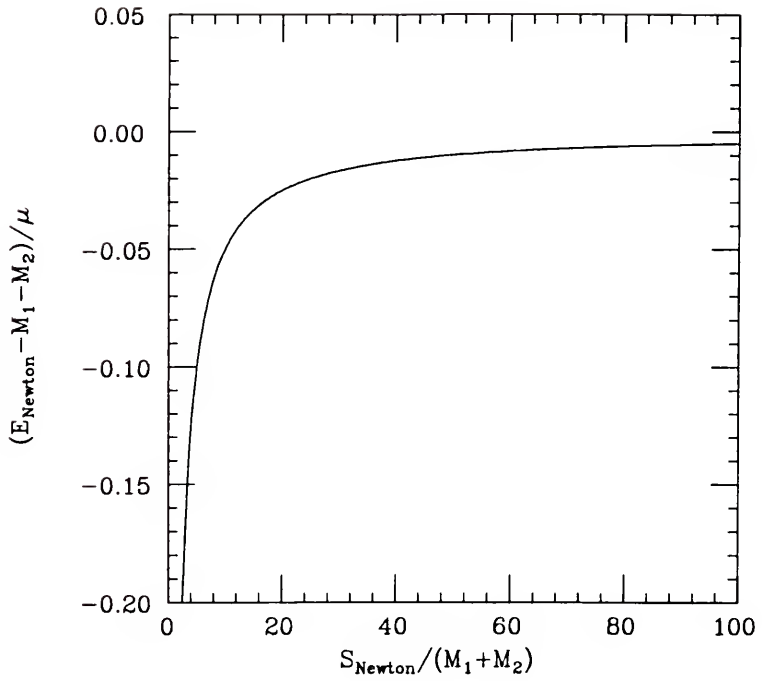

FIGURE 6: Single Parameter Newtonian Circular Orbits. The binding energy per reduced mass as a function of separation per total mass. A single curve describes all possible Newtonian orbits in terms of one parameter, the scaled total angular momentum j_{total}.

An interesting result occurs when the following rescaling is performed:

$$\frac{(E_N - M_{total})}{\mu} = -\frac{1}{2j_{total}^2} \tag{5.22}$$

$$\frac{s_N}{M_{total}} = j_{total}^2 \ . \tag{5.23}$$

When equation (5.22) is plotted as a function of equation (5.23), a single curve results which represents all possible stable circular orbits of a binary system in Newtonian mechanics, as shown in Figure 6.

The post-Newtonian approximation developed out of a study of the equations of motion in a gravitational system described by general relativity.[46] The equations of motion in general relativity are given by the geodesic equation,

$$\frac{d^2x^\mu}{d\tau^2} = \Gamma^\mu_{\ \nu\lambda}\frac{dx^\nu}{d\tau}\frac{dx^\lambda}{d\tau} \tag{5.24}$$

where τ is the proper time. The coordinate accelerations can be derived from equation (5.24) and are found to be

$$\begin{aligned}\frac{d^2x^i}{dt^2} &= -\Gamma^i_{\ 00} - 2\Gamma^i_{\ 0j}\frac{dx^j}{dt} - \Gamma^i_{\ jk}\frac{dx^j}{dt}\frac{dx^k}{dt} \\ &\quad + \left(\Gamma^0_{\ 00} + 2\Gamma^0_{\ 0j}\frac{dx^j}{dt} - \Gamma^0_{\ jk}\frac{dx^j}{dt}\frac{dx^k}{dt}\right)\frac{dx^i}{dt}\end{aligned} \tag{5.25}$$

where the indices i, j, and k range over the spatial coordinates. In the Newtonian limit all velocities in equation (5.25) are neglected, leading to

$$\frac{d^2x^i}{dt^2} \approx -\Gamma^i_{\ 00} \approx \frac{1}{2}g^{ij}\frac{\partial g_{00}}{dx^j} \approx -\frac{\bar{M}}{\bar{r}^2} \ , \tag{5.26}$$

where the $\bar{M}$ and the $\bar{r}$ are the relevant mass and separation in a Newtonian binary system. For a Newtonian system the relevant velocity $\bar{v}$ is related to the potential energy by

$$\bar{v}^2 = \frac{\bar{M}}{\bar{r}} \ . \tag{5.27}$$

Thus in the Newtonian limit the accelerations given in equation (5.26) are calculated to order $\left(\frac{\bar{v}^2}{\bar{r}}\right)$. The post-Newtonian approximation carries the calculation of the accelerations to one higher order in $\bar{v}^2$, that is to order $\left(\frac{\bar{v}^4}{\bar{r}}\right)$. The order to which the connection coefficients in equation (5.25) must be determined can simply be read off. The metric is then expressed as a correction to a flat background metric using an expansion series of terms in powers of $\bar{v}^2$.

The equations of motion derived in the post-Newtonian approximation can be integrated[47] for a binary system of point masses and an effective potential energy constructed in terms of the separation r (in the Einstein-Infeld-Hoffmann gauge) and total angular momentum J_{total}

$$E_{PN}(r, J_{total}) = \frac{J_{total}^2}{2\mu r^2} - \frac{\mu M_{total}}{r} - \frac{J_{total}^4 (M_{total} - 3\mu)}{8 M_{total} \mu^3 r^4} - \frac{J_{total}^2 (3M_{total} + \mu)}{2\mu r^3} + \frac{\mu M_{total}^2}{2r^2} \tag{5.28}$$

where the masses μ and M_{total} are given by equations (5.18) and (5.17).[48] For given masses and angular momentum, the stable circular orbits are found by solving for the zeros of the first derivative with respect to r of equation (5.28) that also correspond to a positive second derivative with respect to r of equation (5.28). It is interesting to notice that the post-Newtonian approximation also has the feature of an innermost stable circular orbit which is determined by simultaneously solving for the zeros of the first and second derivatives with respect to r in equation (5.28). For the case of equal masses the innermost stable circular orbit is found at a total angular momentum of $J_{total} \approx 4.2876 \mu M_{total}$ and a separation of $s \approx 19.81 M_1$. The binding energy for this orbit is found to be 0.85% of the total rest mass energy available when the two masses are infinitely far away and at rest. These features of the post-Newtonian effective

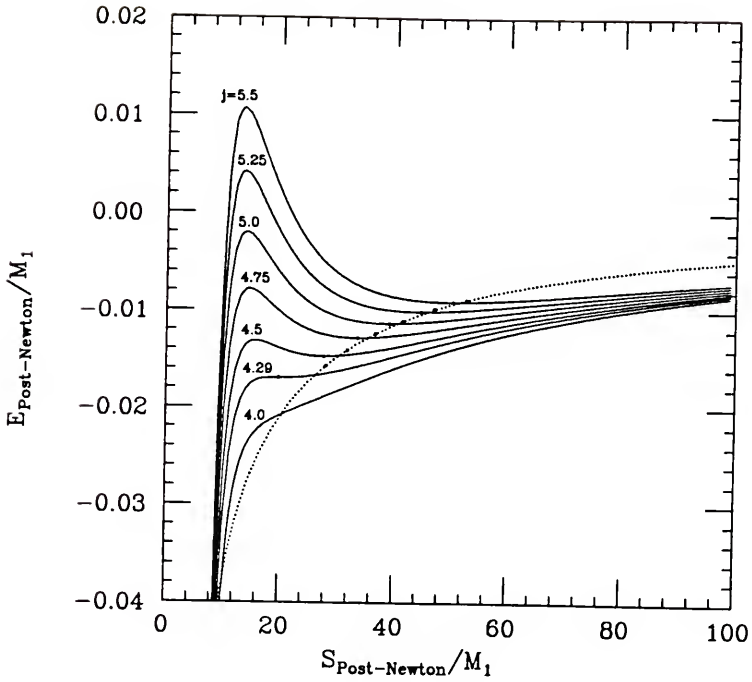

FIGURE 7: Post-Newtonian Effective Potential for Equal Masses. Stable circular orbits are located at the minima. Unstable circular orbits are located at the maxima. No orbits exist for J_{total} less than $\approx 4.2876\mu M_{total}$. The dotted line locates the numerically derived stable circular orbits.

potential energy are illustrated in Figure 7 for several different values of the total angular momentum J_{total} in the case of two equal masses.

Since the post-Newtonian approximation is only valid when the speed of the particles are very small compared to the speed of light, the closer, faster, unstable circular orbits will be less accurately determined by this approximation. Consequently, they will not be compared to numerical findings.

The numerical results of Table 5 for two black holes of equal masses reveal several interesting features. There is an innermost stable circular orbit found at a total angular momentum of $J_{total} \approx 0.84 M_1 M_2$. This is a considerably smaller value of angular momentum then that of the innermost stable orbit in the post-Newtonian approximation. However, the Newtonian approximation has stable orbits for any non-zero angular momentum. This innermost stable circular orbit for the numerical results is located at a separation of $s \approx 1.13 M_1$. The binding energy of this orbit is 17.18% of the total rest mass energy available when the two masses are infinitely far away and at rest. This is very close to the binding energy of 17.72% of the total rest mass energy that a Newtonian calculation would give for this angular momentum.

The numerical results also reveal unstable circular orbits inside the separation for the innermost stable circular orbit. The position of these unstable circular orbits have not been determined accurately since the binary system is undoubtedly evolving rapidly through the emission of gravitational radiation.

The Hamiltonian of equation (3.16) provides an effective potential energy for the circular orbits whereby stable circular orbits are located at the minima and unstable circular orbits are located at the maxima. Figure 8 illustrates these effective potential energy curves for the case of equal mass black holes

TABLE 5: Numerical Stable Circular Orbits for Equal Masses

j_{total}	s/M_1	m_1/M_1	M_{total}/M_1	E_o/M_1	ΩM_1	u^ϕ
0.84	1.13	0.750692	2.112751	1.65639436	1.24503	0.7036
0.85	1.19	0.758342	2.083652	1.66172030	1.15255	0.6857
0.90	1.37	0.778896	2.036690	1.68478020	0.93910	0.6442
1.00	1.65	0.803998	2.014120	1.72181645	0.73036	0.6022
1.30	2.40	0.849706	2.014870	1.79884909	0.44733	0.5372
1.50	2.92	0.870195	2.021581	1.83490281	0.34885	0.5088
1.60	3.19	0.878814	2.024294	1.85005175	0.31138	0.4961
2.00	4.39	0.906376	2.029113	1.89737083	0.20483	0.4493
2.20	5.10	0.917466	2.027682	1.91514164	0.16690	0.4255
2.40	5.93	0.927455	2.023912	1.92995159	0.13496	0.4000
2.50	6.40	0.932149	2.021233	1.93638889	0.12067	0.3863
2.60	6.93	0.936684	2.018113	1.94223806	0.10735	0.3719
2.70	7.52	0.941086	2.014625	1.94753545	0.09489	0.3566
3.00	9.78	0.953514	2.003297	1.96042452	0.06264	0.3063
3.25	12.38	0.962574	1.995479	1.96819869	0.04252	0.2632
3.50	15.58	0.969822	1.990978	1.97390342	0.02896	0.2256
3.70	18.46	0.974295	1.989377	1.97738415	0.02182	0.2015
3.85	20.76	0.977015	1.988904	1.97952878	0.01796	0.1864
4.00	23.17	0.979301	1.988813	1.98136239	0.01499	0.1736
4.29†	28.03	0.982772	1.989208	1.98421423	0.01097	0.1538
4.50	31.83	0.984767	1.989725	1.98589822	0.00893	0.1421
5.00	41.46	0.988223	1.991108	1.98890032	0.00584	0.1211
6.00	64.00	0.992307	1.993452	1.99255313	0.00294	0.0941
7.00	89.72	0.994488	1.995088	1.99463499	0.00174	0.0782
8.00	119.82	0.995861	1.996194	1.99594383	0.00112	0.0669
9.00	153.86	0.996771	1.996972	1.99682134	0.00076	0.0586
10.00	191.87	0.997408	1.997537	1.99744007	0.00054	0.0522
11.00	234.32	0.997875	1.997958	1.99789326	0.00040	0.0470
12.00	279.93	0.998220	1.998280	1.99823532	0.00031	0.0429
13.00	330.06	0.998490	1.998532	1.99850003	0.00024	0.0394
14.00	383.90	0.998701	1.998733	1.99870910	0.00019	0.0365
15.00	441.98	0.998871	1.998895	1.99887737	0.00015	0.0340
17.50	604.56	0.999174	1.999187	1.99917726	0.00010	0.0290
20.00	791.59	0.999369	1.999377	1.99937114	0.00006	0.0253

Note: Units with $G = c = 1$, $M_2 = M_1$, $m_2 = m_1$, and $v^\phi = u^\phi$.
† Actual value of $j_{total} \equiv J_{total}/M_1M_2$ is 4.287597023.

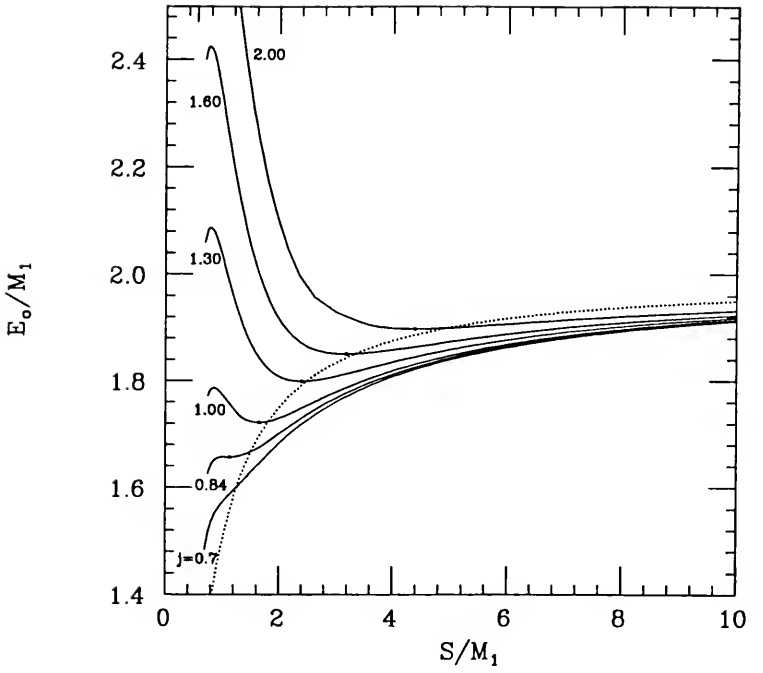

FIGURE 8: Numerical Effective Potential for Equal Mass Black Holes. Stable circular orbits are located at the minima. Unstable circular orbits are located at the maxima. No orbits exist for $J_{total}/M_1M_2 < 0.84$, where J_{total} is the total angular momentum and $M_1 = M_2$ are the irreducible masses of the black holes. The position of the Newtonian stable circular orbits are represented by the dotted line.

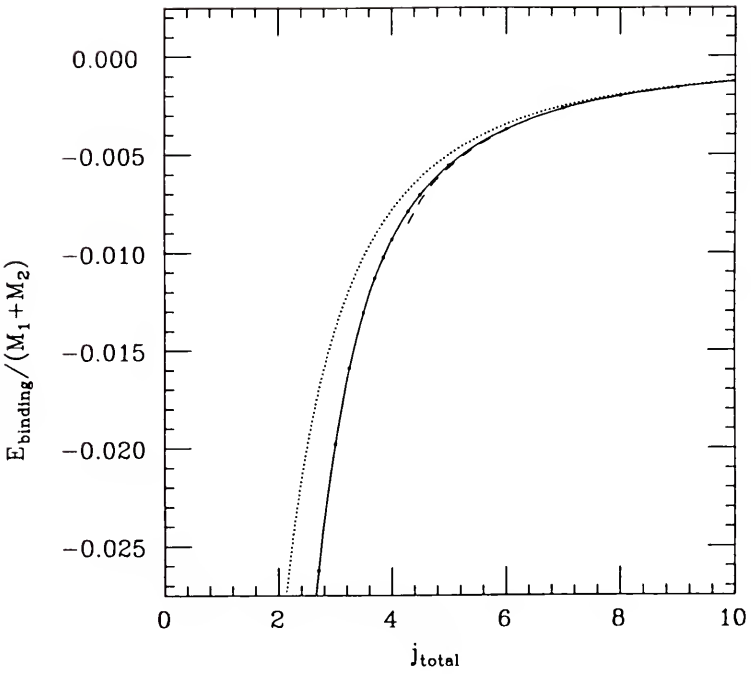

FIGURE 9: Numerical Binding Energy of Equal Mass Black Holes. The binding energy per total mass $(E_o - M_1 - M_2)/(M_1 + M_2)$ of two black holes in stable circular orbits is plotted against the angular momentum $j_{total} = J_{total}/(M_1 M_2)$ for the equal mass case $M_2 = M_1$. The dotted line represents the Newtonian approximation. The dashed line represents the post-Newtonian approximation.

for several values of total angular momentum J_{total}. Since the extremized mass is more accurately determined as a function of the angular momentum, it is useful to compare the numerical binding energy derived from the variational principle of the stable circular orbits as a function of total angular momentum to the values obtained in the Newtonian and post-Newtonian approximations as illustrated in Figure 9 and cataloged in Table 6.

A summary of the results for stable circular orbits found by the three different methods, Newtonian, post-Newtonian, and numerical for equal mass black holes are presented for comparison in Table 6. At the largest tabulated value of the scaled angular momentum, $j_{total} = 20$, the binding energies of the three methods are within $\sim 0.6\%$ of each other. In addition, the post-Newtonian and numerical results are within $\sim 0.03\%$ of each other. Excluding the Newtonian value, the separations between the two black holes are within $\sim 0.04\%$ for this large a value of j_{total}. When the compared to the Newtonian separation, they differ by substantially larger amounts. This results partially from the difference in the gauges. It can be shown that the post-Newtonian's Einstein-Hoffmann-Infeld gauge relates to the Newtonian gauge for equal masses by

$$r_{PN} = \frac{2r_N^2}{(2r_N + 17M)} \tag{5.29}$$

where M is the mass of a single black hole.[47] This accounts for most of the discrepancies at large values of j_{total}. In addition all expressions for the radial separation approach each other at very large values of j_{total}. To provide an example of what is meant by very large values of j_{total}, the planet Mercury orbits the Sun with roughly $j_{total} \approx 3100$. This is at a separation of $s \approx 9.6 \times 10^6$ solar mass units. Yet relativistic effect are observable for Mercury.

TABLE 6: Comparison of Stable Circular Orbits for Equal Masses

	Newtonian		Post-Newtonian		Numerical	
j_{total}	s/M_1	$E_{Binding}/M_1$	s/M_1	$E_{Binding}/M_1$	s/M_1	$E_{Binding}/M_1$
0.80	1.28	0.3906250				
0.84	1.41	0.3543084			1.13	0.3436056
0.85	1.45	0.3460208			1.19	0.3382797
0.90	1.62	0.3086420			1.37	0.3152198
1.00	2.00	0.2500000			1.65	0.2781836
1.30	3.38	0.1479290			2.40	0.2011509
1.50	4.50	0.1111111			2.92	0.1650972
2.00	8.00	0.0625000			4.39	0.1026292
2.50	12.50	0.0400000			6.40	0.0636111
3.00	18.00	0.0277778			9.78	0.0395755
3.50	24.50	0.0204082			15.58	0.0260966
4.00	32.00	0.0156250			23.17	0.0186376
4.29†	36.77	0.0135992	19.81	0.0170059	28.03	0.0157858
4.50	40.50	0.0123457	27.72	0.0147733	31.83	0.0141018
5.00	50.00	0.0100000	39.14	0.0113541	41.46	0.0110997
6.00	72.00	0.0069444	62.42	0.0075077	64.00	0.0074469
7.00	98.00	0.0051020	88.96	0.0053850	89.72	0.0053650
8.00	128.00	0.0039063	119.25	0.0040653	119.82	0.0040562
9.00	162.00	0.0030864	153.43	0.0031830	153.86	0.0031787
10.00	200.00	0.0025000	191.55	0.0025622	191.87	0.0025599
11.00	242.00	0.0020661	233.63	0.0021080	234.32	0.0021067
12.00	288.00	0.0017361	279.70	0.0017654	279.93	0.0017647
13.00	338.00	0.0014793	329.74	0.0015004	330.06	0.0015000
14.00	392.00	0.0012755	383.78	0.0012911	383.90	0.0012909
15.00	450.00	0.0011111	441.81	0.0011229	441.98	0.0011226
17.50	612.50	0.0008163	604.36	0.0008226	604.56	0.0008227
20.00	800.00	0.0006250	791.90	0.0006287	791.59	0.0006289

Note: Units with $G = c = 1$, $M_2 = M_1$. Empty cells are j_{total} without orbits.
† Actual value of $j_{total} \equiv J_{total}/M_1M_2$ is 4.287597023.

Comparisons of the smaller values of j_{total} in Table 6 are restricted by the innermost stable circular orbit of the post-Newtonian approximation at $j_{total} \approx 4.2876$. At this value of the scaled angular momentum, the numerical binding energy differs from the post-Newtonian value by $\sim 7.5\%$. While the same numerical binding energy differs from the Newtonian value by $\sim 14\%$. However, the separations show deviations by as much as $\sim 30\%$ among individual entries at this particular value of j_{total}.

By the time the scaled angular momentum has fall just below the value of $j_{total} \approx 4.0$, at a separation of $s \approx 23M_1$, the binary system satisfies the angular momentum constraints of a Kerr black hole, $J_{total} < M_{total}^2$. The total angular momentum is now small enough for the two black holes to coalesce into one black hole.

5.3 Arbitrary Mass Ratios

When the irreducible masses are comparable but not equal, the only analytic checks that can be made on the numerical results involve the same approximations as in the equal masses case. Tables 7 through 22 list results for irreducible mass ratios ranging from 0.005 to 0.75. All mass ratios were found to have innermost stable orbits. These innermost stable circular orbits will not satisfy the restrictions placed on the secular time scale except in the test particle limit. Thus the exact location for these innermost stable circular orbit have not been determined for these tabulate mass ratios. However, the tables do present several other interesting features. The smallest value of the scaled total angular momenta presented rise abruptly from a mass ratio of 0.02 to the mass ratio of 0.01 used for the test particle comparisons. This reflects

TABLE 7: Numerical Masses for Mass Ratio 0.005

j_{total}	m_1	m_2	M_{total}	$E_\circ$
3.85	0.99969653	0.00469653	1.00501470	1.004780601
4.00	0.99975828	0.00475828	1.00493453	1.004805138
4.50	0.99983888	0.00483888	1.00490563	1.004856914
5.00	0.99987994	0.00487994	1.00491333	1.004888482
6.00	0.99992221	0.00492221	1.00493539	1.004925707
7.00	0.99994448	0.00494448	1.00495136	1.004946719

Note: Units with $G = c = 1$, and $M_2 = 0.005M_1$.
All masses in units of the irreducible mass M_1.
$E_\circ$ is the extremized mass.

TABLE 8: Numerical Orbits for Mass Ratio 0.005

j_{total}	s/M_1	$(E_\circ - M_1)/M_2$	ΩM_1	u^ϕ	v^ϕ
3.85	7.736	0.9561202	0.0608471	0.00249	0.46820
4.00	9.840	0.9610275	0.0401259	0.00203	0.39281
4.50	15.014	0.9713828	0.0198039	0.00150	0.29584
5.00	20.320	0.9776964	0.0120916	0.00123	0.24447
6.00	31.633	0.9851414	0.0060107	0.00095	0.18919
7.00	44.528	0.9893438	0.0035434	0.00079	0.15700

Note: Units with $G = c = 1$, and $M_2 = 0.005M_1$.
M_1 and M_2 are irreducible masses.
$E_\circ$ is the extremized mass.

TABLE 9: Numerical Masses for Mass Ratio 0.02

j_{total}	m_1	m_2	M_{total}	$E_\circ$
2.75	0.99521115	0.01521115	1.03379608	1.015516061
3.00	0.99591166	0.01591166	1.03120167	1.016760196
3.25	0.99646441	0.01646441	1.02935342	1.017763075
3.50	0.99710462	0.01710462	1.02667011	1.018555245
3.70	0.99813953	0.01813953	1.02192645	1.019007721
3.85	0.99887718	0.01887718	1.01990598	1.019143988
4.00	0.99906465	0.01906465	1.01971587	1.019235831
5.00	0.99952583	0.01952583	1.01965901	1.019560807
6.00	0.99969351	0.01969351	1.01974529	1.019707186
7.00	0.99978101	0.01978101	1.01980834	1.019789455

Note: Units with $G = c = 1$, and $M_2 = 0.02M_1$.
All masses in units of the irreducible mass M_1.
$E_\circ$ is the extremized mass.

TABLE 10: Numerical Orbits for Mass Ratio 0.02

j_{total}	s/M_1	$E_{binding}/M_1$	ΩM_1	u^ϕ	v^ϕ
2.75	1.581	0.0044839	0.6018193	0.03494	0.91628
3.00	1.938	0.0032398	0.4749567	0.03107	0.88941
3.25	2.320	0.0022369	0.3837010	0.02810	0.86214
3.50	2.945	0.0014448	0.2836760	0.02383	0.81166
3.70	4.866	0.0009923	0.1351638	0.01523	0.64246
3.85	8.397	0.0008560	0.0531325	0.00918	0.43696
4.00	10.182	0.0007642	0.0381970	0.00786	0.38104
5.00	20.580	0.0004392	0.0119706	0.00486	0.24149
6.00	32.118	0.0002928	0.0059197	0.00374	0.18639
7.00	45.153	0.0002105	0.0034982	0.00310	0.15485

Note: Units with $G = c = 1$, and $M_2 = 0.02M_1$.
M_1 and M_2 are irreducible masses.
$E_\circ$ is the extremized mass.

TABLE 11: Numerical Masses for Mass Ratio 0.03

j_{total}	m_1	m_2	M_{total}	$E_\circ$
2.00	0.98931792	0.01931792	1.06138741	1.016584626
2.50	0.99265326	0.02265326	1.04785160	1.022291645
3.00	0.99451994	0.02451994	1.04264424	1.025799245
3.25	0.99534476	0.02534476	1.04000908	1.027071996
3.50	0.99629503	0.02629503	1.03640449	1.028055840
3.70	0.99784213	0.02784213	1.03074025	1.028552262
3.85	0.99837031	0.02837031	1.02978813	1.028734445
4.00	0.99862660	0.02862660	1.02955457	1.028867896
5.00	0.99929551	0.02929551	1.02949354	1.029347856
6.00	0.99954520	0.02954520	1.02962145	1.029565115
7.00	0.99967752	0.02967752	1.02971454	1.029687245

Note: Units with $G = c = 1$, and $M_2 = 0.03M_1$.
All masses in units of the irreducible mass M_1.
$E_\circ$ is the extremized mass.

TABLE 12: Numerical Orbits for Mass Ratio 0.03

j_{total}	s/M_1	$E_{binding}/M_1$	ΩM_1	u^ϕ	v^ϕ
2.00	0.895	0.0134154	1.1498122	0.06764	0.96094
2.50	1.530	0.0077084	0.6253444	0.04931	0.90771
3.00	2.225	0.0042008	0.4026169	0.04064	0.85516
3.25	2.710	0.0029280	0.3150749	0.03613	0.81757
3.50	3.535	0.0019442	0.2201997	0.02980	0.74871
3.70	6.437	0.0014477	0.0844748	0.01728	0.52652
3.85	8.690	0.0012656	0.0503511	0.01331	0.42424
4.00	10.408	0.0011321	0.0370075	0.01155	0.37361
5.00	20.777	0.0006521	0.0118638	0.00722	0.23927
6.00	32.467	0.0004349	0.0058513	0.00555	0.18443
7.00	46.000	0.0003128	0.0034044	0.00457	0.15204

Note: Units with $G = c = 1$, and $M_2 = 0.03M_1$.
M_1 and M_2 are irreducible masses.
$E_\circ$ is the extremized mass.

TABLE 13: Numerical Masses for Mass Ratio 0.05

j_{total}	m_1	m_2	M_{total}	E_o
2.00	0.98618288	0.03618288	1.07469854	1.032107290
2.50	0.98959226	0.03959226	1.06913405	1.039332489
3.00	0.99216046	0.04216046	1.06402802	1.044097928
3.25	0.99343593	0.04343593	1.06047468	1.045815044
3.50	0.99510707	0.04510707	1.05491658	1.047080584
3.70	0.99681013	0.04681013	1.05033803	1.047672297
3.85	0.99741997	0.04741997	1.04950343	1.047946351
4.00	0.99779170	0.04779170	1.04921957	1.048157502
5.00	0.99885167	0.04885167	1.04916977	1.048934558
6.00	0.99925833	0.04925833	1.04938034	1.049289185
7.00	0.99947298	0.04947298	1.04953321	1.049488741

Note: Units with $G = c = 1$, and $M_2 = 0.05M_1$.
All masses in units of the irreducible mass M_1.
E_o is the extremized mass.

TABLE 14: Numerical Orbits for Mass Ratio 0.05

j_{total}	s/M_1	$E_{binding}/M_1$	ΩM_1	u^ϕ	v^ϕ
2.00	1.291	0.0178927	0.7622651	0.07829	0.90599
2.50	1.882	0.0106675	0.4919043	0.06696	0.85894
3.00	2.668	0.0059021	0.3210902	0.05658	0.80005
3.25	3.287	0.0041850	0.2436785	0.04970	0.75124
3.50	4.587	0.0029194	0.1491445	0.03831	0.64579
3.70	7.314	0.0023277	0.0684667	0.02537	0.47539
3.85	9.166	0.0020536	0.0464748	0.02105	0.40494
4.00	10.797	0.0018425	0.0351909	0.01856	0.36140
5.00	21.246	0.0010654	0.0115760	0.01178	0.23417
6.00	33.183	0.0007108	0.0057129	0.00905	0.18052
7.00	46.912	0.0005113	0.0033378	0.00746	0.14912

Note: Units with $G = c = 1$, and $M_2 = 0.05M_1$.
M_1 and M_2 are irreducible masses.
E_o is the extremized mass.

TABLE 15: Numerical Masses for Mass Ratio 0.10

j_{total}	m_1	m_2	M_{total}	E_o
1.50	0.96942701	0.06942701	1.13189937	1.055075030
2.00	0.97766857	0.07766857	1.12568338	1.072392655
2.50	0.98301146	0.08301146	1.12164905	1.083307383
3.00	0.98746657	0.08746657	1.11471227	1.090556404
3.25	0.98984134	0.08984134	1.10917634	1.093062048
3.50	0.99270186	0.09270186	1.10230585	1.094788009
3.70	0.99447404	0.09447404	1.09944393	1.095656279
3.85	0.99530621	0.09530621	1.09867516	1.096130421
4.00	0.99590759	0.09590759	1.09834592	1.096512528
5.00	0.99781730	0.09781730	1.09840889	1.097968995
6.00	0.99858302	0.09858302	1.09881713	1.098643511
7.00	0.99899478	0.09899478	1.09910846	1.099023876

Note: Units with $G = c = 1$, and $M_2 = 0.10M_1$.
All masses in units of the irreducible mass M_1.
E_o is the extremized mass.

TABLE 16: Numerical Orbits for Mass Ratio 0.10

j_{total}	s/M_1	$E_{binding}/M_1$	ΩM_1	u^ϕ	v^ϕ
1.50	1.101	0.0449250	0.9359655	0.13920	0.89103
2.00	1.700	0.0276073	0.5611091	0.11946	0.83452
2.50	2.402	0.0166926	0.3693877	0.10531	0.78184
3.00	3.446	0.0094436	0.2302418	0.08783	0.70549
3.25	4.377	0.0069380	0.1626380	0.07480	0.63706
3.50	6.305	0.0052120	0.0903454	0.05583	0.51377
3.70	8.501	0.0043437	0.0543652	0.04372	0.41843
3.85	10.105	0.0038696	0.0405219	0.03825	0.37121
4.00	11.670	0.0034875	0.0317865	0.03440	0.33654
5.00	22.359	0.0020310	0.0109701	0.02241	0.22287
6.00	34.737	0.0013565	0.0054660	0.01729	0.17258
7.00	49.191	0.0009761	0.0031821	0.01424	0.14229

Note: Units with $G = c = 1$, and $M_2 = 0.10M_1$.
M_1 and M_2 are irreducible masses.
E_o is the extremized mass.

TABLE 17: Numerical Masses for Mass Ratio 0.25

j_{total}	m_1	m_2	M_{total}	E_o
1.00	0.91749572	0.16749572	1.27236282	1.119868108
1.50	0.94351167	0.19351167	1.27376855	1.172302223
2.00	0.95818493	0.20818493	1.27628112	1.201679315
2.50	0.96874165	0.21874165	1.27222378	1.220490492
3.00	0.97798722	0.22798722	1.26099682	1.232518093
3.25	0.98261884	0.23261884	1.25375920	1.236433004
3.50	0.98664235	0.23664235	1.24865925	1.239162147
3.70	0.98899046	0.23899046	1.24678896	1.240728389
3.85	0.99032198	0.24032198	1.24616044	1.241659789
4.00	0.99138940	0.24138940	1.24588521	1.242439740
5.00	0.99524254	0.24524254	1.24647167	1.245545408
6.00	0.99689374	0.24689374	1.24739243	1.247018742
7.00	0.99779160	0.24779160	1.24803711	1.247853748

Note: Units with $G = c = 1$, and $M_2 = 0.25M_1$.
All masses in units of the irreducible mass M_1.
E_o is the extremized mass.

TABLE 18: Numerical Orbits for Mass Ratio 0.25

j_{total}	s/M_1	$E_{binding}/M_1$	ΩM_1	u^ϕ	v^ϕ
1.00	0.931	0.1301319	1.2124576	0.28080	0.84839
1.50	1.616	0.0776978	0.6229878	0.23882	0.76799
2.00	2.385	0.0483207	0.3870633	0.21371	0.70953
2.50	3.390	0.0295095	0.2453116	0.18698	0.64452
3.00	5.065	0.0174819	0.1371181	0.14972	0.54472
3.25	6.575	0.0135670	0.0903202	0.12477	0.46912
3.50	8.740	0.0108379	0.0561351	0.10096	0.38964
3.70	10.734	0.0092716	0.0396855	0.08680	0.33919
3.85	12.296	0.0083402	0.0315972	0.07880	0.30971
4.00	13.896	0.0075603	0.0257684	0.07240	0.28569
5.00	25.652	0.0044546	0.0095039	0.04890	0.19489
6.00	39.618	0.0029813	0.0047840	0.03795	0.15158
7.00	55.978	0.0021463	0.0027955	0.03132	0.12517

Note: Units with $G = c = 1$, and $M_2 = 0.25M_1$.
M_1 and M_2 are irreducible masses.
E_o is the extremized mass.

TABLE 19: Numerical Masses for Mass Ratio 0.50

j_{total}	m_1	m_2	M_{total}	E_o
0.80	0.83684048	0.33684048	1.52902426	1.252472405
0.83	0.84358456	0.34358456	1.51964016	1.262647030
0.84	0.84550107	0.34550107	1.51791192	1.265832485
0.86	0.84960450	0.34960450	1.51312388	1.271950636
0.88	0.85280116	0.35280116	1.51194069	1.277757531
0.90	0.85610483	0.35610483	1.51001902	1.283287716
1.00	0.86995908	0.36995908	1.50704021	1.307633153
1.50	0.91172222	0.41172222	1.51976045	1.385011755
2.00	0.93566766	0.43566766	1.52545804	1.428501109
2.50	0.95292775	0.45292775	1.51983104	1.455911098
3.00	0.96759739	0.46759739	1.50575813	1.472954303
3.50	0.97935488	0.47935488	1.49483587	1.482426376
4.00	0.98604687	0.48604687	1.49270298	1.487524095
5.00	0.99212891	0.49212891	1.49408400	1.492592825
6.00	0.99483686	0.49483686	1.49564738	1.495035123
7.00	0.99632427	0.49632427	1.49672629	1.496423778

Note: Units with $G = c = 1$, and $M_2 = 0.50M_1$.
All masses in units of the irreducible mass M_1.
E_o is the extremized mass.

TABLE 20: Numerical Orbits for Mass Ratio 0.50

j_{total}	s/M_1	$E_{binding}/M_1$	ΩM_1	u^ϕ	v^ϕ
0.80	0.864	0.2475276	1.4966484	0.48416	0.80868
0.83	0.927	0.2373530	1.3625346	0.46896	0.79345
0.84	0.945	0.2341675	1.3270032	0.46514	0.78938
0.86	0.987	0.2280494	1.2515638	0.45611	0.77978
0.88	1.022	0.2222425	1.1978199	0.45067	0.77348
0.90	1.059	0.2167123	1.1430301	0.44449	0.76635
1.00	1.237	0.1923668	0.9363742	0.42123	0.73753
1.50	2.126	0.1149882	0.4757421	0.36085	0.65063
2.00	3.168	0.0714989	0.2860676	0.31964	0.58669
2.50	4.585	0.0440889	0.1725007	0.27509	0.51575
3.00	6.982	0.0270457	0.0908495	0.21677	0.41751
3.50	11.370	0.0175736	0.0405442	0.15526	0.30572
4.00	17.174	0.0124759	0.0203963	0.11729	0.23300
5.00	31.016	0.0074072	0.0078222	0.08098	0.16163
6.00	47.673	0.0049649	0.0039705	0.06313	0.12616
7.00	67.266	0.0035762	0.0023254	0.05215	0.10426

Note: Units with $G = c = 1$, and $M_2 = 0.50M_1$.
M_1 and M_2 are irreducible masses.
E_o is the extremized mass.

TABLE 21: Numerical Masses for Mass Ratio 0.75

j_{total}	m_1	m_2	M_{total}	E_o
0.82	0.78322430	0.53322430	1.84229277	1.446064194
0.83	0.78940386	0.53940386	1.81975573	1.450800478
0.84	0.79394315	0.54394315	1.80662714	1.455263913
0.86	0.80098080	0.55098080	1.79119016	1.463613948
0.88	0.80715847	0.55715847	1.78008201	1.471379824
0.90	0.81221052	0.56221052	1.77396050	1.478675615
1.00	0.83246008	0.58246008	1.76029885	1.510134604
1.50	0.88836870	0.63836870	1.76961585	1.607389908
2.00	0.91931986	0.66931986	1.77628956	1.661346226
2.50	0.94142692	0.69142692	1.76944950	1.695104326
3.00	0.95984375	0.70984375	1.75358352	1.715932396
3.50	0.97401575	0.72401575	1.74245215	1.727591551
4.00	0.98222554	0.73222554	1.74044445	1.734012927
5.00	0.98990091	0.73990091	1.74238088	1.740484339
6.00	0.99336337	0.74336337	1.74440238	1.743618175
7.00	0.99527678	0.74527678	1.74578981	1.745402830

Note: Units with $G = c = 1$, and $M_2 = 0.75M_1$.
All masses in units of the irreducible mass M_1.
E_o is the extremized mass.

TABLE 22: Numerical Orbits for Mass Ratio 0.75

j_{total}	s/M_1	$E_{binding}/M_1$	ΩM_1	u^ϕ	v^ϕ
0.82	0.963	0.3039358	1.4526745	0.63183	0.76752
0.83	1.011	0.2991995	1.3524250	0.61504	0.75220
0.84	1.048	0.2947361	1.2837045	0.60368	0.74153
0.86	1.109	0.2863861	1.1848341	0.58765	0.72604
0.88	1.166	0.2786202	1.1035990	0.57415	0.71267
0.90	1.216	0.2713244	1.0420676	0.56431	0.70265
1.00	1.447	0.2398654	0.8246488	0.52854	0.66476
1.50	2.540	0.1426101	0.4000700	0.44618	0.57004
2.00	3.813	0.0886538	0.2360295	0.39338	0.50668
2.50	5.557	0.0548957	0.1396559	0.33741	0.43859
3.00	8.484	0.0340676	0.0726496	0.26633	0.35000
3.50	13.570	0.0224084	0.0333776	0.19480	0.25813
4.00	20.232	0.0159871	0.0171888	0.14927	0.19848
5.00	36.262	0.0095157	0.0066826	0.10390	0.13842
6.00	55.633	0.0063818	0.0034033	0.08116	0.10817
7.00	78.522	0.0045972	0.0019915	0.06703	0.08935

Note: Units with $G = c = 1$, and $M_2 = 0.75M_1$.
M_1 and M_2 are irreducible masses.
E_o is the extremized mass.

the trend towards tightly bound innermost stable orbits that mass ratios above 0.02 have in common with the case of equal masses. Below a mass ratio of $\sim$ 0.01 the numerical results compare favorably to the analytic test particle values as seen in Tables 7 and 8. In addition, it is interesting to note in Tables 19 and 20 that the mass ratio having the lowest scaled total angular momentum is 0.50 with a scaled total angular momentum of $j_{total} \approx 0.80$. The energy of the system in these tables is presented as the binding energy in all cases except the mass ratio of 0.005 which is represented as the energy per mass to be consistent with the test particle description. Notice that this mass ratio has an energy per mass of 0.9561202 for the same scaled angular momentum of $j_{total} = 3.85$. This is only 0.04% different from the value for the mass ratio of 0.01 given in Table 4.

5.4 Gravitational Radiation

Introducing the global time symmetry forces the two black holes into stationary orbits. This approximation to the true geometry of the binary black hole system will accurately model the the actual geometry as long as the time scale for secular effects due to gravitational radiation reaction are large when compared to the dynamical time scale. To determine the magnitude of the secular effects the energy and angular momentum carried away by the gravitational radiation must be approximated.

Systems interacting through purely gravitational exchanges will not exhibit dipole radiation. This is because the dipole moment couples to the linear and angular momenta of the sources and the total linear and angular momenta are conserved in a gravitational system. However, the next higher moment,

the quadrupole moment, will in general radiate away energy and momentum. The reduced quadrupole moment for a distribution of mass is given by

$$\begin{aligned} \mathcal{I}_{jk} &\equiv \sum_{\ell} m_{\ell} \left(x_{\ell j} x_{\ell k} - \frac{1}{3} \delta_{jk} r_{\ell}^2 \right) \\ &= \int \rho \left(x_j x_k - \frac{1}{3} \delta_{jk} r^2 \right) d^3x \ . \end{aligned} \tag{5.30}$$

The total power radiated, or the dimensionless luminosity, in the form of gravitational quadrupole radiation is given by

$$L_{GW} = \frac{dE_{GW}}{dt} = \frac{1}{5} \left\langle \frac{d^3\mathcal{I}_{jk}}{dt^3} \frac{d^3\mathcal{I}_{jk}}{dt^3} \right\rangle \ . \tag{5.31}$$

The total angular momentum radiated away by the gravitational quadrupole radiation is given by

$$\frac{dJ^i_{GW}}{dt} = \frac{2}{5} \epsilon^{ijk} \left\langle \frac{d^2\mathcal{I}_{j\ell}}{dt^2} \frac{d^3\mathcal{I}_{\ell k}}{dt^3} \right\rangle \tag{5.32}$$

where the angle brackets $\langle \ \rangle$ represent averaging over several characteristic cycles of the source since the energy of gravitational radiation can not be localized to within a wavelength.

For two black holes in circular orbits about each other, the mass-energy density ρ appearing in equation (5.30) is given by

$$\rho = m_1 \delta^3(\vec{x} - \vec{x}_{o_1}) + m_2 \delta^3(\vec{x} - \vec{x}_{o_2}) \tag{5.33}$$

where m_1 and m_2 are the masses of the two black holes located at $\vec{x}_{o_1}$ and $\vec{x}_{o_2}$. Evaluating equation (5.30) for this mass energy density in Cartesian coordinates gives the following components to the quadrupole moment for the binary black holes:

$$\mathcal{I}_{xx} = m_1 x_{o_1}^2 \left(cos^2(\Omega t) - \frac{1}{3} \right) + m_2 x_{o_2}^2 \left(cos^2(\Omega t) - \frac{1}{3} \right) \tag{5.34}$$

$$\mathcal{I}_{yy} = m_1 x_{o_1}^2 \left(sin^2(\Omega t) - \frac{1}{3} \right) + m_2 x_{o_2}^2 \left(sin^2(\Omega t) - \frac{1}{3} \right) \tag{5.35}$$

$$\mathcal{I}_{zz} = -\frac{1}{3} \left(m_1 x_{o_1}^2 + m_2 x_{o_2}^2 \right) \tag{5.36}$$

$$\mathcal{I}_{xy} = \mathcal{I}_{yx} = m_1 x_{o_1}^2 \left(cos(\Omega t) sin(\Omega t) \right) + m_2 x_{o_2}^2 \left(cos(\Omega t) sin(\Omega t) \right) \tag{5.37}$$

$$\mathcal{I}_{xz} = \mathcal{I}_{zx} = 0 \tag{5.38}$$

$$\mathcal{I}_{yz} = \mathcal{I}_{zy} = 0 \ . \tag{5.39}$$

Equations (5.31) and (5.32) for the rate of energy and angular momentum loss require the second and third time derivatives of the quadrupole moment $\mathcal{I}_{jk}$. The second derivative with respect to time generates the following components:

$$\frac{d^2 \mathcal{I}_{xx}}{dt^2} = -2\Omega^2 \left(m_1 x_{o_1}^2 + m_2 x_{o_2}^2 \right) cos(2\Omega t) \tag{5.40}$$

$$\frac{d^2 \mathcal{I}_{yy}}{dt^2} = 2\Omega^2 \left(m_1 x_{o_1}^2 + m_2 x_{o_2}^2 \right) cos(2\Omega t) \tag{5.41}$$

$$\frac{d^2 \mathcal{I}_{zz}}{dt^2} = 0 \tag{5.42}$$

$$\frac{d^2 \mathcal{I}_{xy}}{dt^2} = \frac{d^2 \mathcal{I}_{yx}}{dt^2} = -2\Omega^2 \left(m_1 x_{o_1}^2 + m_2 x_{o_2}^2 \right) sin(2\Omega t) \tag{5.43}$$

$$\frac{d^2 \mathcal{I}_{xz}}{dt^2} = \frac{d^2 \mathcal{I}_{zx}}{dt^2} = 0 \ . \tag{5.44}$$

The third derivative with respect to time generates the following components:

$$\frac{d^3\mathcal{I}_{xx}}{dt^3} = 4\Omega^3\left(m_1 x_{o_1}^2 + m_2 x_{o_2}^2\right) sin(2\Omega t) \tag{5.45}$$

$$\frac{d^3\mathcal{I}_{yy}}{dt^3} = -4\Omega^3\left(m_1 x_{o_1}^2 + m_2 x_{o_2}^2\right) sin(2\Omega t) \tag{5.46}$$

$$\frac{d^3\mathcal{I}_{zz}}{dt^3} = 0 \tag{5.47}$$

$$\frac{d^3\mathcal{I}_{xy}}{dt^3} = \frac{d^3\mathcal{I}_{yx}}{dt^3} = -4\Omega^3\left(m_1 x_{o_1}^2 + m_2 x_{o_2}^2\right) cos(2\Omega t) \tag{5.48}$$

$$\frac{d^2\mathcal{I}_{xz}}{dt^2} = \frac{d^2\mathcal{I}_{zx}}{dt^2} = 0\ . \tag{5.49}$$

Substitution into equation (5.31), the dimensionless luminosity is found to be

$$\begin{aligned} L_{GW} &= \frac{1}{5}\left\langle \frac{d^3\mathcal{I}_{xx}}{dt^3} + \frac{d^3\mathcal{I}_{yy}}{dt^3} + \frac{d^3\mathcal{I}_{xy}}{dt^3} + \frac{d^3\mathcal{I}_{yx}}{dt^3} \right\rangle \\ &= \frac{32}{5}\Omega^6\left(m_1 x_{o_1}^2 + m_2 x_{o_2}^2\right)^2 \left\langle sin^2(2\Omega t) + cos^2(2\Omega t)\right\rangle \\ &= \frac{32}{5}\mu^2 s^4 \Omega^6 \end{aligned} \tag{5.50}$$

where μ is the reduced mass of the system and s is the separation between the two black holes. Next substitute into equation (5.32) to find the rate at which the system losses angular momentum

$$\frac{dJ_{GW}^x}{dt} = 0 \tag{5.51}$$

$$\frac{dJ_{GW}^y}{dt} = 0 \tag{5.52}$$

$$\frac{dJ^z_{GW}}{dt} = \frac{2}{5}\left\langle \frac{d^2\mathcal{I}_{xx}}{dt^2}\frac{d^3\mathcal{I}_{xy}}{dt^3} + \frac{d^2\mathcal{I}_{xy}}{dt^2}\frac{d^3\mathcal{I}_{yy}}{dt^3} - \frac{d^2\mathcal{I}_{yx}}{dt^2}\frac{d^3\mathcal{I}_{xx}}{dt^3} - \frac{d^2\mathcal{I}_{yy}}{dt^2}\frac{d^3\mathcal{I}_{yx}}{dt^3}\right\rangle$$
$$= \frac{32}{5}\Omega^5\left(m_1 x^2_{o_1} + m_2 x^2_{o_2}\right)^2\left\langle sin^2(2\Omega t) + cos^2(2\Omega t)\right\rangle$$
$$= \frac{32}{5}\mu^2 s^4 \Omega^5 \ . \tag{5.53}$$

The x and y components are naturally zero since the motion of the two black holes is restricted to the $x-y$ plane. The results for equations (5.50) and (5.53) reveal the following relationship between the luminosity and the magnitude of the rate of angular momentum loss for a gravitational system

$$L_{GW} = \Omega\left(\frac{dJ_{GW}}{dt}\right) \ . \tag{5.54}$$

The application of equation (5.50) to the extremized geometries having scaled angular momenta over the range of stable circular orbits allows for a measure of the accuracy that a particular solution has to the actual physical binary system of black holes. These dimensionless luminosities are listed in Table 23 and plotted in Figure 10 for equal mass black holes. The luminosity reaches a value of $L_{GW} \approx 1$ at a scaled angular momentum of $j_{total} \approx 1$, and at a separation of $s \approx 1.7M_1$. This is to large a luminosity to consider the results accurate. A more reasonable limit on the luminosity might be $L_{GW} \approx 0.01$. This occurs at $j_{total} \approx 2.40$, at a separation of $s \approx 5.9M_1$.

Also useful in determining a comparison of the secular time scale to the dynamic time scale is the approximation to the energy radiated away per orbit given by $(\frac{2\pi}{\Omega})L_{GW}$. This quantity becomes comparable to the binding energy at a scaled angular momentum of $j_{total} \approx 3.25$, at a separation of $s \approx 12.4M_1$. This is where one orbit loses roughly the same amount of energy in the form

TABLE 23: Gravitational Quadrupole Radiation for Equal Masses

j_{total}	s/M_1	μ/M_1	ΩM_1	L_{GW}	$(2\pi/\Omega)L_{GW}$‡	$E_{Binding}$‡
0.84	1.13	0.37535	1.25e+00	5.48e+00	2.77e+01	0.34361
0.85	1.19	0.37917	1.15e+00	4.32e+00	2.36e+01	0.33828
0.90	1.37	0.38945	9.39e-01	2.36e+00	1.58e+01	0.31522
1.00	1.65	0.40200	7.30e-01	1.16e+00	9.99e+00	0.27818
1.30	2.40	0.42485	4.47e-01	3.08e-01	4.34e+00	0.20115
1.50	2.92	0.43510	3.49e-01	1.58e-01	2.85e+00	0.16510
1.60	3.19	0.43941	3.11e-01	1.16e-01	2.34e+00	0.14995
2.00	4.39	0.45319	2.05e-01	3.60e-02	1.10e+00	0.10263
2.20	5.10	0.45873	1.67e-01	1.97e-02	7.41e-01	0.08486
2.40	5.93	0.46373	1.35e-01	1.03e-02	4.78e-01	0.07005
2.50	6.40	0.46607	1.21e-01	7.23e-03	3.76e-01	0.06361
2.60	6.93	0.46834	1.07e-01	4.95e-03	2.90e-01	0.05776
2.70	7.52	0.47054	9.49e-02	3.30e-03	2.19e-01	0.05246
3.00	9.78	0.47676	6.26e-02	8.04e-04	8.06e-02	0.03958
3.25	12.38	0.48129	4.25e-02	2.06e-04	3.04e-02	0.03180
3.50	15.58	0.48491	2.90e-02	5.23e-05	1.14e-02	0.02610
3.70	18.46	0.48715	2.18e-02	1.91e-05	5.49e-03	0.02262
3.85	20.76	0.48851	1.80e-02	9.52e-06	3.33e-03	0.02047
4.00	23.17	0.48965	1.50e-02	5.02e-06	2.10e-03	0.01864
4.29†	28.03	0.49139	1.10e-02	1.67e-06	9.54e-04	0.01579
4.50	31.83	0.49238	8.93e-03	8.07e-07	5.68e-04	0.01410
5.00	41.46	0.49411	5.84e-03	1.84e-07	1.98e-04	0.01110
6.00	64.00	0.49615	2.94e-03	1.70e-08	3.64e-05	0.00745
7.00	89.72	0.49724	1.74e-03	2.88e-09	1.04e-05	0.00537
8.00	119.82	0.49793	1.12e-03	6.34e-10	3.57e-06	0.00406
9.00	153.86	0.49839	7.62e-04	1.74e-10	1.43e-06	0.00318
10.00	191.87	0.49870	5.44e-04	5.59e-11	6.46e-07	0.00256
11.00	234.32	0.49894	4.01e-04	2.00e-11	3.13e-07	0.00211
12.00	279.93	0.49911	3.07e-04	8.12e-12	1.67e-07	0.00176
13.00	330.06	0.49924	2.39e-04	3.52e-12	9.25e-08	0.00150
14.00	383.90	0.49935	1.90e-04	1.64e-12	5.41e-08	0.00129
15.00	441.98	0.49944	1.54e-04	8.02e-13	3.28e-08	0.00112
17.50	604.56	0.49959	9.58e-05	1.65e-13	1.08e-08	0.00082
20.00	791.59	0.49968	6.39e-05	4.25e-14	4.19e-09	0.00063
25.00	1241.91	0.49980	3.24e-05	4.42e-15	8.56e-10	0.00040
50.00	4991.19	0.49995	4.01e-06	4.16e-18	6.50e-12	0.00010

Note: Units with $G = c = 1$.

† Actual value of $j_{total} \equiv J_{total}/M_1M_2$ is 4.287597023.

‡ In units of the irreducible mass M_1.

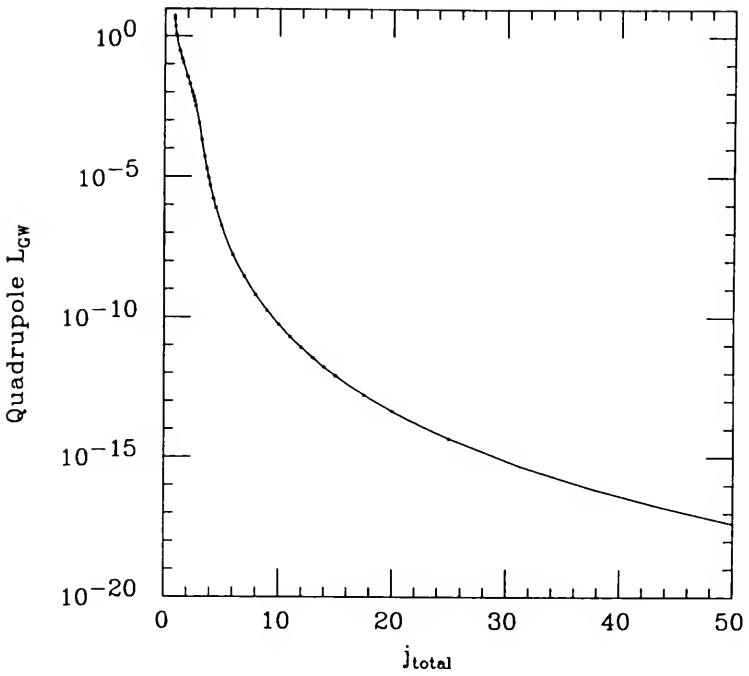

FIGURE 10: Quadrupole Radiation from Equal Mass Black Holes. The quadrupole approximation to the gravitation radiation from two black holes in circular orbits is plotted against the angular momentum $j_{total} = J_{total}/(M_1 M_2)$ for the equal mass case $M_2 = M_1$.

of gravitational quadrupole radiation as the system has lost throughout its entire evolution.

The secular time scale can also be compared with the dynamic time scale by comparing the radial component of the velocity of each black hole to the tangential component of the velocity. This can be accomplished by considering a plot of the binding energy of each stable circular orbit as a function of the separation between the two black holes as in Figure 11, for the equal mass black holes. As the black holes spiral in from their mutual energy and angular momentum loses, they will slowly move inward from a quasi-stable orbit. The change in the binding energy must account for the luminosity of the gravitational radiation to conserve energy. Thus the following definition emerges

$$\frac{ds}{dt} = \left(\frac{dE_{binding}}{dt}\right)\left(\frac{dE_{binding}}{ds}\right)^{-1} \tag{5.55}$$

where the $\left(\frac{dE}{ds}\right)$ term on the right hand side of equation (5.55) is taken from the plot. The $\left(\frac{dE}{dt}\right)$ term is given by the dimensionless Luminosity of equation (5.50). In the case of equal mass black holes the $\left(\frac{ds}{dt}\right)$ is roughly twice the radial component of the velocity. Thus the radial velocity is approximated by

$$v_{radial} \approx \frac{1}{2}\left(\frac{L_{GW}}{\left(\frac{dE_{binding}}{ds}\right)}\right) \tag{5.56}$$

for two equal mass black holes. The numerical results for the radial and tangential components of the velocity are shown in Figure 12. The radial component is smaller than the tangential component for separations larger than $s \approx 5.9M_1$. At roughly this separation the scaled angular momentum has a value of $j_{total} \approx 2.40$ and the dimensionless luminosity for the quadrapole gravitational radiation has a value of $L_{GW} \approx 0.01$, providing stronger justification for the previously discussed limit for the luminosity.

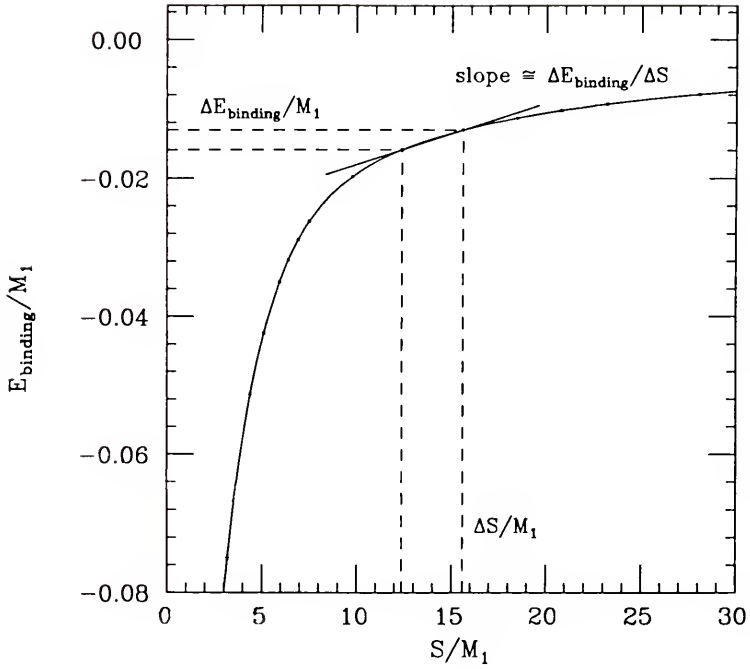

FIGURE 11: Numerical Binding Energy versus Separation. The binding energy per mass M_1 is plotted for the stable circular orbits of equal mass black holes as a function of their separation s/M_1. The slope at any point along this curve is used in conjunction with the luminosity to determine the radial velocity of the black holes.

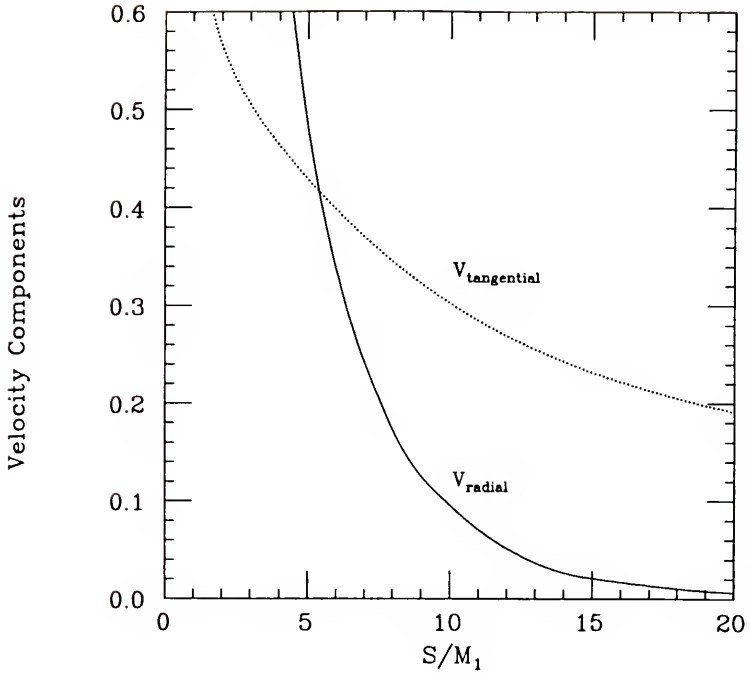

FIGURE 12: Numerical Components of Velocity. The radial and tangential components of the velocity for the equal mass black holes as a function of the separation between the two equal mass black holes in quasi-stable orbits.

5.5 Apparent Horizons

During the true evolution of the binary system of two black holes energy and total angular momentum are lost through the emission of gravitational radiation. The dimensionless luminosity of this radiation increases as the binary system becomes more tightly bound. Eventually, the time scale for the spiralling collapse becomes comparable to an orbital period. Assuming at this stage of the evolution that the total angular momentum of the binary system is less than the total mass of the binary system, the two black holes will coalesce, destined to become a single axisymmetric Kerr black hole.

The coalescence of two black holes into one is marked by the presence of an event horizon enclosing both black holes. Since the determination of the event horizon requires knowledge of the global structure of the space-time geometry and since the initial data is given on a partial Cauchy surface in the variational method, it is not possible to determine the event horizon from the numerical results. Even if the global structure of the space-time was derivable, the limitations of numerical calculations make specification of the event horizon difficult.

However, the apparent horizon can be specified on any space-like hypersurface without knowing the global structure of space-time. When a space-time is stationary the apparent horizon will coincide with the event horizon, but in general the existence of an apparent horizon implies the existence of an event horizon either outside or coinciding with its surface.[34]

The apparent horizon is a two dimensional surface characterized by having outgoing orthogonal null geodesics with zero convergence ρ_e which satisfies

$$\rho_e = \Re e \left(m^\nu \bar{m}^\nu \nabla_\nu l_\mu \right) = 0 \tag{5.57}$$

where m^μ is a complex null vector over the two dimensional surface, $\bar{m}^\mu$ is its complex conjugate, and l^μ is an outgoing null vector spanning the same two dimensional surface. This can be put into a more useful form for numerical relativity involving the geometric quantities on the hypersurface Σ_τ. Consider a space-like unit vector s^μ lying in Σ_τ and everywhere orthogonal to the apparent horizon, then s^μ will satisfy the following equations

$$\gamma_{\mu\nu} s^\mu s^\nu = 1 \tag{5.58}$$

$$\mathrm{D}_\mu s^\mu - K^\nu{}_\nu + K_{\mu\nu} s^\mu s^\nu = 0 \tag{5.59}$$

where D_μ is the covariant derivative on the hypersurface Σ_τ, and $K_{\mu\nu}$ is the extrinsic curvature tensor.

For time symmetric black hole solutions, the extrinsic curvature $K_{\mu\nu} = 0$. This reduces equation (5.59) to

$$\mathrm{D}_\mu s^\mu = 0 \tag{5.60}$$

which is the equation for a minimal (or extremal) surface. In the time symmetric solutions, the outermost apparent horizon is a minimal surface and will have less area than the event horizon. This provides for a means, via the area theorem, to place an upper bound on the amount of gravitational radiation emitted. The apparent horizons of two equal mass black holes in the time symmetric approximation have been investigated extensively in the literature. It has been found that the apparent horizon encloses the two black holes when their separation reaches $1.53m$, where m is the mass of either hole and the maximum energy available for gravitational radiation has been found to be 1.16% of the total initial rest mass of the two black holes.[45,49,50,51] While the time

symmetric solutions are far from being the correct geometry for an evolving binary black hole system, these numbers are useful for comparisons.

The method of actually finding the apparent horizons in a three dimensional numerical relativity solution[52] for a space-time geometry consists of introducing a scalar function $\mathcal{T}$ on the hypersurface Σ_τ defined by

$$\mathcal{T}(r,\theta,\phi) = r - \mathcal{H}(\theta,\phi) \tag{5.61}$$

where $\mathcal{H}(\theta,\phi)$ can be written as a series expansion in spherical harmonics

$$\mathcal{H}(\theta,\phi) = \sum_{\ell=0}^{\infty}\sum_{m=-\ell}^{\ell} c_{\ell m} Y_{\ell m}(\theta,\phi)\ . \tag{5.62}$$

The gradient of this scalar function points in the direction of the normal vector to the apparent horizon s^μ determined by

$$s_\nu = \frac{\mathrm{D}_\nu \mathcal{T}}{\sqrt{(\mathrm{D}_\sigma \mathcal{T})(\mathrm{D}^\sigma \mathcal{T})}}\ . \tag{5.63}$$

The apparent horizon is defined by the vanishing of the scalar function

$$\mathcal{T}(r,\theta,\phi) = 0 \tag{5.64}$$

which gives the radial coordinate to any point having angular coordinates (θ,ϕ) as being

$$r = \mathcal{H}(\theta,\phi) = \sum_{\ell=0}^{\infty}\sum_{m=-\ell}^{\ell} c_{\ell m} Y_{\ell m}(\theta,\phi)\ . \tag{5.65}$$

Substituting $\mathcal{T}(r,\theta,\phi)$ into equation (5.59) gives after a bit of algebra, the following equation for the apparent horizon

$$\begin{aligned}\mathrm{D}^\mu \mathrm{D}_\mu \mathcal{T} &= \mathrm{D}^\mu \mathrm{D}_\mu \mathcal{T} \\ &+ \sum_{\mu\neq\nu}\left\{\frac{(\mathrm{D}_\mu \mathcal{T})(\mathrm{D}_\nu \mathcal{T})(\mathrm{D}^\mu \mathrm{D}_\nu \mathcal{T})}{(\mathrm{D}_\sigma \mathcal{T})(\mathrm{D}^\sigma \mathcal{T})} - \frac{K^{\mu\nu}(\mathrm{D}_\mu \mathcal{T})(\mathrm{D}_\nu \mathcal{T})}{\sqrt{(\mathrm{D}_\sigma \mathcal{T})(\mathrm{D}^\sigma \mathcal{T})}}\right\}\ .\end{aligned} \tag{5.66}$$

This peculiar form of equation (5.59) will become extremely useful in an iterative scheme to be developed, but first consider the common term appearing on both sides of equation (5.66):

$$\begin{aligned} \mathrm{D}^{\mu}\mathrm{D}_{\mu}\mathcal{T} = &-\frac{1}{2}\left(\frac{\partial ln(\gamma)}{\partial x^{\mu}}\right)\left(\frac{\partial \mathcal{T}}{\partial x^{\nu}}\right)\gamma^{\mu\nu} \\ &+\left(\frac{\partial \gamma^{\mu\nu}}{\partial x^{\mu}}\right)\left(\frac{\partial \mathcal{T}}{\partial x^{\nu}}\right)+\gamma^{\mu\nu}\left(\frac{\partial^2 \mathcal{T}}{\partial x^{\mu}\partial x^{\nu}}\right) \end{aligned} \tag{5.67}$$

where $\gamma = det(\gamma_{\mu\nu})$. The last term on the right hand side of equation (5.67) contains the flat Laplacian differential operator ∇^2. By substituting equation (5.67) into both sides of equation (5.66) and cancelling all terms from both sides except a term proportional to the flat Laplacian, which is scaled by Ψ^{-4}, the following equation for the apparent horizon develops:

$$\begin{aligned} \Psi^{-4}\nabla^2\mathcal{T} = &\ \Psi^{-4}\nabla^2\mathcal{T} \\ &+\sum_{\mu\neq\nu}\left\{\frac{(\mathrm{D}_{\mu}\mathcal{T})(\mathrm{D}_{\nu}\mathcal{T})(\mathrm{D}^{\mu}\mathrm{D}_{\nu}\mathcal{T})}{(\mathrm{D}_{\sigma}\mathcal{T})(\mathrm{D}^{\sigma}\mathcal{T})}-\frac{K^{\mu\nu}(\mathrm{D}_{\mu}\mathcal{T})(\mathrm{D}_{\nu}\mathcal{T})}{\sqrt{(\mathrm{D}_{\sigma}\mathcal{T})(\mathrm{D}^{\sigma}\mathcal{T})}}\right\} \end{aligned} \tag{5.68}$$

where the actual choice of Ψ is somewhat arbitrary, but in order to convey more information about the hypersurface, it is chosen to be the conformal factor given in equation (4.18). The action of the flat Laplacian operator ∇^2 on the scalar function $\mathcal{T}$ gives

$$\begin{aligned} \nabla^2\mathcal{T}(r,\theta,\phi) &= \nabla^2\left(r-\mathcal{H}(\theta,\phi)\right) \\ &= \frac{2}{r}-\frac{1}{r^2}\left[\frac{1}{sin\theta}\frac{\partial}{\partial\theta}\left(sin\theta\frac{\partial\mathcal{H}}{\partial\theta}\right)+\frac{1}{sin^2\theta}\frac{\partial^2\mathcal{H}}{\partial\phi^2}\right] \\ &= \frac{2}{r}-\frac{1}{r^2}\left[\sum_{\ell=0}^{\infty}\sum_{m=-\ell}^{\ell}\ell(\ell+1)c_{\ell m}Y_{\ell m}(\theta,\phi)\right]. \end{aligned} \tag{5.69}$$

By substituting equation (5.69) into both sides of equation (5.68) and performing a little algebra, the equation for the apparent horizon becomes

$$\begin{aligned} \sum_{\ell=0}^{\infty}\sum_{m=-\ell}^{\ell}\ell(\ell+1)c_{\ell m}Y_{\ell m}(\theta,\phi) = &\sum_{\ell=0}^{\infty}\sum_{m=-\ell}^{\ell}\ell(\ell+1)c_{\ell m}Y_{\ell m}(\theta,\phi) \\ &-r^2\Psi^4\sum_{\mu\neq\nu}\left\{\frac{(\mathrm{D}_{\mu}\mathcal{T})(\mathrm{D}_{\nu}\mathcal{T})(\mathrm{D}^{\mu}\mathrm{D}_{\nu}\mathcal{T})}{(\mathrm{D}_{\sigma}\mathcal{T})(\mathrm{D}^{\sigma}\mathcal{T})}-\frac{K^{\mu\nu}(\mathrm{D}_{\mu}\mathcal{T})(\mathrm{D}_{\nu}\mathcal{T})}{\sqrt{(\mathrm{D}_{\sigma}\mathcal{T})(\mathrm{D}^{\sigma}\mathcal{T})}}\right\}. \end{aligned} \tag{5.70}$$

Now multiply both sides of equation (5.70) by $Y^*_{\ell' m'}(\theta,\phi) sin\theta d\theta d\phi$ and integrate over the two-sphere. The result is

$$c_{\ell m} = c_{\ell m} - \frac{1}{\ell(\ell+1)} \int_0^{2\pi} \int_0^{\pi} Y^*_{\ell m}(\theta,\phi) \left\{ r^2 \Psi^4 F(r,\theta,\phi) \right\}_{\{r=\mathcal{H}\}} sin\theta d\theta d\phi \quad (5.71)$$

where the function $F(r,\theta,\phi)$ appearing in the integrand is given by

$$F(r,\theta,\phi) = \sum_{\mu \neq \nu} \left[\frac{(\mathrm{D}_\mu \mathcal{T})(\mathrm{D}_\nu \mathcal{T})(\mathrm{D}^\mu \mathrm{D}_\nu \mathcal{T})}{(\mathrm{D}_\sigma \mathcal{T})(\mathrm{D}^\sigma \mathcal{T})} - \frac{K^{\mu\nu}(\mathrm{D}_\mu \mathcal{T})(\mathrm{D}_\nu \mathcal{T})}{\sqrt{(\mathrm{D}_\sigma \mathcal{T})(\mathrm{D}^\sigma \mathcal{T})}} \right] . \quad (5.72)$$

Notice that the portion of the integrand within the { } must be evaluated on the apparent horizon, that is at $r = \mathcal{H}(\theta,\phi)$. Equation (5.71) states that when the apparent horizon is known in terms of a series expansion in spherical harmonics as in equation (5.65), the integral on the right hand side of equation (5.71) must vanish.

One limitation of equation (5.71) is that the coefficients $c_{\ell m}$ are determined only for values of $(\ell > 0)$. The coefficient c_{00} is determined by solving for the root of equation (5.61), which satisfies equation (5.64). An iterative scheme for finding the apparent horizon can now be outlined. Consider the following form of equation (5.71),

$$c^{(n+1)}_{\ell m} = c^{(n)}_{\ell m} - \frac{1}{\ell(\ell+1)} \int_0^{2\pi} \int_0^{\pi} Y^*_{\ell m}(\theta,\phi) \left\{ r^2 \Psi^4 F(r,\theta,\phi) \right\}_{\{r=\mathcal{H}^{(n)}\}} sin\theta d\theta d\phi \quad (5.73)$$

where the superscript index n refers to the level of the iteration. Define the change in the value of the coefficients $c_{\ell m}$ with each iteration as $\delta c^{(n)}_{\ell m}$, then this change defined as

$$\delta c^{(n)}_{\ell m} = c^{(n+1)}_{\ell m} - c^{(n)}_{\ell m} \quad (5.74)$$

will upon substitution, satisfy the equation

$$\delta c_{\ell m}^{(n)} = -\frac{1}{\ell(\ell+1)} \int_0^{2\pi} \int_0^{\pi} Y_{\ell m}^*(\theta,\phi) \left\{ r^2 \Psi^4 F(r,\theta,\phi) \right\}_{\{r=\mathcal{H}^{(n)}\}} sin\theta d\theta d\phi \ . \quad (5.75)$$

These $\delta c_{\ell m}^{(n)}$'s amounts to a correction factor to any reasonable approximation to the value of the coefficients $c_{\ell m}$. In the event that the correct values of the coefficients are used on the right hand side of equation (5.75), the correction to these coefficients will be zero. Iteratively this comes about by

$$\lim_{n\to\infty} \delta c_{\ell m}^{(n)} = 0 \ . \quad (5.76)$$

The schematic procedure for finding the apparent horizon goes as follows. Guess a sufficiently reasonable choice of coefficients $c_{\ell m}^{(0)}$ for the apparent horizon, then the following is true

$$\begin{aligned} \mathcal{T}^{(0)} &= r^{(0)} - \mathcal{H}^{(0)}(\theta,\phi) \\ &= r^{(0)} - \sum_{\ell=0}^{\infty} \sum_{m=-\ell}^{\ell} c_{\ell m}^{(0)} Y_{\ell m}(\theta,\phi) \\ &= 0 \ . \end{aligned} \quad (5.77)$$

This locates the position of the apparent horizon as $r^{(0)}$. Use equation (5.75) to find the corrections to the $c_{\ell m}^{(0)}$ with $(\ell > 0)$. Then determine the newer $c_{\ell m}^{(1)}$ for $(\ell > 0)$ by

$$c_{\ell m}^{(1)} = c_{\ell m}^{(0)} + \delta c_{\ell m}^{(0)} \ , \text{ for } (\ell > 0) \ . \quad (5.78)$$

To find the new value of $c_{00}^{(1)}$, the following equation derived from equation (5.70) with $(\ell = m = 0)$ must be solved

$$\int_0^{2\pi} \int_0^{\pi} Y_{00}^*(\theta,\phi) \left\{ r^2 \Psi^4 F(r,\theta,\phi) \right\}_{\{r=\mathcal{H}^{(1)}\}} sin\theta d\theta d\phi = 0 \quad (5.79)$$

where the r is evaluated using the updated $c_{\ell m}^{(1)}$'s and a guess is made for the value of $c_{00}^{(1)}$. The guess is updated according to the type of algorithm employed

for root solving. The complete set of $c_{\ell m}^{(1)}$'s can now be used to find all of the $c_{\ell m}^{(2)}$'s in a similar fashion. This iterative process can be continued until the desired accuracy with respect to the true $c_{\ell m}$'s is achieved.

Although the apparent horizon for the trial geometry of equations (4.16) through (4.28) has not been determined with this method to date, a similar method has been applied to the time symmetric solution for two and three black holes.[51,52] In a numerical calculation the actual series expansion must be truncated to some finite ℓ_{max} and the number of iterations of the $c_{\ell m}^{(n)}$'s must also remain finite. The question of what constitutes a reasonable initial guess for the apparent horizon must also be addressed. A reasonable starting surface should build on results already achieved. Thus the time symmetric solutions can be utilized to initialize the outlined procedure when the separation between the two black holes is large.[45] Once the sequence of apparent horizons for closer separations begins to evolve, the sequence can be used to extrapolate the initial guess to the position of the apparent horizon for the next closer separation.

CHAPTER 6
SUMMARY AND CONCLUSIONS

The trial geometry used in this first application of the variational principle for the total mass has extended the present day understanding of the gravitational interaction of two bodies as described by general relativity. Although the results are restricted to a system of two black holes in circular orbits about each other, the characteristic of such orbits are found in regions previously exceeding the limitations of the Newtonian and post-Newtonian approximations. For example the post-Newtonian approximation to two equal mass point sources finds no stable circular orbits for a scaled total angular momentum $j_{total} < 4.29$. Taking a critical luminosity of $L_{GW} \approx 1.0 \times 10^{-2}$ as too large to justify a stationary system, then the numerical results can be propitiously considered for scaled total angular momenta greater than $j_{total} \approx 2.4$. Even restricting the critical value of luminosity to $L_{GW} \approx 1.0 \times 10^{-3}$ allows for acceptance of scaled total angular momenta as low as $j_{total} \approx 3.0$. This is a more conservative limit to impose. At just above $j_{total} \approx 3.0$ the system is losing roughly the same amount of energy per orbit as it has lost through its entire evolution. In addition, the Regge-Wheeler potential which describes multipole perturbations of a Schwarzschild black hole's geometry is peaked for quadrupole perturbations at an isotropic radius of $1.743M$, where M is the mass of the black hole.[53] Treating the summed masses of the two black holes as M, this peak is traversed by the two black holes at a separation of $s \approx 7.0M_1$

in isotropic coordinates. The two black holes cross over this peak with a scaled total angular momentum of $j_{total} \approx 2.6$ with a luminosity of just a few parts in one thousand.

In part, the justification for such claims comes from the ability of this trial geometry to reproduce known orbital parameters. In the test particle limit this geometry favorably compares to the analytic result down to the innermost stable circular orbit that was numerically obtained. Unfortunately, the innermost orbit occurred at a scaled angular momentum of $j_{total} \approx 3.85$ some 11% greater than the analytic value of $2\sqrt{3}$. Even so, the energy per mass of $0.9565079M_1$ for the test particle found numerically at this angular momentum is within 0.2% of the analytic value of $0.95830523M_1$. The radial separation of any orbit is not accurately determined by the variational principle. This is clearly seen for the test particle's innermost stable circular orbit found numerically. The numerical separation of $s = 7.95M_1$ differs by approximately 60% from the analytic value of $s = 4.95M_1$.

When considering the accuracy of the results for black holes of equal masses, the post-Newtonian approximation compared extremely well where applicable. The presence of the innermost stable circular orbit at a scaled total angular momentum of $j_{total} \approx 4.29$ is significantly above the value of 0.84 found numerically. However, one must remember that the post-Newtonian approximation is valid only for small velocities. At $j_{total} \approx 4.29$, the black holes have tangential speeds of roughly 15% the speed of light. The post-Newtonian approximation is stressed for accuracy at this angular momentum. Still the numerical binding energy of $0.0157858M_1$ at this scaled angular momentum differs by less than 8% from the post-Newtonian binding energy of $0.0170059M_1$. The energy of the binary system of black holes as determined by these two

methods agree to within 0.06%. Again the separation between the two black holes is shown to be imprecisely predicted through the variational principle. The numerical result of $s = 28.03M_1$ differs from the post-Newtonian result of $s = 19.81M_1$ by 40%. This is not to say that the post-Newtonian separation is accurate. It only suggest the degree of uncertainty that exist in the value of the separation between these result.

Combining the results of a sequence of scaled angular momenta for two black holes of equal mass allow for a sketch of the evolution of the two holes as they slowly spiral in on each other. At very large separations the two black hole are orbiting each other, their motion accurately described by simple Newtonian mechanics. The gravitational radiation is accurately determined through the quadrupole moment approximation. The system loses energy and angular momentum in the form of gravitational radiation. When the scaled angular momentum reaches a value of $j_{total} \approx 10$ at a separation of $s \approx 192M_1$, the Newtonian approximation to the binding energy is $\sim 2.5\%$ in disagreement with the post-Newtonian and numerical values which still agree to within 0.09% of each other. The luminosity of the quadrupole gravitational radiation is roughly $L_{GW} \approx 6 \times 10^{-11}$, and with each orbit the system is losing $\sim 6 \times 10^{-7} M_1$ of its energy. Once the system has decayed down to a scaled angular momentum of $j_{total} \approx 4$, at a separation of $s \approx 23.17M_1$, the system will possess a sufficiently small angular momentum, $J_{total} < M_{total}^2$, for the remainder of its evolution to settle into a Kerr black hole. By this stage the system has radiated away 0.9% of its total mass and is losing energy at a rate of roughly 0.1% of the total mass with each orbit. The black holes will pass through the quadrupole peak in the Regge-Wheeler potential when $j_{total} \approx 2.6$, at an isotropic separation of $s \approx 7.0M_1$. The luminosity has risen to $L_{GW} \approx 5 \times 10^{-3}$ as the energy

loss per orbit climbs to 15% of the total mass. The evolution has now taken a feverish pace but instantaneously the system should still be accurately approximated by the numerical results. At roughly this separation the orbital frequency has a value of $\Omega \approx 0.095 M_1^{-1}$. This corresponds to a quadrupole radiation frequency of $0.19 M_1^{-1}$ which is in resonance with the quadrupole normal mode frequency of a Schwarzschild black hole of mass $2M_1$.[25] By now the system has lost $\sim 0.06 M_1$ of its origin energy at frequencies less than this quadrupole normal mode. As the scaled angular momentum drops to a value of $j_{total} \approx 2.4$ at a separation of $s \approx 5.93 M_1$ the dimensionless luminosity has reached $L_{GW} \approx 1.0 \times 10^{-2}$. The secular time scale for radiation effects is no longer large compared to the dynamical time scale. At this limit the results of the variational principle for the mass should be taken with much less confidence. Up to this point the system has radiated away $0.07 M_1$. With reasonable assurance the system is expected to lose at least $\sim 3\%$ of its initial total mass in the form of gravitational radiation.

In conclusion, it has been shown that the variational principle for the total mass is an extremely powerful technique for studying the binary system of black holes, going beyond the limitations of the approximate methods of the Newtonian and post-Newtonian equations of motion. The method does rely on a reasonable choice of trial geometry. This particular trial geometry has been through many permutations in an effort to achieve the test particle limit with greater accuracy. With it the solutions to stable circular orbits have been mapped out and a lower limit on the amount of gravitation radiation emitted as two equal mass black holes coalesce has been determined. In the future this technique is expected to undergo several modifications. One modification naturally is to find a better trial geometry satisfying Einstein's equations to

higher orders. It is also very important to incorporate gravitational radiation into the variational principle to model the dissipative effect in the physical system. Inevitably, there will be progress at actually solving Einstein's equations numerically. With present day algorithms for solving partial differential equations on a grid, an initial guess to the solution is needed. These and future applications of the variational principle may provide such initial guesses, as well as, improve the understanding of extremely relativistic gravitational systems.

APPENDIX
COMPUTER PROGRAM

The C source code used to numerically study the two black holes' trial geometry within the context of the variational method for the total mass is presented. Several typesetting constraints have made the source code slightly incompatible with the C language. However, only a slight familiarity with the C language will make these differences transparent to the reader. The complete C code was developed in several modules, each of which is given with a short description. Several excellent references exist on some of the fundamental numerical methods employed.[54,55]

Extreme5b.c is the main module of the C code. Variables are initialized and tested for consistency here. This module is also responsible for all output with external mass storage devices and communicates all initial data to the remainder of the C code.

```
/* Extreme5b.c */
/* Test algorithm for minimization routines.
   Calculates initial constants for trial geometry 5B.
*/
# include < stdio.h>
# include < math.h>
# include < assert.h>
# define YES        1
# define NO         0
# define FIND_MIN   YES
```

```
# define STEST        0.5
# define TOL          4.0e−5
# define INTGRLEPS    1.0e−9
# define PI           3.14159265359
# define EPSILON      1.0e−10
# define FILENAME     "R1J429.DAT"
# define FTABULAR     "R1TBL429.DAT"
# define M1IRRBLE     1.000
# define M2IRRBLE     1.000
# define JDENSITY     4.287597023
# define INNERS       27.750
# define OUTERS       28.251
# define SIZES        0.25
FILE *fP;
FILE *fT;
long int TIMES;
int EQ_Masses_Flag = 0;
double Rmax   =  100000.00,
       M1irr  =  M1IRRBLE,
       M2irr  =  M2IRRBLE,
       Sbegin =   OUTERS,
       Send   =   INNERS,
       DeltaS =   −SIZES,
       Sstart =   6*(M1IRRBLE+M2IRRBLE),
       Jtotal =   JDENSITY*M1IRRBLE*M2IRRBLE;
              /*(−) set in 1st call to initialization(s) */
double radError =   INTGRLEPS,
       thetaError = INTGRLEPS,
       phiError =   INTGRLEPS;

double U, V, M1, M2, X1, X2, omega; /* Set in prmtrzd */
int check_initialization(s,jtotal)
 double s,jtotal;
{
 if (  (fabs(1 − (X1 − X2)/s) >  EPSILON)
```

```
    ||   (fabs(1 - V/X2/omega) >  EPSILON)
    ||   (fabs(1 - U/X1/omega) >  EPSILON)
   ||  (fabs(1 - (M1*U*X1/sqrt(1-U*U) + M2*V*X2/sqrt(1-V*V))/jtotal)
              >  EPSILON)
    ||   (fabs(M1*U/sqrt(1-U*U) + M2*V/sqrt(1-V*V)) >  EPSILON)
    ||   (fabs(M1irr - M1*(1+M2/(2*s))) >  EPSILON)
    ||   (fabs(M2irr - M2*(1+M1/(2*s))) >  EPSILON))
   {
    printf("Check Setup.\n\n  U/X1 = %f   V/X2 = %f
                          s = %f   X1-X2 = %f\n\n",
                          omega, V/X2, s, X1 - X2);
    printf("jtotal = %f  ?= J1  + J2 =  %f  +  %f  = %f\n\n", jtotal,
          M1*U*X1/sqrt(1-U*U), M2*V*X2/sqrt(1-V*V) ,
          M1*U*X1/sqrt(1-U*U) + M2*V*X2/sqrt(1-V*V));
    printf("Ptotal = P1 + P2 = %f  +  %f = %f\n\n",
          M1*U/sqrt(1-U*U), M2*V/sqrt(1-V*V) ,
          M1*U/sqrt(1-U*U) + M2*V/sqrt(1-V*V));
    printf("M1irr = %f = M1 * (1 + M2/(2*s)) = %f\n",
          M1irr, M1 * (1 + M2/(2*s)));
    printf("M2irr = %f = M2 * (1 + M1/(2*s)) = %f\n",
          M2irr, M2 * (1 + M1/(2*s)));
    printf("U = %f   V = %f\n\n", U, V);
    printf("\n Hit a Key ( < x Return>  to cancel) . . .\n");
    if ('x' == getchar()) return( 0 );
    else return( 1 );
   }
 return( 1 );
}
int initialization(s)
 double s;
{
 double b,c,tmp1,tmp2;
 double mu, Eschw, Jschw, Sschw;
 double Mtotal;
 if (Jtotal < = 0.0)
```

```
{   /* Fix the total angular momentum once and for all. */
  /* For Test particle around Schwarzschild,
        isotropic radial coord. = Sstart. */
  Mtotal = M1irr + M2irr;
  mu = M1irr * M2irr /Mtotal;
  Sschw = Sstart * (1+Mtotal/(2*Sstart))*(1+Mtotal/(2*Sstart));
  Eschw = mu * (Sschw - 2*Mtotal) / sqrt(Sschw*(Sschw - 3*Mtotal));
  Jschw = mu * Sschw * sqrt(Mtotal/(Sschw - 3*Mtotal));
  Jtotal = Jschw;
  tmp1 = (1-2*Mtotal/Sschw) * (1 + pow(Jtotal/(mu*Sschw),2.0));
  tmp2 = (1-2*Mtotal/Sschw) * (1 + pow(Jtotal/(Mtotal*Sschw),2.0));
  printf("Extreme.initialization Sstart %g Sschw %g Eschw %g\n",
        Sstart, Sschw, Eschw);
  printf( "Compare Eschw %g with [ ]^ 1/2 mu %g\n", Eschw,
      sqrt(tmp1)*mu );
  printf("  Jtotal/(mu*Mtotal) %g <  2 sqrt(3) %g\n",
                        Jtotal/(mu*Mtotal), 2*sqrt(3.0));
  assert(fP != NULL);
  fprintf(fP,"Extreme.initialization Sstart %g Sschw %g Eschw %g\n",
        Sstart, Sschw, Eschw);
  fprintf(fP,"Compare Eschw %g with [ ]^ 1/2 mu + M %g\n", Eschw,
      sqrt(tmp2)*mu);
  fprintf(fP,"  Jtotal/(mu*Mtotal) %g <  2 sqrt(3) %g\n",
                        Jtotal/(mu*Mtotal), 2*sqrt(3.0));
 }
b = 2*s - M1irr + M2irr;
c = -2*s*M1irr;
M1 = (-b+sqrt(b*b-4*c))/2.0;
b = 2*s - M2irr + M1irr;
c = -2*s*M2irr;
M2 = (-b+sqrt(b*b-4*c))/2.0;
U =   Jtotal / s / sqrt(M1*M1 + Jtotal*Jtotal/(s*s));
V = - Jtotal / s / sqrt(M2*M2 + Jtotal*Jtotal/(s*s));
X1 =   M2 * sqrt(1-U*U) * s / (M1 * sqrt(1-V*V) + M2 * sqrt(1-U*U));
X2 = - M1 * sqrt(1-V*V) * s / (M1 * sqrt(1-V*V) + M2 * sqrt(1-U*U));
```

```
omega = U / X1;
if (!check_initialization(s,Jtotal)) return( 0 );
else return( 1 );
}
main()
{
double a,b,c,fa,fb,fc,fm,prmtrzd(),xmin,fmin,brent();
double s,brent(),prmtrzd();
fP = fopen(FILENAME, "a+");
assert(fP != NULL);
if ( fabs(M1irr - M2irr) <  EPSILON ) EQ_Masses_Flag = 1;
fmin = M1irr + M2irr;
assert (fP != NULL);
fprintf(fP,"\n M1irr%g M2irr%g SNewt%g
            Rmax%g\n DeltaS %g Error %g\n",
            M1irr, M2irr, Sstart, Rmax, DeltaS, radError);
                /* For scanning */
/* NOTE: Must scane hi to lo values of separation! */
for (s = Sbegin ; s > = Send; s += DeltaS)
  {
   fm = prmtrzd(s);
   if ((fm <  fmin)& & (s >  STEST))
     {
      a = s;
      b = a + DeltaS/5.0;
     }
   fmin = fm;
  }
     /* For finding the extremum */
if (FIND_MIN == YES)
 {
  mnbrak(& a,& b,& c,& fa,& fb,& fc,prmtrzd);
  printf("f(x) = %g  at  x = %g \n",fa,a);
  printf("f(x) = %g  at  x = %g \n",fb,b);
  printf("f(x) = %g  at  x = %g \n",fc,c);
```

```
    fprintf(fP,"f(x) = %g  at  x = %g \n",fa,a);
    fprintf(fP,"f(x) = %g  at  x = %g \n",fb,b);
    fprintf(fP,"f(x) = %g  at  x = %g \n",fc,c);
    fflush(fP);
    fmin = brent(a,b,fb,c,prmtrzd,TOL,& xmin);
    if ((fT = fopen(FTABULAR,"a+")) != NULL)
      {
       fprintf(fT,"% 1d\n",1);
       fclose(fT);
      }
    printf("Extremized Mass = %15.9g at the Separation=%15.9f\n"
           ,fmin,xmin);
    fprintf(fP,"\n Extremized Mass = %15.9g  at  the Separation=%15.9f\n"
              ,fmin,xmin);
  }
 fclose(fP);
}
double prmtrzd(s)
 double s;
{
 double Minf,Mmax,mVP;
 double VaryIntegral();
 if (!initialization(s)) return( 0.0 );
 Minf = M1 / sqrt(1-U*U) + M2 / sqrt(1-V*V);
 mVP = VaryIntegral()/(16*PI) - omega * Jtotal; /* Second term is
                                  from Version A of the V.P. */
 Mmax = Minf - mVP;
 printf("Jtotal %f Minf %13.9f - mVP %13.9f = %13.9f S = %f\n",
        Jtotal,Minf, mVP, Mmax, X1-X2);
 fprintf(fP, "Jtotal %f Minf %13.9f - mVP %13.9f = %13.9f S = %f\n",
             Jtotal,Minf, mVP, Mmax, X1-X2);
 printf("U = %g V = %g and OMEGA = %g \n",U,V,omega);
 fprintf(fP,"U = %13.9g V = %13.9g and OMEGA = %13.9g \n"
          ,U,V,omega);
 fflush(fP);
```

```
if ((fT = fopen(FTABULAR,"a+")) != NULL)
  {
   fprintf(fT,"\n %7.4f %7.4f % 11.8f %18.14 f%18.14f %18.14f",
              M1irr,M2irr,Jtotal,X1−X2, Mmax, omega);
   fprintf(fT,"\n %17.14f %17.14f %17.14f %17.14f %17.14f %17.14f % 1d",
                 M1,    M2,    Minf,  mVP,   U,     V,     0);
   fclose(fT);
  }
 return(Mmax);
}
```

Bracket.c is responsible for finding a sufficiently tight range of separation parameters which bracket the extreme, in this case minimum, value of the total mass of the binary black hole system. The algorithm utilized the "Golden Section Search" based on a self replicating interval ratio of 0.61803. The convergence rate is only linear in the number of applications, so the algorithm is only used to guarentee the presence of an extremum and establish the optimum interval spacing allowing the latest three evaluations to employ parabolic interpolation in the next module.

```
/* Bracket.c */
/* Routine for Initially Bracketing a Minimum */
#include <math.h>
#include <stdio.h>
#define GOLD        1.618033988750
#define GLIMIT     100.0
#define TINY        1.0e−16
#define MAX(a,b)      ((a) > (b) ? (a) : (b))
#define SIGN(a,b)     ((b) > 0.0 ? fabs(a) : −fabs(a))
#define SHFT(a,b,c,d) (a)=(b);(b)=(c);(c)=(d);
void mnbrak(ax,bx,cx,fa,fb,fc,func)
 double *ax,*bx,*cx,*fa,*fb,*fc;
```

```
double (*func)();
{
double ulim,u,r,q,fu,dum;
*fa = (*func)(*ax);
*fb = (*func)(*bx);
if (*fb > *fa)
  {
   SHFT(dum,*ax,*bx,dum)
   SHFT(dum,*fb,*fa,dum)
  }
*cx = (*bx) + GOLD * (*bx - *ax);
*fc = (*func)(*cx);
while (*fb > *fc)
    {
     r = (*bx - *ax) * (*fb - *fc);
     q = (*bx - *cx) * (*fb - *fa);
     u = (*bx) - ((*bx - *cx) * q - (*bx - *ax) * r)
              / (2.0 * SIGN(MAX(fabs(q-r),TINY),q-r));
     ulim = (*bx) + GLIMIT * (*cx - *bx);
     if ((*bx - u) * (u - *cx) > 0.0)
       {
        fu = (*func)(u);
        if (fu < *fc)
          {
           *ax = (*bx);
           *bx = u;
           *fa = (*fb);
           *fb = fu;
           return;
          }
        else if (fu > *fb)
          {
           *cx = u;
           *fc = fu;
           return;
```

```
            }
          u = (*cx) + GOLD * (*cx - *bx);
          fu = (*func)(u);
          }
        else if ((*cx - u) * (u - ulim) > 0.0)
          {
          fu = (*func)(u);
          if (fu < *fc)
            {
            SHFT(*bx,*cx,u,*cx + GOLD * (*cx - *bx))
            SHFT(*fb,*fc,fu,(*func)(u))
            }
          }
        else if ((u - ulim) * (ulim - *cx) >= 0.0)
          {
          u = ulim;
          fu = (*func)(u);
          }
        else
          {
          u = (*cx) + GOLD * (*cx - *bx);
          fu = (*func)(u);
          }
        SHFT(*ax,*bx,*cx,u)
        SHFT(*fa,*fb,*fc,fu)
      }
}
```

Brent.c uses a very powerful one dimensional minimization technique which tracks the the progress of the the search in order to decide which of two method to use to continue the search. A parabolic interpolation is applied to each successive evaluation while satisfactory convergence rates are achieved. The convergence of the method is superlinear, possessing a convergence rate

that increases with each successive evaluation. In the event that such rapid convergence falters, the algorithm will utilize the "Golden Section Search".

```
/* Brent.c */
/* Routine to isolate the minimum of a one parameter
   function once it is bracketed by mnbrak()      */
#include <math.h>
#include <stdio.h>
#define ITMAX       100
#define CGOLD       0.38196601125
#define ZEPS        1.0e-10
#define SIGN(a,b)   ((b) > 0.0 ? fabs(a) : -fabs(a))
#define SHFT(a,b,c,d) (a)=(b);(b)=(c);(c)=(d);
double brent(ax,bx,fbx,cx,f,tol,xmin)
 double ax,bx,fbx,cx,tol,*xmin;
 double (*f)();
{
 int iter;
 double a,b,d,etemp,fu,fv,fw,fx,p,q,r,tol1,tol2,u,v,w,x,xm;
 double e = 0.0;
 a = ((ax < cx) ? ax : cx);
 b = ((ax > cx) ? ax : cx);
 x = w = v = bx;
 fw = fv = fx = fbx;
 for (iter = 1;iter <= ITMAX;iter++)
   {
    xm = 0.5 * (a + b);
    tol2 = 2.0 * (tol1 = tol * fabs(x) + ZEPS);
    if (fabs(x-xm) <= (tol2 - 0.5 * (b - a)))
      {
       *xmin = x;
       return(fx);
      }
    if (fabs(e) > tol1)
```

```
  {
   r = (x - w) * (fx - fv);
   q = (x - v) * (fx - fw);
   p = (x - v) * q - (x - w) * r;
   q = 2.0 * (q - r);
   if (q > 0.0) p = -p;
   q = fabs(q);
   etemp = e;
   e = d;
   if (fabs(p) >= fabs(0.5*q*etemp)||p <= q*(a-x)||p >= q*(b-x))
     {
      d = CGOLD * (e=(x >= xm ? a-x : b-x));
     }
   else
     {
      d = p / q;
      u = x + d;
      if (u-a < tol2 || b-u < tol2)
        d = SIGN(tol1,xm-x);
     }
  }
else
  {
   d = CGOLD * (e=(x >= xm ? a-x : b-x));
  }
u = (fabs(d) >= tol1 ? x+d : x + SIGN(tol1,d));
fu = (*f)(u);
if (fu <= fx)
  {
   if ( u >= x) a = x; else b = x;
   SHFT(v,w,x,u)
   SHFT(fv,fw,fx,fu)
  }
else
  {
```

```
        if (u < x) a = u; else b = u;
        if (fu <= fw || w == x)
          {
          v = w;
          w = u;
          fv = fw;
          fw = fu;
          }
        else if (fu <= fv || v == x || v == w)
          {
          v = u;
          fv = fu;
          }
      }
    }
  printf"Too many iterations in BRENT()\n");
  *xmin = x;
  return(fx);
}
```

Evaluate.c controls the process of evaluating the complete three dimensional volume integral. Depending on the locations and masses of the two black holes, the volume is divided up into several regions possessing useful symmetries. Each region is evaluated differently depending on the local symmetry of the region. A local spherical coordinate system is established allowing all regions to be evaluated with a single spherically symmetric integration routine.

```
/* Evaluate.c */
#include <stdio.h>
#include <math.h>
#include <assert.h>
#define fmax(a,b) (((a) > (b)) ? (a) : (b))
#define fmin(a,b) (((a) < (b)) ? (a) : (b))
```

```
/* double VaryIntegral(void)  calculates the entire variational integral.
   This integral is broken up into a number of parts.
   First the hot spots near each black hole are done. Then working
   from the inside out,
        From r = 0 to the inside edge of the more massive black hole.
        If the holes themselves overlap:
          The situation is ultrarelativistic. Might as well just integrate
          from the origin out to infinity with no messing around.
          OR, for the time being, set the maximum radius of a given hole
          at its offset from the origin.
        else if the holes radii overlap :
          From inner edge of more massive to inner edge of less massive.
          From inner edge of less massive to outer edge of more massive
          From outer edge of more massive to outer edge of less massive.
        else they don't overlap:
          Across diameter of more massive.
          Between the holes.
          Across diameter of less massive.
        endif.
        Finally, from outer edge of outer hole to infinity.
double full_VaryIntegral(double xoff,double yoff,double zoff,double rmin,
                double rmax)
does the full variational integral centered at the offset,
from rmin to rmax.
double part_VaryIntegral(double x1, double r1, double x2, double r2,
                    double rmin, double rmax);
does the variational integral centered at the origin but avoids the
hot spots around each hole.
*/
extern FILE *fP;
extern int EQ_Masses_Flag;
extern long int TIMES;
extern double U, V, M1, M2, X1, X2, omega;
extern double Rmax;
double R1, R2; /* Radii of the hot spots around the holes. */
```

```
/*
double VolumeIntegral(double (*integrand)(double x, double y, double z),
                double rmin, double rmax,
                double xoff, double yoff, double zoff,
                double x1, double r1, double x2, double r2, int holes);
*/
double full_VaryIntegral(xoff,yoff,zoff,rmin,rmax)
 double xoff,yoff,zoff,rmin,rmax;
{
 double VolumeIntegral(),VPintegrand();
 return VolumeIntegral(VPintegrand, rmin, rmax, xoff, yoff, zoff,
                0.0, 0.0, 0.0, 0.0, 0); /* 0 is no holes.*/
}
double part_VaryIntegral(x1,r1,x2,r2,rmin,rmax)
 double x1,r1,x2,r2,rmin,rmax;
{
 double VolumeIntegral(),VPintegrand();
 return VolumeIntegral(VPintegrand, rmin, rmax, 0.0, 0.0, 0.0,
                x1, r1, x2, r2, 1); /* 1 is hole(s). */
}
int dcomp(d1,d2)
 double *d1,*d2;
{
 if (*d1 >= *d2) return 1;
 else return -1;
}
double VaryIntegral()
{
 double r[4],absX1, absX2,outer2,VParound2;
 double VP1,VP2,VPinnermost,VPinner,VPmiddle,VPouter,VPoutermost;
 double full_VaryIntegral(),part_VaryIntegral();

 assert(fP != NULL);
 absX1 = fabs(X1);
 absX2 = fabs(X2);
```

```
if (EQ_Masses_Flag)
  {
   R1 = fmin(2.0*M1,fabs(X2-X1)/4.0);
   R2 = R1;
  }
else
  {
   R1 = fmin(2.0*M1, fabs(X2-X1)/4.0);
   R2 = fmin(100.0*M2, fabs(X2-X1)/4.0);
  }
printf("\nM1 %g  R1 %g X1 %g\nM2 %g R2 %g X2 %g\n",
        M1, R1, X1, M2, R2, X2);
fprintf(fP, "\nM1 %g  R1 %g X1 %g\nM2 %g R2 %g X2 %g\n",
             M1, R1, X1, M2, R2, X2);
r[0] = fabs(absX1 - R1);
r[1] = absX1 + R1;
r[2] = fabs(absX2 - R2);
r[3] = absX2 + R2;
qsort(r, 4, sizeof(double), dcomp);
printf("Sorted Radii %g %g %g %g\n", r[0], r[1], r[2], r[3]);
fprintf(fP,"Sorted Radii %g %g %g %g\n",r[0],r[1],r[2],r[3]);
TIMES = 0;
VP1 = full_VaryIntegral(X1, 0.0, 0.0, 0.001*M1, R1);
printf("TIMES %ld  Hole #1 %g\n", TIMES, VP1);
fprintf(fP,"TIMES %ld  Hole #1 %g\n", TIMES, VP1);
fflush(fP);
if (M2 < 0.99*M1)
  {
   TIMES = 0;
   outer2 = fmin(10*M2,R2);
   VParound2 = full_VaryIntegral(X2,0.0,0.0,0.001*M2,outer2);
   printf("TIMES %ld  Around Hole #2 %g\n", TIMES,VParound2);
   fprintf(fP, "TIMES %ld  Around Hole #2 %g\n",TIMES,VParound2);
   fflush(fP);
  }
```

```
else
 {
  VParound2 = 0.0;
  outer2 = 0.001*M2;
 }
TIMES = 0;
if (EQ_Masses_Flag)
  VP2 = VP1;
else
  VP2 = full_VaryIntegral(X2, 0.0, 0.0, outer2, R2);
printf("TIMES %ld  Hole #2 %g\n", TIMES, VP2);
fprintf(fP, "TIMES %ld  Hole #2 %g\n", TIMES, VP2);
fflush(fP);
if (R1 < absX1 && R2 < absX2)
  {
   TIMES = 0;
   VPinnermost = full_VaryIntegral(0.0, 0.0, 0.0, 0.0, r[0]);
   fprintf(fP, "TIMES %ld innermost %g\n",TIMES,VPinnermost);
   printf("TIMES %ld innermost %g\n",TIMES,VPinnermost);
   fflush(fP);
  }
else
  VPinnermost = 0.0; /* else there is no innermost region. */
TIMES = 0;
VPinner = part_VaryIntegral(X1,R1,X2,R2,r[0],r[1]);
printf("TIMES %ld inner %g\n",TIMES, VPinner);
fprintf(fP,"TIMES %ld  inner %g\n",TIMES,VPinner);
fflush(fP);
TIMES = 0;
VPmiddle = part_VaryIntegral(X1,R1,X2,R2,r[1],r[2]);
printf("TIMES %ld Middle %g\n",TIMES,VPmiddle);
fprintf(fP,"TIMES %ld Middle %g\n",TIMES,VPmiddle);
fflush(fP);
TIMES = 0;
VPouter = part_VaryIntegral(X1,R1,X2,R2,r[2],r[3]);
```

```
  printf("TIMES %ld Outer %g\n",TIMES,VPouter);
  fprintf(fP,"TIMES %ld Outer %g\n",TIMES,VPouter);
  fflush(fP);
  TIMES = 0;
  VPoutermost = full_VaryIntegral(0.0,0.0,0.0,r[3],Rmax);
  printf("TIMES %ld outermost %g\n",TIMES,VPoutermost);
  fprintf(fP,"TIMES %ld outermost %g\n",TIMES,VPoutermost);
  fflush(fP);
  return (VP1+VParound2+VP2+VPinnermost+VPinner+VPmiddle
          +VPouter+VPoutermost);
}
```

Fastvol.c is the module actually responsible for the numerical evaluation of the integrand over a region described by spherical coordinates. A very powerful extension of the Romberg method is used on each of the three dimensions to guarantee accuracy over regions which contain prodigious structure, as is the case near the throats of the black holes. The integration tracks trouble spots within each one dimensional integration and concentrates on these regions by locally adding more functional evaluations to the integrand in the context of the Romberg scheme.

```
/* FastVol.c */
/* Has step size halving control. */
/* A quality controlled integrator over a spherical volume.
   This allows for an offset and for the presence of two holes
   in the region of integration.
*/
#include <stdio.h>
#include <math.h>
#include <assert.h>
#define M_PI      3.14159265359
#define SMALL     1.0e-7
```

```
#define VERYSMALL 1.0e-10
#define JMAX     15 /* Max halves.=KMAX fast,>KMAX otherwise*/
#define KMAX      5 /* Romberg of order 2K */
#define LMAX     16 /* 2 ** (KMAX-1) */
#define KMIN      3
#define fmin(a,b) (((a) < (b)) ? (a) : (b))
extern FILE *fP;
extern long int TIMES;
extern double radError,
              thetaError,
              phiError;
int HOLES;
double local_x1,
       local_x2,
       local_r1,
       local_r2,
       local_xoff,
       local_yoff,
       local_zoff,
       local_radius,
       local_theta;
double  (*local_integrand)();
void polint(xa,ya,n,x,y,dy)
 int n;
 double *xa,*ya,x,*y,*dy;
{
 int i, m, ns = 1;
 double den, dif, dift, ho, hp, w;
 double c[JMAX+2], d[JMAX+2];
 dif = fabs(x-xa[1]);
 for (i = 1; i <= n; i++)
    {
     if ((dift = fabs(x - xa[i])) < dif)
       {
        ns = i;
```

```
        dif = dift;
       }
     c[i] = ya[i];
     d[i] = ya[i];
    }
 *y = ya[ns--];
 for (m = 1; m < n; m++)
    {
     for (i = 1; i <= n-m; i++)
        {
         ho = xa[i] - x;
         hp = xa[i+m] - x;
         w = c[i+1] - d[i];
         if ((den = ho-hp) == 0.0) assert(0);
         den = w/den;
         d[i] = hp * den;
         c[i] = ho * den;
        }
     *y += (*dy = (2*ns < (n-m) ? c[ns+1] : d[ns--]));
    }
}
double trapzd(funct,a,b,n,current_s,current_it)
 int n,*current_it;
 double (*funct)(),a,b,*current_s;
{
 long int j;
 double tnm, del, sum, x, f;
 assert(a!=b);
 if (n == 1)
   {
    *current_it = 1; /* number pts to be added next call. */
    return (*current_s = 0.5 * (b-a) * ((*funct)(a) + (*funct)(b)));
   }
 else
   {
```

```
    tnm = (double) *current_it;
    del = (b-a)/tnm;
    x = a + 0.5 * del;
    sum = 0.0;
    for (j = 0; j < *current_it; j++)
      {
       sum += (f = (*funct)(x));
       x = x + del;
      }
    *current_it *= 2;
    return (*current_s = 0.5 * ( *current_s + (b-a)*sum/tnm));
   }
}
double Qromb(integrand,a,b,error)
 double (*integrand)(),a,b,error;
{
 int curr_it,j, k;
 double ss, dss,s[JMAX+2], h[JMAX+2],curr_s;
 double trapzd();
 void polint();
 h[1] = 1.0;
 for (j = 1; j <= JMAX; j++)
    {
     s[j] = trapzd(integrand, a, b, j, &curr_s, &curr_it);
     if (j >= KMIN)
       {
        k = fmin(j, KMAX);
        polint(&h[j-k], &s[j-k], k, 0.0, &ss, &dss);
        if (fabs(dss) < error /* * fabs(ss) */)
          { /* success */
           return ss;
          }
/*
        print_inter = 1;
        polint(&h[j-k], &s[j-k], k, 0.0, &ss, &dss);
```

```
*/
        }
      s[j+1] = s[j];
      h[j+1] = 0.25*h[j];
     }
 assert(0); /* Too many steps. */
 return 0.0;
}
/* Qrombinf */
/* allows region of integration to extend out to infinity. */
#define FUNC(x) ((*funk)(1.0/(x))/((x)*(x)))
double inf_trapzd(funk,f,a,b,n,it,s)
 int n,*it;
 double (*funk)(),*f,a,b,*s;
/* The array f[] contains all but the last needed
   refinement of the function. */
{
 int j,l,lstart,lplus;
 double tnm,del,sum,x;
 assert(a!=b);
 if (n == 1)
   {
    *it = 1; /* number of points to be added on the next call. */
    return (*s = 0.5 * (b-a) * (f[0] + f[LMAX]));
   }
 else
   {
    tnm = (double) *it;
    if (n < KMAX)
      {
       lplus = LMAX / *it;
       lstart = lplus / 2;
       for (sum = 0.0, l = lstart; l < LMAX; l += lplus)
          {
           sum += f[l];
```

```
        }
      }
    else
      {
       del = (b-a)/tnm;
       x = a + 0.5 * del;
       assert(*it == LMAX/2);
       for (sum = 0.0, j = 0; j < *it; j++)
         {
          f[1+2*j] = FUNC(x);
          sum += f[1+2*j];
          x = x + del;
         }
      }
    *it *= 2;
    return (*s = 0.5 * ( *s + (b-a)*sum/tnm));
   }
}
double inf_QrombSlave(funk,f,a,b,error)
 double (*funk)(),*f,a,b,error;
{
 int curr_it,l,j;
 double curr_s,ss,dss,s[JMAX+2],h[JMAX+2],
        first_f[LMAX+1],first_s,second_s;
 double inf_trapzd(),inf_QrombSlave();
 void polint();
/*
 printf("enter QrombS from %g to %g\n", a, b);
 for (l = 0; l <= LMAX; l +=2)
    {
     printf("l %d  f %g\n", l, f[l]);
    }
*/
 h[1] = 1.0;
 for (j = 1; j <= JMAX; j++)
```

```
    {
     s[j] = inf_trapzd(funk, f, a, b, j, &curr_it, &curr_s);
     if (j >= KMAX)
       {
        polint(&h[j-KMAX], &s[j-KMAX], KMAX, 0.0, &ss, &dss);
                    ss, error, dss); */
        if (fabs(dss) < error /* * fabs(ss) */)
          { /* success */
           return ss;
          }
        else
          { /* halve the interval and recurse. */
           for (l = 0; l <= LMAX/2; l++)
              {
               first_f[2*l] = f[l];
              }
           first_s = inf_QrombSlave(funk, first_f, a, (b+a)/2.0, error);
           for (l = 0; l <= LMAX/2; l++)
              {
               first_f[2*l] = f[l+LMAX/2];
              }
           second_s = inf_QrombSlave(funk, first_f, (b+a)/2.0, b, error);
           return first_s + second_s;
          }
       }
     assert(j < KMAX);
     s[j+1] = s[j];
     h[j+1] = 0.25*h[j];
    }
 assert(0); /* Too many steps. */
 return 0;
}
double inf_QrombDriver(funk,aa,bb,error)
double (*funk)(),aa,bb,error;
{
```

```
int l;
double f[LMAX+1], del, a, b, x;
double inf_QrombSlave();
b = 1.0/aa;
a = 1.0/bb;
del = (b - a)/LMAX;
for (l = 0; l <= LMAX; l += 2)
   {
    x = a + l * del;
    f[l] = FUNC(x);
   }
/* printf("inf_QrombDriver error %g\n", error); */
return inf_QrombSlave(funk, f, a, b, error);
}
#undef FUNC
double New_trapzd(funct,f,a,b,n,it,s)
int n,*it;
double (*funct)(),*f,a,b,*s;
/* The array f[] contains all but the last needed refinement
  of the function. */
{
int j, l, lstart, lplus;
double tnm, del, sum, x;
assert(a!=b);
if (n == 1)
  {
   *it = 1; /* number of points to be added on the next call. */
   return (*s = 0.5 * (b-a) * (f[0] + f[LMAX]));
  }
else
  {
   tnm = (double) *it;
   if (n < KMAX)
     {
      lplus = LMAX / *it;
```

```
      lstart = lplus / 2;
      for (sum = 0.0, l = lstart; l < LMAX; l += lplus)
        {
         sum += f[l];
        }
     }
   else
     {
      del = (b-a)/tnm;
      x = a + 0.5 * del;
      assert(*it == LMAX/2);
      for (sum = 0.0, j = 0; j < *it; j++)
        {
         f[1+2*j] = (*funct)(x);
         sum += f[1+2*j];
         x = x + del;
        }
     }
   *it *= 2;
   return (*s = 0.5 * ( *s + (b-a)*sum/tnm));
  }
}
double QrombSlave(func,f,a,b,error)
 double (*func)(),*f,a,b,error;
{
 int j,l,curr_it;
 double curr_s,ss,dss,s[JMAX+2],h[JMAX+2],
       first_f[LMAX+1],first_s,second_s;
 double New_trapzd(),QrombSlave();
 void polint();

 h[1] = 1.0;
 for (j = 1; j <= JMAX; j++)
   {
    s[j] = New_trapzd(func, f, a, b, j, &curr_it, &curr_s);
```

```
    if (j >= KMAX)
      {
       polint(&h[j-KMAX], &s[j-KMAX], KMAX, 0.0, &ss, &dss);
       if (fabs(dss) < error /* * fabs(ss) */)
         { /* success */
          return ss;
         }
       else
         { /* halve the interval and recurse. */
          for (l = 0; l <= LMAX/2; l++)
             {
              first_f[2*l] = f[l];
             }
          first_s = QrombSlave(func, first_f, a, (b+a)/2.0, error);
          for (l = 0; l <= LMAX/2; l++)
             {
              first_f[2*l] = f[l+LMAX/2];
             }
          second_s = QrombSlave(func, first_f, (b+a)/2.0, b, error);
          return first_s + second_s;
         }
      }
    assert(j < KMAX);
    s[j+1] = s[j];
    h[j+1] = 0.25*h[j];
   }
 assert(0); /* Too many steps. */
 return 0;
}
double QrombDriver(func,a,b,error)
 double (*func)(),a,b,error;
{
 int l;
 double f[LMAX+1], del;
 double QrombSlave();
```

```
 for (l = 0; l <= LMAX; l += 2)
    {
     del = (b - a)/LMAX;
     f[l] = (*func)(a + l * del);
    }
 return QrombSlave(func, f, a, b, error);
}
double volume_element(rad,the,phi)
 double rad,the,phi;
{
 double x,y,z,Jacobian, ret;
 TIMES++;
 if (!(TIMES % 5000))
   printf("volume_element TIMES %ld\n", TIMES);
/*
 x = rad*sin(the)*cos(phi);
 y = rad*sin(the)*sin(phi);
 z = rad*cos(the);
*/
/* We have the holes on the x-axis but the grid points are
   clustered near small values of theta.  So let
   (x,y,z) -> (y,z,x) to put the phi = 0 axis
   at the x-axis.
*/
 y = rad*sin(the)*cos(phi) + local_yoff;
 z = rad*sin(the)*sin(phi) + local_zoff;
 x = rad*cos(the) + local_xoff;
 Jacobian = rad*rad*sin(the);
 assert(local_integrand != NULL);
 ret = (*local_integrand)(x,y,z);
 ret = ret * Jacobian;
 return(ret);
}
double phi_integrand(phi)
 double phi;
```

```
{
 double result,volume_element();
 result = volume_element(local_radius, local_theta, phi);
 return result;
}
double theta_integrand(theta)
 double theta;
{
 double result, phi_upper, phi_lower;
 double Qromb(),phi_integrand();
 local_theta = theta;
 if (sin(theta) < SMALL) return 0.0;
 phi_lower = 0.0; /* only one quarter covered from symmetry. */
 phi_upper = M_PI/2.0;
 result = 4.0 * Qromb(phi_integrand,phi_lower,phi_upper,phiError);
 return result;
}
double radial_integrand(r)
 double r;
{
 double result,theta_upper,theta_lower,costheta;
 double QrombDriver(),theta_integrand();
 if (fabs(r) < VERYSMALL) return 0.0;
 local_radius = r;
 if (HOLES)
   {
    assert(local_x1 > local_x2); /* else limits of costheta wrong? */
    costheta = (local_x1 * local_x1 - local_r1 * local_r1 + r * r)
            / (2 * local_x1 * r);
    if (costheta < 1.0 && costheta > -1.0)
      {
       theta_lower = acos(costheta);
      }
    else
      {
```

```
      theta_lower = 0.0;
     }
   costheta = (local_x2 * local_x2 - local_r2 * local_r2 + r * r)
         / (2 * local_x2 * r);
   if (costheta < 1.0 && costheta > -1.0)
     {
      theta_upper = acos(costheta);
     }
   else
     {
      theta_upper = M_PI;
     }
  }
 else
  {
   theta_upper = M_PI;
   theta_lower = 0.0;
  }
 result=
 QrombDriver(theta_integrand,theta_lower,theta_upper,thetaError);
 return result;
}
double VolumeIntegral(integrand,rmin,rmax,xoff,
                  yoff,zoff,x1,r1,x2,r2,holes)
 int holes;
 double (*integrand)(),rmin,rmax,
       xoff,yoff,zoff,x1,r1,x2,r2;
{
 double result;
 double QrombDriver(),inf_QrombDriver(),
       radial_integrand();
 local_xoff = xoff;
 local_yoff = yoff;
 local_zoff = zoff;
 local_integrand = integrand;
```

```
HOLES = holes;
if (holes != 0)
  {
   local_x1 = x1;
   local_x2 = x2;
   local_r1 = r1;
   local_r2 = r2;
  }
else
  {
   local_x1 = 0;
   local_x2 = 0;
   local_r1 = 0;
   local_r2 = 0;
  }
printf("FastVol.VolumeIntegral from %f to %f\n",rmin,rmax);
if(fabs(rmax-rmin) < VERYSMALL) return 0.0;
if (HOLES == 0 && rmin > 0.1 && rmax > 20.0)
  { /* use inf functions. */
   result = inf_QrombDriver(radial_integrand,rmin,rmax,radError);
  }
else
  {
   if (HOLES==0&&local_xoff!=0.0&&rmin<SMALL) rmin=SMALL;
   result =
   QrombDriver(radial_integrand, rmin, rmax, radError);
  }
return result;
}
```

Scalar5b.c is where the all necessary geometric quantities for evaluating the integrand of the variational method are determined. The evaluation is carried out based on the location of the infinitesimal volume element in terms

of Cartesian coordinates. This module is the most time consuming element of the entire program, carrying out on the order of two thousand floating point operations for each infinitesimal volume element evaluated.

```
/* Scalar5b.c */
#include <math.h>
#include <stdio.h>
double VPintegrand(x,y,z)
  double x,y,z;
{
  double rho1,drho1_dx,drho1_dy,drho1_dz,d2rho1_dxdx,
     d2rho1_dydy,d2rho1_dzdz,d2rho1_dxdy,d2rho1_dxdz,
     d2rho1_dydz,d2rho1_dydx,d2rho1_dzdx,d2rho1_dzdy;
  double rho2,drho2_dx,drho2_dy,drho2_dz,d2rho2_dxdx,
     d2rho2_dydy,d2rho2_dzdz,d2rho2_dxdy,d2rho2_dxdz,
     d2rho2_dydz,d2rho2_dydx,d2rho2_dzdx,d2rho2_dzdy;
  double common,dcommon_drho1,dcommon_drho2,
     dcommon_dx,dcommon_dy,dcommon_dz;
  double d2common_drho1drho1,d2common_drho1drho2,
     d2common_drho2drho2,d2common_dxdx,d2common_dydy,
     d2common_dzdz,d2common_dxdy,d2common_dxdz,
     d2common_dydz,d2common_dydx,d2common_dzdx,
     d2common_dzdy;
  double PSI,dPSI_drho1,dPSI_drho2,dPSI_dx,
     dPSI_dy,dPSI_dz;
  double d2PSI_drho1drho1,d2PSI_drho1drho2,
     d2PSI_drho2drho2,d2PSI_dxdx,d2PSI_dydy,
     d2PSI_dzdz,d2PSI_dxdy,d2PSI_dxdz,
     d2PSI_dydz,d2PSI_dydx,d2PSI_dzdx,d2PSI_dzdy;
  double psi1,dpsi1_drho1,dpsi1_drho2,dpsi1_dx,
     dpsi1_dy,dpsi1_dz;
  double d2psi1_drho1drho1,d2psi1_drho1drho2,
     d2psi1_drho2drho2,d2psi1_dxdx,d2psi1_dydy,d2psi1_dzdz,
     d2psi1_dxdy,d2psi1_dxdz,d2psi1_dydz,d2psi1_dydx,
```

```
    d2psi1_dzdx,d2psi1_dzdy;
double psi2,dpsi2_drho1,dpsi2_drho2,dpsi2_dx,
    dpsi2_dy,dpsi2_dz;
double d2psi2_drho1drho1,d2psi2_drho1drho2,
    d2psi2_drho2drho2,d2psi2_dxdx,d2psi2_dydy,d2psi2_dzdz,
    d2psi2_dxdy,d2psi2_dxdz,d2psi2_dydz,d2psi2_dydx,
    d2psi2_dzdx,d2psi2_dzdy;
double QU_PSI,dQU_PSI_drho1,dQU_PSI_drho2,
    dQU_PSI_dx,dQU_PSI_dy,dQU_PSI_dz;
double d2QU_PSI_drho1drho1,d2QU_PSI_drho1drho2,
    d2QU_PSI_drho2drho2,d2QU_PSI_dxdx,d2QU_PSI_dydy,
    d2QU_PSI_dzdz,d2QU_PSI_dxdy,d2QU_PSI_dxdz,
    d2QU_PSI_dydz,d2QU_PSI_dydx,d2QU_PSI_dzdx,
    d2QU_PSI_dzdy;
double qu_psi1,dqu_psi1_drho1,dqu_psi1_drho2,
    dqu_psi1_dx,dqu_psi1_dy,dqu_psi1_dz;
double d2qu_psi1_drho1drho1,d2qu_psi1_drho1drho2,
    d2qu_psi1_drho2drho2,d2qu_psi1_dxdx,d2qu_psi1_dydy,
    d2qu_psi1_dzdz,d2qu_psi1_dxdy,d2qu_psi1_dxdz,
    d2qu_psi1_dydz,d2qu_psi1_dydx,d2qu_psi1_dzdx,
    d2qu_psi1_dzdy;
double qu_psi2,dqu_psi2_drho1,dqu_psi2_drho2,
    dqu_psi2_dx,dqu_psi2_dy,dqu_psi2_dz;
double d2qu_psi2_drho1drho1,d2qu_psi2_drho1drho2,
    d2qu_psi2_drho2drho2,d2qu_psi2_dxdx,d2qu_psi2_dydy,
    d2qu_psi2_dzdz,d2qu_psi2_dxdy,d2qu_psi2_dxdz,
    d2qu_psi2_dydz,d2qu_psi2_dydx,d2qu_psi2_dzdx,
    d2qu_psi2_dzdy;
double a1,da1_drho1,da1_drho2,da1_dx,da1_dy,da1_dz;
double d2a1_drho1drho1,d2a1_drho1drho2,d2a1_drho2drho2,
    d2a1_dxdx,d2a1_dydy,d2a1_dzdz,d2a1_dxdy,
    d2a1_dxdz,d2a1_dydz,d2a1_dydx,d2a1_dzdx,d2a1_dzdy;
double a2,da2_drho1,da2_drho2,da2_dx,da2_dy,da2_dz;
double d2a2_drho1drho1,d2a2_drho1drho2,d2a2_drho2drho2,
    d2a2_dxdx,d2a2_dydy,d2a2_dzdz,d2a2_dxdy,
```

```
    d2a2_dxdz,d2a2_dydz,d2a2_dydx,d2a2_dzdx,d2a2_dzdy;
double alpha1,dalpha1_drho1,dalpha1_drho2,dalpha1_dx,dalpha1_dy,
    dalpha1_dz;
double d2alpha1_drho1drho1,d2alpha1_drho1drho2,d2alpha1_drho2drho2,
    d2alpha1_dxdx,d2alpha1_dydy,d2alpha1_dzdz,d2alpha1_dxdy,
    d2alpha1_dxdz,d2alpha1_dydz,d2alpha1_dydx,d2alpha1_dzdx,
    d2alpha1_dzdy;
double alpha2,dalpha2_drho1,dalpha2_drho2,dalpha2_dx,dalpha2_dy,
    dalpha2_dz;
double d2alpha2_drho1drho1,d2alpha2_drho1drho2,d2alpha2_drho2drho2,
    d2alpha2_dxdx,d2alpha2_dydy,d2alpha2_dzdz,d2alpha2_dxdy,
    d2alpha2_dxdz,d2alpha2_dydz,d2alpha2_dydx,d2alpha2_dzdx,
    d2alpha2_dzdy;
double sq_alpha1,dsq_alpha1_drho1,dsq_alpha1_drho2,
    dsq_alpha1_dx,dsq_alpha1_dy,dsq_alpha1_dz;
double d2sq_alpha1_drho1drho1,d2sq_alpha1_drho1drho2,
    d2sq_alpha1_drho2drho2,d2sq_alpha1_dxdx,d2sq_alpha1_dydy,
    d2sq_alpha1_dzdz,d2sq_alpha1_dxdy,d2sq_alpha1_dxdz,
    d2sq_alpha1_dydz,d2sq_alpha1_dydx,d2sq_alpha1_dzdx,
    d2sq_alpha1_dzdy;
double sq_alpha2,dsq_alpha2_drho1,dsq_alpha2_drho2,
    dsq_alpha2_dx,dsq_alpha2_dy,dsq_alpha2_dz;
double d2sq_alpha2_drho1drho1,d2sq_alpha2_drho1drho2,
    d2sq_alpha2_drho2drho2,d2sq_alpha2_dxdx,d2sq_alpha2_dydy,
    d2sq_alpha2_dzdz,d2sq_alpha2_dxdy,d2sq_alpha2_dxdz,
    d2sq_alpha2_dydz,d2sq_alpha2_dydx,d2sq_alpha2_dzdx,
    d2sq_alpha2_dzdy;
double gxx,dgxx_drho1,dgxx_drho2,dgxx_dx,dgxx_dy,dgxx_dz;
double d2gxx_drho1drho1,d2gxx_drho1drho2,d2gxx_drho2drho2,
    d2gxx_dxdx,d2gxx_dydy,d2gxx_dzdz,d2gxx_dxdy,d2gxx_dxdz,
    d2gxx_dydz,d2gxx_dydx,d2gxx_dzdx,d2gxx_dzdy;
double gyy,dgyy_drho1,dgyy_drho2,dgyy_dx,dgyy_dy,dgyy_dz;
double d2gyy_drho1drho1,d2gyy_drho1drho2,d2gyy_drho2drho2,
    d2gyy_dxdx,d2gyy_dydy,d2gyy_dzdz,d2gyy_dxdy,d2gyy_dxdz,
    d2gyy_dydz,d2gyy_dydx,d2gyy_dzdx,d2gyy_dzdy;
```

```
double gzz,dgzz_drho1,dgzz_drho2,dgzz_dx,dgzz_dy,dgzz_dz;
double d2gzz_drho1drho1,d2gzz_drho1drho2,d2gzz_drho2drho2,
   d2gzz_dxdx,d2gzz_dydy,d2gzz_dzdz,d2gzz_dxdy,d2gzz_dxdz,
   d2gzz_dydz,d2gzz_dydx,d2gzz_dzdx,d2gzz_dzdy;
double beta_X,beta_Y,beta_Z,beta_z,gXX,gYY,gZZ;
double lapse,K,K_AB_K_ab;
double K1xx,K1yy,K1zz,K1xy,K1yx,K1yz,K1zy,K1xz,K1zx;
double K2xx,K2yy,K2zz,K2xy,K2yx,K2yz,K2zy,K2xz,K2zx;
double K_xx,K_yy,K_zz,K_xy,K_yx,K_yz,K_zy,K_xz,K_zx;
double K_XX,K_YY,K_ZZ,K_XY,K_YX,K_XZ,K_ZX,K_YZ,K_ZY;
double beta_y,dbeta_y_drho1,dbeta_y_drho2,
   dbeta_y_dx,dbeta_y_dy,dbeta_y_dz;
double beta_x,dbeta_x_drho1,dbeta_x_drho2,
   dbeta_x_dx,dbeta_x_dy,dbeta_x_dz;
double D_x_beta_y,D_y_beta_y,D_z_beta_y,
   D_x_beta_x,D_y_beta_x,D_z_beta_x,
   D_x_beta_z,D_y_beta_z,D_z_beta_z;
double G_xxx,G_xxy,G_xyx,G_xxz,G_xzx,G_xyy,
   G_xyz,G_xzy,G_xzz,G_yxx,G_yxy,G_yyx,G_yxz,
   G_yzx,G_yyy,G_yyz,G_yzy,G_yzz,G_zxx,G_zxy,
   G_zyx,G_zxz,G_zzx,G_zyy,G_zyz,G_zzy,G_zzz,
G_Xxx,G_Xxy,G_Xyx,G_Xxz,G_Xzx,G_Xyy,G_Xyz,
   G_Xzy,G_Xzz,G_Yxx,G_Yxy,G_Yyx,G_Yxz,G_Yzx,
   G_Yyy,G_Yyz,G_Yzy,G_Yzz,G_Zxx,G_Zxy,G_Zyx,
   G_Zxz,G_Zzx,G_Zyy,G_Zyz,G_Zzy,G_Zzz;
double R,S2,S;
extern double U,V,M1,M2,X1,X2,omega;
{
  if (0) exit(0);
  S2 = (X1-X2)*(X1-X2);
  S = sqrt(S2);
  rho1 = sqrt( (x-X1)*(x-X1) + y*y/(1-U*U) + z*z );
  drho1_dx = (x-X1)/rho1;
  drho1_dy = y/((1-U*U)*rho1);
  drho1_dz = z/rho1;
```

```
d2rho1_dxdx = 1/rho1 − (x−X1)/(rho1*rho1) * drho1_dx;
d2rho1_dydy = 1/(1−U*U)/rho1 − y/(1−U*U)/(rho1*rho1)*drho1_dy;
d2rho1_dzdz = 1/rho1 − z/(rho1*rho1) * drho1_dz;
d2rho1_dydx = d2rho1_dxdy = −drho1_dx * drho1_dy/rho1;
d2rho1_dzdy = d2rho1_dydz = −drho1_dy * drho1_dz/rho1;
d2rho1_dzdx = d2rho1_dxdz = −drho1_dz * drho1_dx/rho1;
rho2 = sqrt( (x−X2)*(x−X2) + y*y/(1−V*V) + z*z );
drho2_dx = (x−X2)/rho2;
drho2_dy = y/(1−V*V)/rho2;
drho2_dz = z/rho2;
d2rho2_dxdx = 1/rho2 − (x−X2)/(rho2*rho2) * drho2_dx;
d2rho2_dydy = 1/(1−V*V)/rho2 − y/(1−V*V)/(rho2*rho2)*drho2_dy;
d2rho2_dzdz = 1/rho2 − z/(rho2*rho2) * drho2_dz;
d2rho2_dydx = d2rho2_dxdy = −drho2_dx * drho2_dy/rho2;
d2rho2_dzdy = d2rho2_dydz = −drho2_dy * drho2_dz/rho2;
d2rho2_dzdx = d2rho2_dxdz = −drho2_dz * drho2_dx/rho2;
PSI = 1 + M1/(2*rho1) + M2/(2*rho2);
dPSI_drho1 = −M1/(2*rho1*rho1);
dPSI_drho2 = −M2/(2*rho2*rho2);
d2PSI_drho1drho1 = M1/((rho1)*(rho1)*(rho1));
d2PSI_drho2drho2 = M2/((rho2)*(rho2)*(rho2));
d2PSI_drho1drho2 = 0;
QU_PSI = ((PSI)*(PSI)*(PSI)*(PSI));
dQU_PSI_drho1 = 4*(QU_PSI/PSI)*dPSI_drho1;
dQU_PSI_drho2 = 4*(QU_PSI/PSI)*dPSI_drho2;
d2QU_PSI_drho1drho1 = 12*((PSI*dPSI_drho1)*(PSI*dPSI_drho1))
   + 4*(QU_PSI/PSI)*d2PSI_drho1drho1;
d2QU_PSI_drho2drho2 = 12*((PSI*dPSI_drho2)*(PSI*dPSI_drho2))
   + 4*(QU_PSI/PSI)*d2PSI_drho2drho2;
d2QU_PSI_drho1drho2 = 12 * PSI * PSI * dPSI_drho1 * dPSI_drho2
   + 4 *(QU_PSI/PSI) * d2PSI_drho1drho2;
{ dQU_PSI_dx = dQU_PSI_drho1 * drho1_dx
                + dQU_PSI_drho2 * drho2_dx;
  dQU_PSI_dy = dQU_PSI_drho1 * drho1_dy
                + dQU_PSI_drho2 * drho2_dy;
```

```
 dQU_PSI_dz = dQU_PSI_drho1 * drho1_dz
                + dQU_PSI_drho2 * drho2_dz;
};
{d2QU_PSI_dxdx = d2QU_PSI_drho1drho1*drho1_dx*drho1_dx
    + dQU_PSI_drho1*d2rho1_dxdx
    + d2QU_PSI_drho2drho2*drho2_dx*drho2_dx
    + dQU_PSI_drho2*d2rho2_dxdx
    + 2 * d2QU_PSI_drho1drho2 * drho1_dx * drho2_dx;
 d2QU_PSI_dydy = d2QU_PSI_drho1drho1*drho1_dy*drho1_dy
    + dQU_PSI_drho1*d2rho1_dydy
    + d2QU_PSI_drho2drho2*drho2_dy*drho2_dy
    + dQU_PSI_drho2*d2rho2_dydy
    + 2 * d2QU_PSI_drho1drho2 * drho1_dy * drho2_dy;
 d2QU_PSI_dzdz = d2QU_PSI_drho1drho1*drho1_dz*drho1_dz
    + dQU_PSI_drho1*d2rho1_dzdz
    + d2QU_PSI_drho2drho2*drho2_dz*drho2_dz
    + dQU_PSI_drho2*d2rho2_dzdz
    + 2 * d2QU_PSI_drho1drho2 * drho1_dz * drho2_dz;
 d2QU_PSI_dydx = d2QU_PSI_dxdy
           = d2QU_PSI_drho1drho1 * drho1_dx * drho1_dy
    + d2QU_PSI_drho2drho2 * drho2_dx * drho2_dy
    + d2QU_PSI_drho1drho2
    * (drho1_dx*drho2_dy+drho2_dx*drho1_dy)
    + dQU_PSI_drho1 * d2rho1_dxdy
    + dQU_PSI_drho2 * d2rho2_dxdy;
 d2QU_PSI_dzdy = d2QU_PSI_dydz
           = d2QU_PSI_drho1drho1 * drho1_dy * drho1_dz
    + d2QU_PSI_drho2drho2 * drho2_dy * drho2_dz
    + d2QU_PSI_drho1drho2
    * (drho1_dy*drho2_dz+drho2_dy*drho1_dz)
    + dQU_PSI_drho1 * d2rho1_dydz
    + dQU_PSI_drho2 * d2rho2_dydz;
 d2QU_PSI_dxdz = d2QU_PSI_dzdx
           = d2QU_PSI_drho1drho1 * drho1_dz * drho1_dx
    + d2QU_PSI_drho2drho2 * drho2_dz * drho2_dx
```

```
      + d2QU_PSI_drho1drho2
      * (drho1_dz*drho2_dx+drho2_dz*drho1_dx)
      + dQU_PSI_drho1 * d2rho1_dxdz
      + dQU_PSI_drho2 * d2rho2_dxdz;
};
psi1 = 1 + M1/(2*rho1)
    + M2*M1*M1/(2*S*(M1*M1+4*rho1*rho1));
dpsi1_drho1 = - M1/(2*rho1*rho1)
            - M2*M1*M1*8*rho1
            / (2*S*((M1*M1+4*rho1*rho1)
            * (M1*M1+4*rho1*rho1)) );
dpsi1_drho2 = 0;
d2psi1_drho1drho1 = 2*M1/(2*rho1*rho1*rho1)
                  - M2*M1*M1*8
                  / (2*S*((M1*M1+4*rho1*rho1)
                  * (M1*M1+4*rho1*rho1)) )
                  + M2*M1*M1*8*2*4*2*rho1*rho1
                  / (2*S*((M1*M1+4*rho1*rho1)
                  * (M1*M1+4*rho1*rho1)
                  * (M1*M1+4*rho1*rho1)) );
d2psi1_drho2drho2 = 0;
d2psi1_drho1drho2 = 0;
qu_psi1 = ((psi1)*(psi1)*(psi1)*(psi1));
dqu_psi1_drho1 = 4*(qu_psi1/psi1)*dpsi1_drho1;
dqu_psi1_drho2 = 4*(qu_psi1/psi1)*dpsi1_drho2;
d2qu_psi1_drho1drho1 = 12*((psi1*dpsi1_drho1)*(psi1*dpsi1_drho1))
   + 4*(qu_psi1/psi1)*d2psi1_drho1drho1;
d2qu_psi1_drho2drho2 = 12*((psi1*dpsi1_drho2)*(psi1*dpsi1_drho2))
   + 4*(qu_psi1/psi1)*d2psi1_drho2drho2;
d2qu_psi1_drho1drho2 = 12 * psi1 * psi1 * dpsi1_drho1 * dpsi1_drho2
   + 4 *(qu_psi1/psi1) * d2psi1_drho1drho2;
{ dqu_psi1_dx = dqu_psi1_drho1 * drho1_dx
           + dqu_psi1_drho2 * drho2_dx;
  dqu_psi1_dy = dqu_psi1_drho1 * drho1_dy
           + dqu_psi1_drho2 * drho2_dy;
```

```
  dqu_psi1_dz = dqu_psi1_drho1 * drho1_dz
              + dqu_psi1_drho2 * drho2_dz;
};
psi2 = 1 + M2/(2*rho2)
     + M1*M2*M2/(2*S*(M2*M2+4*rho2*rho2));
dpsi2_drho1 = 0;
dpsi2_drho2 = - M2/(2*rho2*rho2)
              - M1*M2*M2*8*rho2
              / (2*S*((M2*M2+4*rho2*rho2)
              * (M2*M2+4*rho2*rho2)) );
d2psi2_drho1drho1 = 0;
d2psi2_drho2drho2 = 2*M2/(2*rho2*rho2*rho2)
                  - M1*M2*M2*8
                  / (2*S*((M2*M2+4*rho2*rho2)
                  * (M2*M2+4*rho2*rho2)) )
                  + M1*M2*M2*8*2*4*2*rho2*rho2
                  / (2*S*((M2*M2+4*rho2*rho2)
                  * (M2*M2+4*rho2*rho2)
                  * (M2*M2+4*rho2*rho2)) );
d2psi2_drho1drho2 = 0;
qu_psi2 = ((psi2)*(psi2)*(psi2)*(psi2));
dqu_psi2_drho1 = 4*(qu_psi2/psi2)*dpsi2_drho1;
dqu_psi2_drho2 = 4*(qu_psi2/psi2)*dpsi2_drho2;
d2qu_psi2_drho1drho1 = 12*((psi2*dpsi2_drho1)*(psi2*dpsi2_drho1))
   + 4*(qu_psi2/psi2)*d2psi2_drho1drho1;
d2qu_psi2_drho2drho2 = 12*((psi2*dpsi2_drho2)*(psi2*dpsi2_drho2))
   + 4*(qu_psi2/psi2)*d2psi2_drho2drho2;
d2qu_psi2_drho1drho2 = 12 * psi2 * psi2 * dpsi2_drho1 * dpsi2_drho2
   + 4 *(qu_psi2/psi2) * d2psi2_drho1drho2;
{ dqu_psi2_dx = dqu_psi2_drho1 * drho1_dx
              + dqu_psi2_drho2 * drho2_dx;
  dqu_psi2_dy = dqu_psi2_drho1 * drho1_dy
              + dqu_psi2_drho2 * drho2_dy;
  dqu_psi2_dz = dqu_psi2_drho1 * drho1_dz
              + dqu_psi2_drho2 * drho2_dz;
```

```
};
{
  double f,df_drho1,df_drho2,d2f_drho1drho1,d2f_drho1drho2,
     d2f_drho2drho2;
  double g,dg_drho1,dg_drho2,d2g_drho1drho1,d2g_drho1drho2,
     d2g_drho2drho2;
  double h,dh_drho1,dh_drho2,d2h_drho1drho1,d2h_drho1drho2,
     d2h_drho2drho2;
  g = 1+M2/(2*rho2);
  dg_drho2 = -M2/(2*rho2*rho2);
  d2g_drho2drho2 = M2/(rho2*rho2*rho2);
  h = M1/(2*rho1*g);
  dh_drho1 = -h/rho1;
  d2h_drho1drho1 = 2*h/(rho1*rho1);
  dh_drho2 = -h*dg_drho2/g;
  d2h_drho2drho2 = h*(-d2g_drho2drho2
     + 2*dg_drho2*dg_drho2/g)/g;
  d2h_drho1drho2 = -dh_drho1*dg_drho2/g;
  a1 = (1-h)/(1+h);
  da1_drho1 = -2*dh_drho1/((1+h)*(1+h));
  d2a1_drho1drho1 = -2*d2h_drho1drho1/((1+h)*(1+h))
     +4*((dh_drho1)*(dh_drho1)) /((1+h)*(1+h)*(1+h));
  da1_drho2 = -2*dh_drho2/((1+h)*(1+h));
  d2a1_drho2drho2 = -2*d2h_drho2drho2/((1+h)*(1+h))
     +4*((dh_drho2)*(dh_drho2)) /((1+h)*(1+h)*(1+h));
  d2a1_drho1drho2 = -2*d2h_drho1drho2/((1+h)*(1+h))
     +4*dh_drho1*dh_drho2/((1+h)*(1+h)*(1+h));
  if (0) {
    f = 1.0;
    df_drho1 = d2f_drho1drho1 = df_drho2
       = d2f_drho2drho2 = d2f_drho1drho2 = 0.0;
  } else {
    f = 1 + M2*M1*M1/(2*S*(M1*M1+4*rho1*rho1));
    df_drho1 = - M2*M1*M1*8*rho1
       /(2*S*((M1*M1+4*rho1*rho1)*(M1*M1+4*rho1*rho1)) );
```

```
  d2f_drho1drho1 = - M2*M1*M1*8
     /(2*S*((M1*M1+4*rho1*rho1)*(M1*M1+4*rho1*rho1)) )
     + M2*M1*M1*8*2*8*rho1*rho1
     /(2*S*((M1*M1+4*rho1*rho1)
     *(M1*M1+4*rho1*rho1)*(M1*M1+4*rho1*rho1)) );
  df_drho2 = d2f_drho2drho2 = d2f_drho1drho2 = 0;
 }
 alpha1 = a1*f*f;
 dalpha1_drho1 = da1_drho1*f*f + 2*a1*f*df_drho1;
 d2alpha1_drho1drho1 = d2a1_drho1drho1*f*f
                + 4*f*da1_drho1*df_drho1
                + 2*a1*df_drho1*df_drho1
                + 2*f*a1*d2f_drho1drho1;
 dalpha1_drho2 = da1_drho2*f*f
           + 2*a1*f*df_drho2;
 d2alpha1_drho2drho2 = d2a1_drho2drho2*f*f
                + 4*f*da1_drho2*df_drho2
                + 2*a1*df_drho2*df_drho2
                + 2*f*a1*d2f_drho2drho2;
 d2alpha1_drho1drho2 = d2a1_drho1drho2*f*f
                + 2*f*da1_drho1*df_drho2
                + 2*f*da1_drho2*df_drho1
                + 2*a1*df_drho1*df_drho2
                + 2*f*a1*d2f_drho1drho2;
 sq_alpha1 = ((alpha1)*(alpha1));
 dsq_alpha1_drho1 = 2*alpha1*dalpha1_drho1;
 d2sq_alpha1_drho1drho1 = 2*((dalpha1_drho1)*(dalpha1_drho1))
                + 2*alpha1*d2alpha1_drho1drho1;
 dsq_alpha1_drho2 = 2*alpha1*dalpha1_drho2;
 d2sq_alpha1_drho2drho2 = 2*((dalpha1_drho2)*(dalpha1_drho2))
                + 2*alpha1*d2alpha1_drho2drho2;
 d2sq_alpha1_drho1drho2 = 2*dalpha1_drho1*dalpha1_drho2
                + 2*alpha1*d2alpha1_drho1drho2;
}
{
```

```
double f,df_drho1,df_drho2,d2f_drho1drho1,d2f_drho1drho2,
    d2f_drho2drho2;
double g,dg_drho1,dg_drho2,d2g_drho1drho1,d2g_drho1drho2,
    d2g_drho2drho2;
double h,dh_drho1,dh_drho2,d2h_drho1drho1,d2h_drho1drho2,
    d2h_drho2drho2;
g = 1+M1/(2*rho1);
dg_drho1 = -M1/(2*rho1*rho1);
d2g_drho1drho1 = M1/(rho1*rho1*rho1);
h = M2/(2*rho2*g);
dh_drho2 = -h/rho2;
d2h_drho2drho2 = 2*h/(rho2*rho2);
dh_drho1 = -h*dg_drho1/g;
d2h_drho1drho1 = h*(-d2g_drho1drho1
    + 2*dg_drho1*dg_drho1/g)/g;
d2h_drho1drho2 = -dh_drho2*dg_drho1/g;
a2 = (1-h)/(1+h);
da2_drho1 = -2*dh_drho1/((1+h)*(1+h));
d2a2_drho1drho1 = -2*d2h_drho1drho1/((1+h)*(1+h))
    +4*((dh_drho1)*(dh_drho1)) /((1+h)*(1+h)*(1+h));
da2_drho2 = -2*dh_drho2/((1+h)*(1+h));
d2a2_drho2drho2 = -2*d2h_drho2drho2/((1+h)*(1+h))
    +4*((dh_drho2)*(dh_drho2)) /((1+h)*(1+h)*(1+h));
d2a2_drho1drho2 = -2*d2h_drho1drho2/((1+h)*(1+h))
    +4*dh_drho1*dh_drho2/((1+h)*(1+h)*(1+h));
if (0) {
  f = 1.0;
  df_drho1 = d2f_drho1drho1 = df_drho2
      = d2f_drho2drho2 = d2f_drho1drho2 = 0.0;
} else {
  f = 1 + M1*M2*M2/(2*S*(M2*M2+4*rho2*rho2));
  df_drho2 = - M1*M2*M2*8*rho2
      /(2*S*((M2*M2+4*rho2*rho2)*(M2*M2+4*rho2*rho2)) );
  d2f_drho2drho2 = - M1*M2*M2*8
      /(2*S*((M2*M2+4*rho2*rho2)*(M2*M2+4*rho2*rho2)) )
```

```
      + M1*M2*M2*8*2*8*rho2*rho2
      /(2*S*((M2*M2+4*rho2*rho2)
      *(M2*M2+4*rho2*rho2)*(M2*M2+4*rho2*rho2)) );
    df_drho1 = d2f_drho1drho1 = d2f_drho1drho2 = 0;
  }
  alpha2 = a2*f*f;
  dalpha2_drho1 = da2_drho1*f*f
              + 2*a2*f*df_drho1;
  d2alpha2_drho1drho1 = d2a2_drho1drho1*f*f
                  + 4*f*da2_drho1*df_drho1
                  + 2*a2*df_drho1*df_drho1
                  + 2*f*a2*d2f_drho1drho1;
  dalpha2_drho2 = da2_drho2*f*f
              + 2*a2*f*df_drho2;
  d2alpha2_drho2drho2 = d2a2_drho2drho2*f*f
                  + 4*f*da2_drho2*df_drho2
                  + 2*a2*df_drho2*df_drho2
                  + 2*f*a2*d2f_drho2drho2;
  d2alpha2_drho1drho2 = d2a2_drho1drho2*f*f
                  + 2*f*da2_drho1*df_drho2
                  + 2*f*da2_drho2*df_drho1
                  + 2*a2*df_drho1*df_drho2
                  + 2*f*a2*d2f_drho1drho2;
  sq_alpha2 = ((alpha2)*(alpha2));
  dsq_alpha2_drho1 = 2*alpha2*dalpha2_drho1;
  d2sq_alpha2_drho1drho1 = 2*((dalpha2_drho1)*(dalpha2_drho1))
                    + 2*alpha2*d2alpha2_drho1drho1;
  dsq_alpha2_drho2 = 2*alpha2*dalpha2_drho2;
  d2sq_alpha2_drho2drho2 = 2*((dalpha2_drho2)*(dalpha2_drho2))
                    + 2*alpha2*d2alpha2_drho2drho2;
  d2sq_alpha2_drho1drho2 = 2*dalpha2_drho1*dalpha2_drho2
                    + 2*alpha2*d2alpha2_drho1drho2;
}
{ dalpha1_dx = dalpha1_drho1 * drho1_dx
          + dalpha1_drho2 * drho2_dx;
```

```
  dalpha1_dy = dalpha1_drho1 * drho1_dy
             + dalpha1_drho2 * drho2_dy;
  dalpha1_dz = dalpha1_drho1 * drho1_dz
             + dalpha1_drho2 * drho2_dz;
};
{ dalpha2_dx = dalpha2_drho1 * drho1_dx
             + dalpha2_drho2 * drho2_dx;
  dalpha2_dy = dalpha2_drho1 * drho1_dy
             + dalpha2_drho2 * drho2_dy;
  dalpha2_dz = dalpha2_drho1 * drho1_dz
             + dalpha2_drho2 * drho2_dz;
};
{ dsq_alpha1_dx = dsq_alpha1_drho1 * drho1_dx
                + dsq_alpha1_drho2 * drho2_dx;
  dsq_alpha1_dy = dsq_alpha1_drho1 * drho1_dy
                + dsq_alpha1_drho2 * drho2_dy;
  dsq_alpha1_dz = dsq_alpha1_drho1 * drho1_dz
                + dsq_alpha1_drho2 * drho2_dz;
};
{ dsq_alpha2_dx = dsq_alpha2_drho1 * drho1_dx
                + dsq_alpha2_drho2 * drho2_dx;
  dsq_alpha2_dy = dsq_alpha2_drho1 * drho1_dy
                + dsq_alpha2_drho2 * drho2_dy;
  dsq_alpha2_dz = dsq_alpha2_drho1 * drho1_dz
                + dsq_alpha2_drho2 * drho2_dz;
};
common = QU_PSI - U*U*(sq_alpha1-qu_psi1)/(1-U*U)
   - V*V*(sq_alpha2-qu_psi2)/(1-V*V);
dcommon_drho1 = dQU_PSI_drho1
   - (U*U/(1-U*U))*(dsq_alpha1_drho1 - dqu_psi1_drho1)
   - (V*V/(1-V*V))*(dsq_alpha2_drho1 - dqu_psi2_drho1);
dcommon_drho2 = dQU_PSI_drho2
   - (U*U/(1-U*U))*(dsq_alpha1_drho2 - dqu_psi1_drho2)
   - (V*V/(1-V*V))*(dsq_alpha2_drho2 - dqu_psi2_drho2);
d2common_drho1drho1 = d2QU_PSI_drho1drho1
```

```
    - (U*U/(1-U*U))*(d2sq_alpha1_drho1drho1
    - d2qu_psi1_drho1drho1)
    - (V*V/(1-V*V))*(d2sq_alpha2_drho1drho1
    - d2qu_psi2_drho1drho1);
d2common_drho2drho2 = d2QU_PSI_drho2drho2
    - (U*U/(1-U*U))*(d2sq_alpha1_drho2drho2
    - d2qu_psi1_drho2drho2)
    - (V*V/(1-V*V))*(d2sq_alpha2_drho2drho2
    - d2qu_psi2_drho2drho2);
d2common_drho1drho2 = d2QU_PSI_drho1drho2
    - (U*U/(1-U*U))*(d2sq_alpha1_drho1drho2
    - d2qu_psi1_drho1drho2)
    - (V*V/(1-V*V))*(d2sq_alpha2_drho1drho2
    - d2qu_psi2_drho1drho2);
{ dcommon_dx = dcommon_drho1 * drho1_dx
            + dcommon_drho2 * drho2_dx;
  dcommon_dy = dcommon_drho1 * drho1_dy
            + dcommon_drho2 * drho2_dy;
  dcommon_dz = dcommon_drho1 * drho1_dz
            + dcommon_drho2 * drho2_dz;
};
{d2common_dxdx = d2common_drho1drho1*drho1_dx*drho1_dx
              + dcommon_drho1*d2rho1_dxdx
              + d2common_drho2drho2*drho2_dx*drho2_dx
              + dcommon_drho2*d2rho2_dxdx
              + 2 * d2common_drho1drho2 * drho1_dx * drho2_dx;
  d2common_dydy = d2common_drho1drho1*drho1_dy*drho1_dy
              +
      dcommon_drho1*d2rho1_dydy
              + d2common_drho2drho2*drho2_dy*drho2_dy
              + dcommon_drho2*d2rho2_dydy
              + 2 * d2common_drho1drho2 * drho1_dy * drho2_dy;
  d2common_dzdz = d2common_drho1drho1*drho1_dz*drho1_dz
              + dcommon_drho1*d2rho1_dzdz
              + d2common_drho2drho2*drho2_dz*drho2_dz
```

```
            + dcommon_drho2*d2rho2_dzdz
            + 2 * d2common_drho1drho2 * drho1_dz * drho2_dz;
  d2common_dydx = d2common_dxdy
            = d2common_drho1drho1 * drho1_dx * drho1_dy
            + d2common_drho2drho2 * drho2_dx * drho2_dy
            + d2common_drho1drho2 *
              (drho1_dx*drho2_dy+drho2_dx*drho1_dy)
            + dcommon_drho1 * d2rho1_dxdy
            + dcommon_drho2 * d2rho2_dxdy;
  d2common_dzdy = d2common_dydz
            = d2common_drho1drho1 * drho1_dy * drho1_dz
            + d2common_drho2drho2 * drho2_dy * drho2_dz
            + d2common_drho1drho2 *
              (drho1_dy*drho2_dz+drho2_dy*drho1_dz)
            + dcommon_drho1 * d2rho1_dydz
            + dcommon_drho2 * d2rho2_dydz;
  d2common_dxdz = d2common_dzdx
            = d2common_drho1drho1 * drho1_dz * drho1_dx
            + d2common_drho2drho2 * drho2_dz * drho2_dx
            + d2common_drho1drho2 *
              (drho1_dz*drho2_dx+drho2_dz*drho1_dx)
            + dcommon_drho1 * d2rho1_dxdz
            + dcommon_drho2 * d2rho2_dxdz;
};
lapse = a1*a2*((((1+M2/(2*S))*(1+M2/(2*S*(1+M1/(2*rho1)))))
   *((1+M2/(2*S))*(1+M2/(2*S*(1+M1/(2*rho1))))))
   * M1*M1*rho2*rho2/(M1*M1*rho2*rho2+4*rho1*rho1*rho1*rho1)
   +(((1+M1/(2*S))*(1+M1/(2*S*(1+M2/(2*rho2)))))*((1+M1/(2*S))
   *(1+M1/(2*S*(1+M2/(2*rho2))))))
   * M2*M2*rho1*rho1/(M2*M2*rho1*rho1+4*rho2*rho2*rho2*rho2)
  +(1-M1*M1*rho2*rho2/(M1*M1*rho2*rho2+4*rho1*rho1*rho1*rho1)
   -M2*M2*rho1*rho1/(M2*M2*rho1*rho1+4*rho2*rho2*rho2*rho2))
   )/sqrt(common/QU_PSI);
{gxx = QU_PSI;
  dgxx_drho1 = dQU_PSI_drho1;
```

```
  dgxx_drho2 = dQU_PSI_drho2;
  d2gxx_drho1drho1 = d2QU_PSI_drho1drho1;
  d2gxx_drho2drho2 = d2QU_PSI_drho2drho2;
  d2gxx_drho1drho2 = d2QU_PSI_drho1drho2;
  dgxx_dx = dQU_PSI_dx;
  dgxx_dy = dQU_PSI_dy;
  dgxx_dz = dQU_PSI_dz;
  d2gxx_dxdx = d2QU_PSI_dxdx;
  d2gxx_dxdy = d2gxx_dydx = d2QU_PSI_dxdy;
  d2gxx_dzdx = d2gxx_dxdz = d2QU_PSI_dxdz;
  d2gxx_dydy = d2QU_PSI_dydy;
  d2gxx_dzdy = d2gxx_dydz = d2QU_PSI_dydz;
  d2gxx_dzdz = d2QU_PSI_dzdz;
};
{gyy = common;
  dgyy_drho1 = dcommon_drho1;
  dgyy_drho2 = dcommon_drho2;
  d2gyy_drho1drho1 = d2common_drho1drho1;
  d2gyy_drho2drho2 = d2common_drho2drho2;
  d2gyy_drho1drho2 = d2common_drho1drho2;
  dgyy_dx = dcommon_dx;
  dgyy_dy = dcommon_dy;
  dgyy_dz = dcommon_dz;
  d2gyy_dxdx = d2common_dxdx;
  d2gyy_dxdy = d2gyy_dydx = d2common_dxdy;
  d2gyy_dzdx = d2gyy_dxdz = d2common_dxdz;
  d2gyy_dydy = d2common_dydy;
  d2gyy_dzdy = d2gyy_dydz = d2common_dydz;
  d2gyy_dzdz = d2common_dzdz;
};
{gzz = QU_PSI;
  dgzz_drho1 = dQU_PSI_drho1;
  dgzz_drho2 = dQU_PSI_drho2;
  d2gzz_drho1drho1 = d2QU_PSI_drho1drho1;
  d2gzz_drho2drho2 = d2QU_PSI_drho2drho2;
```

```
  d2gzz_drho1drho2 = d2QU_PSI_drho1drho2;
  dgzz_dx = dQU_PSI_dx;
  dgzz_dy = dQU_PSI_dy;
  dgzz_dz = dQU_PSI_dz;
  d2gzz_dxdx = d2QU_PSI_dxdx;
  d2gzz_dxdy = d2gzz_dydx = d2QU_PSI_dxdy;
  d2gzz_dzdx = d2gzz_dxdz = d2QU_PSI_dxdz;
  d2gzz_dydy = d2QU_PSI_dydy;
  d2gzz_dzdy = d2gzz_dydz = d2QU_PSI_dydz;
  d2gzz_dzdz = d2QU_PSI_dzdz;
};
gXX = 1/gxx;
gYY = 1/gyy;
gZZ = 1/gzz;
{ double f,df_drho1,df_drho2,df_dx,df_dy,df_dz;
  f = 1 + U*U*M1*M1*rho2*rho2/((1-U*U)*(M1*M1*rho2*rho2
        + 4*((rho1)*(rho1)*(rho1)*(rho1)) )
        + V*V*M2*M2*rho1*rho1/((1-V*V)*(M2*M2*rho1*rho1
        + 4*((rho2)*(rho2)*(rho2)*(rho2)) ));
  df_drho1 = U*U/(1-U*U) * M1*M1*rho2*rho2/(M1*M1*rho2*rho2
     +4*((rho1)*(rho1)*(rho1)*(rho1)) )
     * (-16*((rho1)*(rho1)*(rho1)) /(M1*M1*rho2*rho2
     +4*((rho1)*(rho1)*(rho1)*(rho1)) ))
     + V*V/(1-V*V) * M2*M2*rho1*rho1/(M2*M2*rho1*rho1
     +4*((rho2)*(rho2)*(rho2)*(rho2)) )
     *(2/rho1 - 2*rho1*M2*M2/(M2*M2*rho1*rho1
     +4*((rho2)*(rho2)*(rho2)*(rho2)) ));
  df_drho2 = V*V/(1-V*V) * M2*M2*rho1*rho1/(M2*M2*rho1*rho1
     +4*((rho2)*(rho2)*(rho2)*(rho2)) )
     * (-16*((rho2)*(rho2)*(rho2)) /(M2*M2*rho1*rho1
     +4*((rho2)*(rho2)*(rho2)*(rho2)) ))
     + U*U/(1-U*U) * M1*M1*rho2*rho2/(M1*M1*rho2*rho2
     +4*((rho1)*(rho1)*(rho1)*(rho1)) )
     *(2/rho2 - 2*rho2*M1*M1/(M1*M1*rho2*rho2
     +4*((rho1)*(rho1)*(rho1)*(rho1)) ));
```

```
    { df_dx = df_drho1 * drho1_dx + df_drho2 * drho2_dx;
      df_dy = df_drho1 * drho1_dy + df_drho2 * drho2_dy;
      df_dz = df_drho1 * drho1_dz + df_drho2 * drho2_dz;
    };
    beta_X = -f*omega*y;
    beta_Y = omega*x
          + (U*(sq_alpha1 - qu_psi1)/(1-U*U)
          + (V*(sq_alpha2 - qu_psi2)/(1-V*V)))/gyy;
    beta_Z = 0.0;
    beta_x = gxx * beta_X;
    beta_y = gyy * beta_Y;
    beta_z = gzz * beta_Z;
    dbeta_x_dx = dgxx_dx * beta_X
              - df_dx * omega * y * gxx;
    dbeta_x_dy = dgxx_dy * beta_X
              - f * omega * gxx - df_dy * omega * y * gxx;
    dbeta_x_dz = dgxx_dz * beta_X
                  - df_dz * omega * y * gxx;
    dbeta_y_dx = omega * x * dgyy_dx + omega * gyy
       + U*(dsq_alpha1_dx - dqu_psi1_dx)/(1-U*U)
       + V*(dsq_alpha2_dx - dqu_psi2_dx)/(1-V*V);
    dbeta_y_dy = dgyy_dy * omega * x
       + U*(dsq_alpha1_dy - dqu_psi1_dy)/(1-U*U)
       + V*(dsq_alpha2_dy - dqu_psi2_dy)/(1-V*V);
    dbeta_y_dz = dgyy_dz * omega * x
       + U*(dsq_alpha1_dz - dqu_psi1_dz)/(1-U*U)
       + V*(dsq_alpha2_dz - dqu_psi2_dz)/(1-V*V);
  }
}
{
  G_xxx =  dgxx_dx / 2;
  G_xxy =  dgxx_dy / 2;
  G_xyx = G_xxy;
  G_xxz =  dgxx_dz / 2;
  G_xzx = G_xxz;
```

```
G_xyy = -dgyy_dx / 2;
G_xyz =  0.0;
G_xzy = 0.0;
G_xzz = -dgzz_dx / 2;
G_yxx = -dgxx_dy / 2;
G_yxy =  dgyy_dx / 2;
G_yyx = G_yxy;
G_yxz =  0.0;
G_yzx = 0.0;
G_yyy =  dgyy_dy / 2;
G_yyz =  dgyy_dz / 2;
G_yzy = G_yyz;
G_yzz = -dgzz_dy / 2;
G_zxx = -dgxx_dz / 2;
G_zxy =  0.0;
G_zyx = 0.0;
G_zxz =  dgzz_dx / 2;
G_zzx = G_zxz;
G_zyy = -dgyy_dz / 2;
G_zyz =  dgzz_dy / 2;
G_zzy = G_zyz;
G_zzz =  dgzz_dz / 2;
G_Xxx = gXX * G_xxx;
G_Xxy = gXX * G_xxy;
G_Xyx = G_Xxy;
G_Xxz = gXX * G_xxz;
G_Xzx = G_Xxz;
G_Xyy = gXX * G_xyy;
G_Xyz = gXX * G_xyz;
G_Xzy = G_Xyz;
G_Xzz = gXX * G_xzz;
G_Yxx = gYY * G_yxx;
G_Yxy = gYY * G_yxy;
G_Yyx = G_Yxy;
G_Yxz = gYY * G_yxz;
```

```
G_Yzx = G_Yxz;
G_Yyy = gYY * G_yyy;
G_Yyz = gYY * G_yyz;
G_Yzy = G_Yyz;
G_Yzz = gYY * G_yzz;
G_Zxx = gZZ * G_zxx;
G_Zxy = gZZ * G_zxy;
G_Zyx = G_Zxy;
G_Zxz = gZZ * G_zxz;
G_Zzx = G_Zxz;
G_Zyy = gZZ * G_zyy;
G_Zyz = gZZ * G_zyz;
G_Zzy = G_Zyz;
G_Zzz = gZZ * G_zzz;
}
{
K1xx = U *alpha1*drho1_dy*dgxx_drho1/(2*sqrt(QU_PSI*gyy));
K1zz = U *alpha1*drho1_dy*dgzz_drho1/(2*sqrt(QU_PSI*gyy));
K2xx = V *alpha2*drho2_dy*dgxx_drho2/(2*sqrt(QU_PSI*gyy));
K2zz = V *alpha2*drho2_dy*dgzz_drho2/(2*sqrt(QU_PSI*gyy));
K1yy = U *(-alpha1*drho1_dy*dgyy_drho1
    + 4*gyy*drho1_dy*dalpha1_drho1)/(2*sqrt(QU_PSI*gyy));
K2yy = V *(-alpha2*drho2_dy*dgyy_drho2
    + 4*gyy*drho2_dy*dalpha2_drho2)/(2*sqrt(QU_PSI*gyy));
K1yx = K1xy = U *sqrt(gyy/QU_PSI)*drho1_dx * (dalpha1_drho1
   -alpha1*dgyy_drho1/(2*gyy));
K1yz = K1zy = U *sqrt(gyy/QU_PSI)*drho1_dz * (dalpha1_drho1
   -alpha1*dgyy_drho1/(2*gyy));
K2yx = K2xy = V *sqrt(gyy/QU_PSI)*drho2_dx * (dalpha2_drho2
   -alpha2*dgyy_drho2/(2*gyy));
K2yz = K2zy = V *sqrt(gyy/QU_PSI)*drho2_dz * (dalpha2_drho2
   -alpha2*dgyy_drho2/(2*gyy));
K_xx= K1xx+ K2xx;
K_yy= K1yy+ K2yy;
K_zz= K1zz+ K2zz;
```

```
K_xy= K1xy+ K2xy;
K_yz= K1yz+ K2yz;
K_yx= K1yx+ K2yx;
K_zy= K1zy+ K2zy;
K_xz = 0;
K_zx = 0;
K = gXX * K_xx + gYY * K_yy + gZZ * K_zz;
K_XX = gXX * gXX * K_xx;
K_YY = gYY * gYY * K_yy;
K_ZZ = gZZ * gZZ * K_zz;
K_XY = gXX * gYY * K_xy;
K_YX = K_XY;
K_XZ = gXX * gZZ * K_xz;
K_ZX = K_XZ;
K_YZ = gYY * gZZ * K_yz;
K_ZY = K_YZ;
K_AB_K_ab = K_XX * K_xx + K_XY * K_xy
   + K_XZ * K_xz + K_YX * K_yx + K_YY * K_yy
   + K_YZ * K_yz + K_ZX * K_zx + K_ZY * K_zy
   + K_ZZ * K_zz;
D_x_beta_y = dbeta_y_dx
                - G_Yxy*beta_y - G_Xxy*beta_x;
D_y_beta_y = dbeta_y_dy
                - G_Yyy*beta_y - G_Xyy*beta_x;
D_z_beta_y = dbeta_y_dz
                - G_Yzy*beta_y - G_Xzy*beta_x;
D_x_beta_x = dbeta_x_dx
                - G_Yxx*beta_y - G_Xxx*beta_x;
D_y_beta_x = dbeta_x_dy
                - G_Yyx*beta_y - G_Xyx*beta_x;
D_z_beta_x = dbeta_x_dz
                - G_Yzx*beta_y - G_Xzx*beta_x;
D_x_beta_z =  - G_Yxz*beta_y - G_Xxz*beta_x;
D_y_beta_z =  - G_Yyz*beta_y - G_Xyz*beta_x;
D_z_beta_z =  - G_Yzz*beta_y - G_Xzz*beta_x;
```

```
}
{
  R = - d2gxx_dydy / (gxx * gyy)
      - d2gxx_dzdz / (gxx * gzz)
      - d2gyy_dxdx / (gxx * gyy)
      - d2gyy_dzdz / (gyy * gzz)
      - d2gzz_dxdx / (gxx * gzz)
      - d2gzz_dydy / (gyy * gzz)
      + (dgxx_dy)*(dgxx_dy) / (2*gxx*gxx*gyy)
      + (dgxx_dz)*(dgxx_dz) / (2*gxx*gxx*gzz)
      + (dgyy_dx)*(dgyy_dx) / (2*gxx*gyy*gyy)
      + (dgyy_dz)*(dgyy_dz) / (2*gyy*gyy*gzz)
      + (dgzz_dx)*(dgzz_dx) / (2*gxx*gzz*gzz)
      + (dgzz_dy)*(dgzz_dy) / (2*gyy*gzz*gzz)
      + (dgxx_dx)*(dgyy_dx) / (2*gxx*gxx*gyy)
      + (dgxx_dx)*(dgzz_dx) / (2*gxx*gxx*gzz)
      + (dgxx_dy)*(dgyy_dy) / (2*gxx*gyy*gyy)
      - (dgxx_dy)*(dgzz_dy) / (2*gxx*gyy*gzz)
      - (dgxx_dz)*(dgyy_dz) / (2*gxx*gyy*gzz)
      + (dgxx_dz)*(dgzz_dz) / (2*gxx*gzz*gzz)
      - (dgyy_dx)*(dgzz_dx) / (2*gxx*gyy*gzz)
      + (dgyy_dy)*(dgzz_dy) / (2*gyy*gyy*gzz)
      + (dgyy_dz)*(dgzz_dz) / (2*gyy*gzz*gzz);
}
{
  double D_b_K_XB,D_b_K_YB,D_b_K_ZB,D_x_K_XX,
     D_y_K_XY,D_z_K_XZ,D_x_K_YX,D_y_K_YY,
     D_z_K_YZ,D_x_K_ZX,D_y_K_ZY,D_z_K_ZZ,
     D_X_K,D_Y_K,D_Z_K,measure,scalar;
  scalar = lapse * (R + K*K - K_AB_K_ab)
     + 2 * (  D_x_beta_x * (K_XX - gXX*K)
     +  D_y_beta_y * (K_YY - gYY*K)
     +  D_z_beta_z * (K_ZZ - gZZ*K)
     + (D_x_beta_y + D_y_beta_x) * K_XY
     + (D_x_beta_z + D_z_beta_x) * K_XZ
```

```
      + (D_z_beta_y + D_y_beta_z) * K_ZY);
    measure = sqrt( gxx * gyy * gzz );
    if (0) {
      printf(" x %g,y %g,z %g\n",x,y,z);
      printf("  R  %g measure  %g\n",R,measure);
      printf("  lapse (R + K*K - K_AB_K_ab) %g %g\n",
        lapse,(R + K*K - K_AB_K_ab));
      printf("D_x_beta_x * (K_XX - gXX*K) %g\n",
        D_x_beta_x * (K_XX - gXX*K));
      printf("D_y_beta_y * (K_YY - gYY*K) %g\n",
        D_y_beta_y * (K_YY - gYY*K));
      printf("D_z_beta_z * (K_ZZ - gZZ*K) %g\n",
        D_z_beta_z * (K_ZZ - gZZ*K));
      printf("(D_x_beta_y + D_y_beta_x) * K_XY %g \n",
        (D_x_beta_y + D_y_beta_x) * K_XY);
      printf("(D_x_beta_z + D_z_beta_x) * K_XZ %g \n",
        (D_x_beta_z + D_z_beta_x) * K_XZ);
      printf("(D_z_beta_y + D_y_beta_z) * K_ZY %g \n",
        (D_z_beta_y + D_y_beta_z) * K_ZY);
      printf("returning integrand %g NO r**2 sin(theta)\n",scalar *
        measure);
    }
    return( (measure * scalar) );
  }
}
```

REFERENCES

1. J. Michell, Philos. Trans. 74, 35-57, (1783).

2. P. S. Laplace, *Le Système du monde*, vol. II, Paris, (1795).

3. A. Einstein, Preuss. Akad. Wiss. Berlin, Sitzber. 47, 831-839, (1915).

4. K. Schwarzschild, Sitzber. Deut. Akad. Wiss. Berlin, Kl. Math.-Phys. Tech., 189-196, (1916).

5. S. Chandrasekhar, Astrophys. J. 74, 81-82, (1931).

6. A. S. Eddington, in Minutes of a Meeting of the Royal Astronomical Society, Observatory 58, 37, (1935).

7. L. D. Landau, Phys. Z. Sowjetunion 1, 285, (1932).

8. J. Chadwick, Nature 129, 312, (1932).

9. J. R. Oppenheimer, G. M. Volkoff, Phys. Rev. 55, 374, (1939).

10. J. R. Oppenheimer, H. Snyder, Phys. Rev. 56, 455, (1939).

11. S. Chandrasekhar, in *Highlights of Astronomy*, Vol. 5, P. A. Wayman, ed., Reidel, Dordrecht, Holland, 53, (1980).

12. M. D. Kruskal, Phys. Rev. 119, 1743, (1960).

13. B. K. Harrison, K. S. Thorne, M. Wakano, J. A. Wheeler, *Gravitation Theory and Gravitational Collapse*, University of Chicago Press, Chicago, (1965).

14. J. A. Wheeler, American Scientist 56, 1, (1968).

15. B. L. Webster, P. Murdin, Nature 235, 37-38, (1972).

16. R. P. Kerr, Phys. Rev. Lett. 11, 237-238, (1963).

17. E. T. Newman, E. Couch, K. Chinnapared, A. Exton, A. Prakash, R. Torrence, J. Math. Phys. 6, 918, (1965).

18. C. W. Misner, K. S. Thorne, J. A. Wheeler, *Gravitation*, Freeman, San Francisco, 876, (1973).

19. R. Penrose, Phys. Rev. Lett. 14, 57-59, (1965).

20. W. Isreal, Phys. Rev. 164, 1776-1779, (1967).

21. B. Carter, Phys. Rev. Lett. 26, 331-333, (1970).

22. S. W. Hawking, Commun. Math. Phys. 26, 1344-1346, (1972).

23. R. Penrose, in *Relativity, Groups, and Topology*, C. DeWitt, and B. S. DeWitt, eds., Gordon and Breach, New York, (1964).

24. G. W. Gibbons, Comm. Math. Phys. 27, 87-102, (1972).

25. S. L. Detweiler, in *Sources of Gravitational Radiation*, L. L. Smarr, ed., Cambridge University Press, Cambridge, (1979).

26. R. M. Wald, *General Relativity*, University of Chicago Press, Chicago, (1984).

27. P. S. Arnowitt, S. Deser, C. W. Misner, in *Gravitation: An Introduction to Current Research*, L. Witten, ed., Wiley, New York, (1962).

28. K. Eppley, Phys. Rev. D 16, 1609-1614, (1977).

29. L. L. Smarr, in *Sources of Gravitational Radiation*, L. L. Smarr, ed., Cambridge University Press, Cambridge, (1979).

30. J. K. Blackburn, S. L. Detweiler, In Preparation, (1990).

31. L. D. Landau, E. M. Lifshitz, *The Classical Theory of Fields*, Pergamon, Oxford, (1975).

32. È. Cartan, J. Math. Pures Appl. 1, 141-203, (1922).

33. J. W. York, in *Sources of Gravitational Radiation*, L. L. Smarr, ed., Cambridge University Press, Cambridge, (1979).

34. S. W. Hawking, G. F. R. Ellis, *The Large Scale Structure of Space-Time*, Cambridge University Press, Cambridge, (1973).

35. J. Leray, unpublished, notes from Princeton Institute for Advanced Study, (1952).

36. S. L. Detweiler, in *Frontiers in Numerical Relativity*, C. R. Evans, S. L. Finn, D. W. Hobill, eds., Cambridge University Press, Cambridge, (1989).

37. R. W. Fuller, J. A. Wheeler, Phys. Rev. 128, 778-781, (1962).

38. J. M. Bowen, J. W. York, Phys. Rev. D 21, 2047-2056, (1980).

39. A. Ashtekar, R. O. Hansen, J. Math. Phys. 19, 1542-1566, (1978).

40. J. W. York, *Essays in General Relativity: a festcrift for Abraham Taub*, F. J. Tipler, ed., Academic Press, New York, (1980).

41. T. Regge, C. Teitelboim, Ann. Phys. 88, 286-318, (1974).

42. R. C. Tolman, *Relativity Thermodynamics and Cosmology*, Dover Publications, New York, (1987).

43. R. Penrose, *The Emperor's New Mind*, Oxford University Press, New York, (1989).

44. S. L. Shapiro, S. A. Teukolsky, *Black Holes, White Dwarfs, and Neutron Stars*, John Wiley & Sons, New York, (1983).

45. D. R. Brill, R. W. Lindquist, Phys. Rev. 131, 471-476, (1963).

46. A. Einstein, L. Infeld, B. Hoffmann, Ann. Math. 39, 65-100, (1938).

47. H. P. Robertson, Ann. Math. 39, 100, (1938).

48. J. P. Clark, D. M. Eardley, Ap. J. 215, 311-322, (1977).

49. A. Čadež, Ann. Phys. 83, 449, (1974).

50. N. T. Bishop, Gen. Rel. Grav. 14, 717, (1982).

51. K. Oohara, T. Nakamura, Y. Kojima, Phys. Lett. 107A, 452-455, (1985).

52. T. Nakamura, Y. Kojima, K. Oohara, Phys. Lett. 106A, 235-238, (1984).

53. T. Regge, J. A. Wheeler, Phys. Rev. 108, 1063, (1957).

54. W. H. Press, B. P. Flannery, S. A. Teukolsky, W. T. Vetterling, *Numerical Recipes*, Cambridge University Press, New York, (1986).

55. B. Carnahan, H. A. Luther, J. O. Wilkes, *Applied Numerical Methods*, John Wiley & Sons, New York, (1969).

BIOGRAPHICAL SKETCH

James Kent Blackburn was born on July 15, 1957, in Chattanooga, Tennessee. At the age of three his family moved to Greensboro, North Carolina, and again at the age of five moved to Winston-Salem, North Carolina. It was here on his sixth birthday that his love of science would begin with a small reflecting telescope presented to him by an aunt who also captured his imagination with stories from the orient, where she was stationed as an officer in the United States Navy. It was also the dawn of the Space Age. With each countdown to launch he would attach himself to the television set, following the mission from "t-minus" to "splashdown." During these years he was also developing a love for the outdoors. Weekends would often be times of canoeing, hiking, and camping, and in January, 1973, he became an Eagle Scout in the Boy Scouts of America, as had his father in his boyhood. He completed high school at West Forsyth High School in Winston-Salem, graduating third in his class, in 1975. After high school he entered the University of North Carolina at Chapel Hill in fall of 1975. Here his interests focused on physics and astronomy, and in August of 1979 he graduated with the degree of Bachelor of Science in physics. After graduating from the University of North Carolina at Chapel Hill he entered industry working first as a chemist and then as an electronics technician. By this time his curiosity for science began to erupt, and he began to take graduate courses in physics at Wake Forest University as a part-time

student while working full-time at Western Electric Company. After a year of sleepless nights he was able to secure a fellowship at Wake Forest University and entered as a full-time graduate student in the fall of 1982. Here he studied the basic curriculum in physics, but Wake Forest did not offer a program above the Master of Science level. This brought him to the University of Florida in the fall of 1983. Here his interest in astrophysics began to resurface. Initially his research at the University of Florida was geared toward experimental astrophysics in the space program using the space shuttle. But after the Challenger disaster he found his interests focusing on theoretical astrophysics. A strong predilection towards general relativity and a fascination with computers placed him under the guidance of Steven Detweiler and provided him with the opportunity to work on the binary system of black holes.

I certify that I have read this study and that in my opinion it conforms to acceptable standards of scholarly presentation and is fully adequate, in scope and quality, as a dissertation for the degree of Doctor of Philosophy.

Steven Detweiler, Chairman
Professor of Physics

I certify that I have read this study and that in my opinion it conforms to acceptable standards of scholarly presentation and is fully adequate, in scope and quality, as a dissertation for the degree of Doctor of Philosophy.

James Ipser, Cochairman
Professor of Physics

I certify that I have read this study and that in my opinion it conforms to acceptable standards of scholarly presentation and is fully adequate, in scope and quality. as a dissertation for the degree of Doctor of Philosophy.

James Fry
Associate Professor of Physics

I certify that I have read this study and that in my opinion it conforms to acceptable standards of scholarly presentation and is fully adequate, in scope and quality, as a dissertation for the degree of Doctor of Philosophy.

Richard Field
Professor of Physics

I certify that I have read this study and that in my opinion it conforms to acceptable standards of scholarly presentation and is fully adequate, in scope and quality, as a dissertation for the degree of Doctor of Philosophy.

Stephen Gottesman
Professor of Astronomy

This dissertation was submitted to the Graduate Faculty of the Department of Physics in the College of Liberal Arts and Sciences and to the Graduate School and was accepted as partial fulfillment of the requirements for the degree of Doctor of Philosophy.

May 1990

Dean, Graduate school

UNIVERSITY OF FLORIDA
3 1262 08553 4518